Synthesis of Reactive Distillation Processes

Dissertation

zur Erlangung des akademischen Grades

Doktoringenieur
(Dr.-Ing.)

von Dipl.-Ing. Erik Stein

geb. am 28. März 1970 in Püttlingen

genehmigt durch die Fakultät für Elektrotechnik und Informationstechnik
der Otto-von-Guericke-Universität Magdeburg

Gutachter: Prof. Dr.-Ing. Achim Kienle
                  Prof. Dr.-Ing. habil. Kai Sundmacher

Promotionskolloquium am 14. Juli 2003

Forschungsberichte aus dem Max-Planck-Institut
für Dynamik komplexer technischer Systeme

Band 6

Erik Stein

Synthesis of Reactive Distillation Processes

Shaker Verlag
Aachen 2003

Printed in Germany.

Acknowledgements

This thesis originated while I was working as a research assistant at the Max-Planck-Institute (MPI) for Dynamics of Complex Technical Systems in Magdeburg. Several people have contributed to the success of this work in one way or another.

I thank Prof. Dr.-Ing. Dr.h.c.mult. Ernst-Dieter Gilles for the possibility to work at the Max-Planck-Institute with its outstanding working conditions.

Furthermore, I thank Prof. Dr.-Ing. habil. Kai Sundmacher as an expert in reactive distillation for fruitful discussions and critical reading of the forthcoming text.

Above all, I wish to thank Prof. Dr.-Ing. Achim Kienle for his continuous support and many inspiring discussions. He has been my competent advisor from the very beginning and introduced me to the fascinating world of reactive distillation.

I enjoyed to work at the MPI with its animating and agreeable atmosphere. Many colleagues are "responsible" for these circumstances with their readiness for technical discussions or just everyday questions. Among them, special thanks I address to Martin Häfele and Dr. Michael Mangold for the joint efforts to "settle in".

Last but not least I would like to thank my parents for providing the basis, not only for my professional life. I am very grateful to my wife Marion and our children Niklas, Finian and Junia for their love and encouragement during all these years.

Schifferstadt, August 2003   Erik Stein

Contents

Notation

In general, vectors are denoted as bold face symbols, e.g. $\mathbf{x}$ or $\boldsymbol{\nu}$.

a	activity	
B	bottom flow rate	kmol/s
D	distillate flow rate	kmol/s
Da	Damköhler number	
Da^*	scaled Damköhler number	
E	energy of activation	kJ/kmol
F	feed flow rate	kmol/s
K_{eq}	chemical equilibrium constant	
k_f	forward reaction rate	kmol/s
L	liquid flow rate	kmol/s
M	molar mass	kg/kmol
m	amount of catalyst	kg
N	number of stages	
n	liquid molar holdup	kmol
nc	number of components	
nr	number of reactions	
p	pressure	bar
Q	reboiler duty	kW
r	reflux ratio	
$r(\mathbf{x})$	reaction rate	kmol/s or kmol/(kg s)
$\mathbb{R}$	ideal gas constant	kJ/(kmol K)
s	reboil ratio	
T	temperature	K
t	time	s
V	vapor flow rate	kmol/s
w	weighting factors	
X	transformed liquid mole fraction	
x	liquid mole fraction	
Y	transformed vapor mole fraction	
y	vapor mole fraction	
z	spatial coordinate	m

Greek letters

α	constant relative volatility	
γ	activity coefficient	
ν	stoichiometric coefficient	
ξ	extent of reaction	kmol
τ	dimensionless time	
ϕ	fraction of vaporized feed	

Subscripts

cat	catalyst
$crit$	critical
D	distillate
F	feed
il	inner left column section
ir	inner right column section
re	rectifying section
sd	side draw
st	stripping section
P	product
R	reactor
ref	reference
rx	reaction
s	saturation
T	total

Superscripts

C	combinatorial part
eq	equilibrium
R	residual part
T	transposed

Abbreviations

C_4	hydrocarbons with four carbon atoms
DIB	diisobutene
DME	dimethyl ether
$elka$	extended line of kinetic azeotropy
H_2O	water
iB	isobutene
$MeOH$	methanol
MSS	multiple steady states
$MTBE$	methyl *tert*-butyl ether
nB	1-butene (*n*-butene)
RCM	residue curve map
TBA	*tert*-butyl alcohol

Kurzfassung

Stoffumwandlung und Stofftrennung sind Basisoperationen in der Verfahrenstechnik. Werden diese Grundoperationen in einem Apparat vereint, so spricht man von einem multifunktionellen Prozess. Ein Beispiel dafür ist die Reaktivdestillation (RD), bei der Reaktion und Destillation überlagert werden. Dieses Verfahrenskonzept kann einerseits zu deutlichen Einsparungen führen, andererseits gestaltet sich das Design und die Prozessführung eines solchen multifunktionellen Prozesses schwierig. Neue Phänomene treten auf, die bei den Einzelprozessen nicht vorkommen.

Ziel dieser Arbeit ist es, Kriterien zu identifizieren, bei welchen Stoffsystemen und Reaktionsklassen sich die RD lohnen kann, um eine Entscheidung im frühen Stadium des Prozessentwurfs zu erleichtern. Im Mittelpunkt der Betrachtungen stehen einfache, ideale Stoffsysteme, anhand derer grundlegende Phänomene erkannt und erläutert werden können. Am Ende der Arbeit kommen die gewonnenen Erkenntnisse beim Design von RD-Prozessen mit realen Stoffsystemen zum Tragen.

Zunächst werden die Grundlagen aufgearbeitet, die für den Entwurf von RD-Prozessen benötigt werden. Zu nennen sind hier die Konzepte "Rückstandskurve (Residue Curve)", "Reaktive kinetische Azeotrope" sowie verschiedene Designmethoden. Weiterhin werden Grundlagen der mathematischen Modellierung und Optimierung zusammengefasst.

Bei dem ersten Anwendungsbeispiel handelt es sich um ein binäres ideales Stoffsystem, bei dem in einer Isomerisierungsreaktion die Komponente A in die Komponente B überführt werden soll. Ausgehend von den inhärenten Systemeigenschaften, wie relative Flüchtigkeit und Reaktionskinetik, werden unterschiedliche Prozessvarianten entwickelt und verglichen. Dabei zeigt sich die Relevanz der prinzipiellen Untersuchungen für das konkrete Kolonnendesign.

Im nächsten Schritt werden ternäre ideale Systeme mit unterschiedlichen Reaktionsschemata betrachtet. Analog zum binären System werden zuächst die Basiseigenschaften wie kinetische Azeotrope ermittelt. Davon abhängig sind die unterschiedlichen Prozessvarianten, die zum Teil mit Hilfe bekannter Auslegungsmethoden wie den Fenske-Underwood-Gleichungen für nichtreaktive Kolonnen bestimmt werden. Für das Design der RD-Prozesse wird auf mathematische Optimierungsmethoden zurückgegriffen. Es handelt sich dabei um Probleme der gemischt-ganzzahligen nichtlinearen Programmierung (MINLP), die mit speziellen Werkzeugen gelöst werden. Im Vergleich zum herkömmlichen Prozess, bei dem Reaktion und Stofftrennung in verschiedenen Appa-

raten stattfinden, sind RD-Prozesse – abhängig vom jeweiligen Reaktionsschema – deutlich kostengünstiger bis absolut ungeeignet. Neben dem Reaktionsschema spielen auch konkrete Stoffdaten eine entscheidende Rolle bei der Auswahl des günstigsten Prozesses.

Abschließend werden zwei reale Stoffsysteme betrachtet. Es handelt sich dabei um die reaktive Trennung von eng siedenden Gemischen, hier beispielhaft die Trennung der Isomere Isobuten und 1-Buten. Im ersten Beispielsystem ist der Reaktionspartner Methanol, wodurch sich als Zwischenprodukt Methyl *tert*-Butyl Ether (MTBE) ergibt. Im zweiten Beispielsystem wird Wasser eingesetzt, was zu *tert*-Butylalkohol (TBA) als Zwischenprodukt führt. Die wesentlichen Nebenreaktionen und -produkte werden berücksichtigt, wodurch sich eine etwas andere Fragestellung als bei den idealen Stoffsystemen ergibt. Es zeigt sich, dass das Prozessdesign auf der Basis mathematischer Optimierung bei diesen komplexen Systemen schnell an seine Grenzen stößt, weshalb hier konzeptionelle Überlegungen und Simulationsstudien überwiegen. Um auch bei solchen Systemen Optimierungswerkzeuge nutzbringend einzusetzen, werden Modellvereinfachungen vorgestellt und diskutiert.

Die Untersuchung der verschiedenen Beispielsysteme zeigt, dass für das Design von RD-Prozessen ein profundes Wissen um die komplexen Wechselwirkungen von Reaktion und destillativer Trennung unabdingbar ist. Allerdings läßt sich allein aus diesem Wissen kein optimaler Prozess ableiten. Es erfordert weiterhin Methoden der mathematischen Modellierung und Optimierung, die ausgehend von konzeptionellen Studien zu einer optimalen Lösung führen. Die wesentliche Einschränkung, die einen universellen Einsatz dieser Methodik bei realen industriellen Prozessen verbietet, besteht derzeit darin, dass die verfügbaren Optimierungswerkzeuge solch komplexe Modelle nicht zufriedenstellend lösen können. Unabhängig von der Weiterentwicklung auf der Werkzeugseite besteht die Möglichkeit, bei der Modellierung Vereinfachungen vorzunehmen und so den vielversprechenden Einsatz von Optimierungsmethoden beim Design von Reaktivdestillationsprozessen voranzutreiben.

Chapter 1

Introduction

The combination of the unit operations *reaction* and *separation* in one apparatus is called *reactive distillation* (RD). If the substances only react in the presence of a solid catalyst, this process is also termed *catalytic distillation*. Running reaction and separation simultaneously provides considerably higher economic benefits for some reaction systems compared to the conventional sequential processing. This is mainly due to a reduced downstream processing as the products are removed from the reactants in situ. This is also a main advantage of RD for systems where the conversion is limited by the chemical equilibrium. The continuous removal of products shifts the chemical equilibrium to the product side. Thus, in the ideal case, full conversion can be achieved in a RD column in contrast to a conventional reactor. A further possible advantageous effect of RD is the suppression of side reactions or consecutive reactions leading to an increase in selectivity and yield of the process. Furthermore, some difficult separation problems can be solved using a selective reactive entrainer.

Possibly the most famous example for a successful implementation of RD technology is the Eastman process for the production of methyl acetate [3]. For this esterification reaction it was possible to substitute a conventional process consisting of a reactor and nine separation columns by a single RD column. As methyl acetate is produced in high quantities every year, the economic benefit of this inventive process modification was enormous. Another established process is the production of the fuel additive methyl *tert*-butyl ether (MTBE) from isobutene and methanol. This process will be investigated in more detail in section 3.3.3. Podrebarac et al. [50] provide an overview of implemented and possible applications of the RD technology.

Despite all these advantages, there are some obstacles preventing a successful implementation of RD technology in some cases. Compared to a process flowsheet consisting of separate reactors and columns, the process design for RD columns is more difficult because of the additional degrees of freedom (e.g. selection of catalyst; number and positions of feed inputs; number, lengths and positions of reaction zones). Additionally, new phenomena like reactive azeotropes arise from the interaction of physico-chemical effects which are separated in the conventional processes. Furthermore, the strongly nonlinear behavior of some RD processes requires advanced process control methods.

Thus, the question arises for which reaction systems RD is a profitable alternative. This thesis wants to contribute to enable a profound decision whether RD should be examined or not in an early design stage. The goal is to provide theoretical approaches for a systematic development and design of reactive distillation systems. These approaches will be based on mathematical models of the processes with different degrees of detail. They are optimized with mathematical programming algorithms. Design methods are already established for reaction systems which are determined by the chemical equilibrium. The focus in this thesis is on kinetically controlled reaction systems where the development of design methods is in progress.

In the following, an overview of the current literature on different aspects of this thesis is given. These aspects include distillation synthesis methods, optimization methods (for separation processes), phenomena in reactive distillation like kinetic azeotropes, etc.

Chapter 2 provides fundamental information about the thermodynamics of reaction-separation systems, general phenomena like kinetic azeotropes, analogy between simple reactive distillation and reactive distillation columns, etc. These are necessary requirements for the following process design studies.

Chapter 3 deals with different applications of reactive distillation. In section 3.1, a simple ideal isomerization reaction is considered. This simple system provides some fundamental insight, valid also for more complex systems. In section 3.2, different ideal ternary systems are investigated. Feasible solutions are identified and different process configurations are compared. In section 3.3, reactive distillation is used for the separation of closely boiling mixtures. Starting with an ideal system like in the previous sections, finally two real-world problems are examined in detail, and feasible process configurations are developed for the two realistic nonideal multicomponent mixtures.

1.1 Reactive Distillation

In this thesis, focus is on design and synthesis of reactive distillation systems. Hence in the following, the important literature on these subjects is briefly revisited in chronological order. A nice overview on RD literature from the beginning of the 20th century was written by Pyhälahti [51]. It includes different RD processes (spontaneous reactions, homogeneously and heterogeneously catalyzed processes), column internals, and modeling for design and optimization. Recently, Taylor and Krishna [69] reviewed reactive distillation modeling approaches. While their focus is on the proper description of physico-chemical effects, there is also a short summary on RD design methods.

Duprat et al [22] propose the optimization of a reactive separation system by the construction of empirical formula. This method is efficient for the particular system under consideration (picoline separation). In general, considerable effort is necessary to set up the empirical formula.

Barbosa and Doherty [6, 7] describe a graphical design method for a single feed and double feed reactive distillation column. The design procedure is based on transformed concentration variables for a single chemical equilibrium reaction. By trial and error the minimum reflux ratio is obtained.

Doherty and Buzad [19] relax the assumption of chemical equilibrium and consider the design of a single feed RDC with a single kinetically controlled reaction. The *Damköhler number Da* is introduced as the design parameter related to reaction kinetics. For specified top and bottom product concentrations and given Da, the reflux ratio is varied until a feasible design is found.

Ciric and Gu [15] were the first to propose the optimization of a RD process with mathematical programming methods. The goal is to determine the optimal number of trays, holdup per tray, reflux ratio, condenser and reboiler duties, and feed tray locations. The model formulation requires binary variables resulting in a *mixed integer nonlinear programming (MINLP)* problem. The annualized costs are used as objective function to be minimized. The problem is solved with a modified GBD method in the optimization tool GAMS [9]. See section 1.2 for a description of the algorithms.

Cardoso et al [12] applied the stochastic optimization algorithms *simulated annealing* and *adaptive random search algorithm* to the same process as in Ciric and Gu [15] (ethylene glycol production). A general MINLP model (non-equimolar, non-ideal VLE, distributed feeding and reaction zone) was used in an integrated simulation and optimization

environment. Slightly better optimal solutions were found, demonstrating that heuristic optimization methods are also capable of solving reactive distillation design problems.

Buzad and Doherty [10, 11] developed a fixed point method for the design of reactive distillation columns. The focus is on kinetically controlled reactions with an ideal ternary system as an example. For fixed product concentrations, feasible process configurations are found with different total amounts of holdup for varying Damköhler numbers.

Okasinski and Doherty [47] extended the fixed point design method by Buzad and Doherty to multicomponent non-equimolar reactions with non-ideal VLE. A distribution of the liquid holdup over the column height is allowed.

Pekkanen [48] proposed a *local optimization method* where a local Damköhler number and an effectiveness factor on each tray are optimized. The directional difference between operating lines and desired end products is minimized. This stage-by-stage approach is applicable to single-feed multireaction systems. There is no simultaneous overall optimization like in the approach of Ciric and Gu.

Hauan [32, 33, 40] developed the concept of *phenomena vectors* attributed to the three fundamentally different mechanisms in a reactive distillation column: separation, reaction and mixing. Combining these vectors, fixed points in the composition space are found. For ternary systems the different effects can be visualized instructively. With this method, feasibility criteria for reactive distillation are exploited.

Recently, Chadda et al. [13] showed that the model of an isobaric flash cascade can be used to predict possible top and bottom products of a multicomponent, single-feed RDC. The models of the rectifying and the stripping flash cascade are identical in the limiting cases of no reaction and reaction equilibrium, and thus are their fixed points. However, for kinetically controlled reactions the models differ and different fixed points are obtained.

Stichlmair and Frey [63] investigated the optimal design of RD processes for MTBE and methyl acetate production. They followed a similar approach to that proposed in this thesis: First, possible product regions are determined graphically with the help of distillation lines. Based on these findings, a RD column is modeled with degrees of freedom like feed positions, reaction zones and the like. The resulting MINLP model is optimized to obtain the best process design. Even though this procedure is very similar to the approach in this thesis, there exists an important difference: In this thesis, the main goal is not to find the best RD column configuration for one given reaction scheme but to answer the question if RD is the best option for a certain class of reaction systems. Furthermore, new innovative applications are developed as will be shown in section 3.3.

1.2 Optimization

This section briefly reviews mathematical optimization problems and solution methods. As this is a large field of ongoing research, only those topics will be discussed in more detail that are relevant for the solution of the problems faced in this thesis. For general and more detailed informations on optimization the interested reader is referred to textbooks like [24, 29] or to Ullmann's Encyclopedia [25]. Models to be solved with optimization algorithms can be classified with respect to their following properties:

- dynamic vs. steady state,
- linear vs. nonlinear equations,
- continuous vs. discrete variables.

In the following only steady state (stationary) optimization problems are considered. The most general formulation of *mathematical programming* problems reads

$$
\begin{aligned}
\min_{\mathbf{x},\mathbf{y}} \quad & f(\mathbf{x},\mathbf{y}) \\
\text{s.t.} \quad & \mathbf{g}(\mathbf{x},\mathbf{y}) = \mathbf{0} \\
& \mathbf{h}(\mathbf{x},\mathbf{y}) \leq \mathbf{0} \\
& \mathbf{x} \in I\!R^n \\
& \mathbf{y} \in \{0,1\}^m
\end{aligned}
\tag{1.1}
$$

where f is a scalar *objective function* to be minimized by manipulating *continous variables* $\mathbf{x}$ and *discrete variables* $\mathbf{y}$. The latter are restricted to zero and one without loss of generality and thus are termed *binary variables*. These variables obey *equality constraints* $\mathbf{g}$ as well as *inequality constraints* $\mathbf{h}$. Typical examples for the former are model equations like mass and energy balances, whereas product purity requirements or safety constraints are examples for the latter. Different classes of mathematical programming problems are distinguished as shown in Table 1.1. They will be discussed in more detail in the following.

Linear Programming (LP) problems

If no discrete variables are present and both, the objective function f and the constraints $\mathbf{g}, \mathbf{h}$ are linear in the continous variables $\mathbf{x}$ the simplest form of an optimization formulation is obtained, a *linear programming* (LP) problem. This problem has either

	continous $(\mathbf{x})$	mixed $(\mathbf{x}, \mathbf{y})$
linear $(f, \mathbf{g}, \mathbf{h})$	LP	MILP
nonlinear $(f, \mathbf{g}, \mathbf{h})$	NLP	MINLP

Table 1.1: Classificaton of mathematical programming problems.

- no solution if the constraints are contradictory,

- infinitely many solutions if the objective function coincides with a constraint, or

- exactly one solution if the problem is well posed.

In the latter case, the unique solution is found at a point where two or more constraints are active, a *vertex* of the system. The standard algorithm to solve these problems is the *simplex algorithm* (for details see [24]). It efficiently exploits the basic properties of the problem by searching only among the vertices in the feasible space. Most current commercial codes for solving LP problems are based on extensions of the simplex algorithm and typically are able to handle tens of thousands of variables.

Mixed-Integer Linear Programming (MILP) problems

If some of the optimization variables are restricted to binary (0,1) values and f, $\mathbf{g}$ and $\mathbf{h}$ are all linear, a *mixed-integer linear programming* (MILP) problem is obtained. An intuitive way to solve these problems is to relax the binary variables and treat them as continuous variables between 0 and 1. Unfortunately, there is no guarantee that the solution of the resulting LP problems provides necessary integer values for the 0-1 variables. Rounding to the nearest integer may even lead to infeasible solutions as the following example demonstrates [25]. Consider the pure integer problem

$$\min_{\mathbf{y}} \quad f(\mathbf{y}) = -1.2 \, y_1 - y_2 \qquad \text{(1.2-a)}$$

$$\text{s.t.} \quad 1.2 \, y_1 + 0.5 \, y_2 - 1 \le 0 \qquad \text{(1.2-b)}$$

$$\mathbf{y} \in \{0, 1\}^2 \qquad \text{(1.2-c)}$$

Relaxing y_1 and y_2 yields the solution $\mathbf{y} = [0.715, \ 0.285]$ with $f = -1.148$. Simply rounding to $\mathbf{y} = [1, 0]$ leads to an infeasible solution as the constraint, Eq. (1.2-b), is violated. The optimal solution is $\mathbf{y} = [0, 1]$ with $f = -1$.

The most common approach to solve MILP problems is the *branch and bound* (BB) method. The basic idea is to represent all the 0-1 combinations through a binary tree such as the example shown in Fig. 1.1.
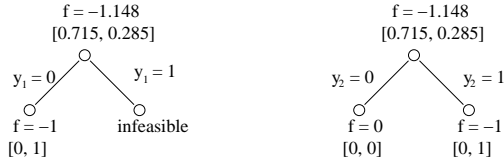

Figure 1.1: Binary solution tree of the MILP problem given in Eqs. (1.2-a) to (1.2-c). Left hand side: initial branching on y_1; right hand side: initial branching on y_2.

At each node of the tree the solution of the (continous) linear program is considered subject to integer constraints for the subset of the binary variables that are fixed in previous branches. The solution to this LP problem is a lower bound to the original MILP problem. If all binary values are either 0 or 1, the corresponding solution provides an upper bound to the MILP problem. If the actual node is infeasible or its LP solution is greater or equal to its best upper bound, the node is fathomed, i.e. it is not investigated any further. Otherwise, it is kept open for further examination by branching. Different branching strategies exist, leading to different intermediate results during the solution procedure. This is demonstrated in Fig. 1.1 where the binary tree on the left hand side corresponds to an initial branching on the first binary variable y_1 and the right hand side to an initial branching on y_2. However, if the MILP solution procedure is driven to completion, a global optimal solution is obtained for this class of problems. Concerning the computational burden, small problems (< 20 binary variables) are solved in seconds to minutes whereas large problems (> 100 binary variables) may require many hours to solve. The computation time depends on the problem structure and the availability of good starting points.

The most widely used MILP solver – and perhaps the most efficient one – is the commercial code CPLEX [16]. It is based on the simplex algorithm combined with sophisticated branch & bound and branch & cut methods. CPLEX is available as a callable library and has an interface to the modeling and optimization environment GAMS [9] which was used throughout this thesis for numerical studies (see below for a short description).

Nonlinear Programming (NLP) problems

The mathematical description of chemical engineering systems typically leads to nonlinear models, from bilinear component material balances to highly nonlinear phase equilibrium relations or reaction kinetics. The algorithms to solve these problems are completely different compared to those for linear problems discussed above. Presuming that only continuous variables are present, the general optimization problem reads

$$
\begin{aligned}
\min_{\mathbf{x}} \quad & f(\mathbf{x}) \\
\text{s.t.} \quad & \mathbf{g}(\mathbf{x}) = \mathbf{0} \\
& \mathbf{h}(\mathbf{x}) \leq \mathbf{0} \\
& \mathbf{x} \in I\!R^n
\end{aligned}
\tag{1.3}
$$

If no constraints are present, the necessary condition for an optimal point $\mathbf{x}^*$ is that f is stationary with respect to all variations in the independent variables $\mathbf{x}$,

$$
\nabla_{\mathbf{x}}^T f = \mathbf{0}^T \qquad \text{at} \quad \mathbf{x} = \mathbf{x}^*.
$$

The point $\mathbf{x}^*$ may, however, be a minimum, maximum or a saddle point. To assure a minimum point, a sufficient condition must be satisfied that the matrix of second derivatives $\nabla_{\mathbf{x}\mathbf{x}} f$ is positive definite at $\mathbf{x}^*$.

In order to solve constrained problems, Eqs. (1.3), the *Lagrangian function* is introduced

$$
L(\mathbf{x}, \boldsymbol{\lambda}, \boldsymbol{\mu}) = f(\mathbf{x}) + \boldsymbol{\lambda}^T \mathbf{g}(\mathbf{x}) + \boldsymbol{\mu}^T \mathbf{h}(\mathbf{x})
$$

where $\boldsymbol{\lambda}$ are termed the *Lagrange multipliers* and $\boldsymbol{\mu}$ the *Kuhn-Tucker multipliers*. The necessary conditions for optimality, the so-called (Karush-) Kuhn-Tucker conditions (KTC) can be derived for this equation.

In the following, two types of solution algorithms are presented in short, see [24] for more detailed informations.

Successive Quadratic Programming

Successive Quadratic Programming (SQP) methods solve a sequence of quadratic programming approximations to a nonlinear programming problem. Quadratic programs (QPs) have a quadratic objective function and linear constraints, and there exist efficient procedures for solving them. The linear constraints are linearizations of the actual constraints about the selected point. The objective is a quadratic approximation to the Lagrangian function, and the algorithm is simply Newton's method applied to the KTC of

the problem. Two characteristics of this class of algorithms shall be mentioned:

The linearization necessitates the evaluation of the Hessian matrix of the Lagrangian function, ∇_x^2, i.e. second derivatives of all problem functions are involved. As this Hessian is not guaranteed to be positive-definite, and further to avoid the computation of second derivatives, the Hessian is approximated by a positive-definite quasi-Newton approximation matrix B. The most common approximation is the BFGS (Broyden, Fletcher, Goldfarb and Shanno) update.

Besides the update strategy, the SQP line search is of crucial importance for the efficiency and robustness of this algorithm. The convergence properties of Newton and quasi-Newton methods strongly depend on the step size chosen per iteration. This step size is determined by line search criteria which usually consist of obtaining a sufficient decrease for some merit function that consists of the objective function and the violated constraints.

Software implementation of the SQP algorithm include NLPQL [56] or the routine E04UCF in the NAG library [46]. Both methods are implemented in the process simulation environment DIVA (see below).

Generalized Reduced Gradient

Gradient-projection and *reduced gradient methods* are based on extending methods for linear constraints to the nonlinear case. They are motivated by the same idea as active set methods for linear constraints – to stay "on" a subset of the nonlinear constraints while reducing the objective function. Achieving this objective requires the ability to adjust the variables so that the active constraints continue to be satisfied exactly at each trial point. In contrast to the case with linear constraints, some sort of iterative correction procedure is required to follow a nonlinear curving constraint boundary. An ideal version of a reduced gradient type method would have the property that all constraints active at the solution are satisfied exactly at every iteration. The differences among the algorithms arise from the variety of techniques used to achieve the aims of staying feasible and reducing the objective function.

One method of this type is the *generalized reduced gradient* (GRG) method. It was first developed in the late 1960s by Jean Abadie [1] and has since been refined by several other researchers. A widely used implementation of the GRG algorithm is CONOPT [21], designed to solve large, sparse problems. It is available as a stand-alone system, as a callable library, or as one of the optimizers callable by the GAMS system (see below).

Both approaches have their advantages and disadvantages. These are summarized in Table 1.2, taken from [24].

Algorithm	Relative advantages	Relative disadvantages
SQP	Usually requires the fewest function and gradient evaluations. Does not attempt to satisfy equalities at each iteration.	Will usually violate nonlinear constraints until convergence, often by large amounts.
GRG	Probably the most robust method. Versatile – especially good for unconstrained or linearly constrained problems but also works well for nonlinear constraints. Once it reaches a feasible solution it remains feasible and then can be stopped at any stage with an improved solution.	Needs to satisfy equalities at each step of the algorithm.

Table 1.2: Comparison of NLP solution algorithms.

Mixed-Integer Nonlinear Programming (MINLP) problems

Many problems, especially in process design or scheduling involve not only continuous variables but also integer values. If the continuous variables are coupled by nonlinear equations and inequalities, a *mixed-integer nonlinear programming problem* (MINLP) is obtained.

$$\min_{\mathbf{x},\mathbf{y}} \quad z = f(\mathbf{x}) + \mathbf{c}^T \mathbf{y}$$
$$\text{s.t.} \quad \mathbf{g}(\mathbf{x}) = \mathbf{0}$$
$$\mathbf{h}(\mathbf{x}) + \mathbf{M}\,\mathbf{y} \leq \mathbf{0} \quad\quad (1.4)$$
$$\mathbf{x} \in I\!R^n$$
$$\mathbf{y} \in \{0,1\}^m$$

Most solution methods require a problem formulation as shown above where the integer (or binary) variables $\mathbf{y}$ must satisfy linear relations. This is no restriction as all problems with binary decision variables can be brought to that form. The following example will demonstrate this special kind of problem formulation. Consider a distillation column with $N-2$ stages, a condenser (1) and a reboiler (N) as shown in Fig. 1.2.

Assume that a variable total feed flow F_{in} enters the column at a single tray. Its position may vary from the uppermost column tray (2) to the lowermost tray ($N-1$). The column trays and thus the potential feed tray positions are represented by binary variables y_j where $y_j = 1$ means that feed is introduced at tray j. As these variables are not allowed
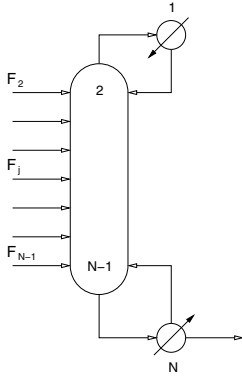
$$F_{in} - \sum_{j=2}^{N-1} F_j = 0 \tag{1.5-a}$$

$$F_j \leq F_{max} \, y_j \qquad j = 2(1)N - 1 \tag{1.5-b}$$

$$1 - \sum_{j=2}^{N-1} y_j = 0 \qquad \text{(single feed)} \tag{1.5-c}$$

$$F_{max} \geq F_{in} \tag{1.5-d}$$

Figure 1.2: MINLP example problem: distillation column feed tray location.

to appear in nonlinear relations with the continuous variables, an intuitive modeling of the individual flow rates

$$F_j = F_{in} \, y_j, \qquad j = 2(1)N - 1$$

is not possible. Instead, a constant F_{max} has to be introduced that replaces the variable F_{in} in Eqs. (1.5-b). These equations select the optimal feed tray, Eq. (1.5-a) assures that the whole amount of F_{in} enters the column, and Eq. (1.5-c) guarantees a single feed tray.

In principle, the class of MINLP problems can be solved with a branch and bound (BB) approach as explained in the previous section. In that case, the examination of each node would require the solution of a nonlinear program (NLP) rather than the solution of a LP. An important drawback of the BB method for MINLP is that the solution of the NLP subproblem is much more expensive, and they canot be updated readily as in the case of the MILP.

As a consequence, alternative solution methods were developed, and the most popular ones will be presented in the following: *Outer Approximation* (OA) [23] and *Generalized Benders Decomposition* (GBD) [28]. The basic idea in both methods is to solve an alternating sequence of NLP subproblems (with fixed binary variables y) and MILP master problems (linear approximations to predict new values for y). The alternation is continued to the point where the predicted lower bound of the MILP master is greater than or equal to the best upper bound obtained from the NLP subproblems. In comparing the two methods, the OA method requires the solution of fewer NLP subproblems and MILP master problems. On the other hand, the MILP master in the OA method is more expensive to

solve, so the GBD method may require less time if the NLP subproblems are inexpensive to solve.

The Outer Approximation algorithm is realized in the software DICOPT (DIscrete Continouous OPTimizer) which has an interface with GAMS. To solve the MILP master problem as well as the NLP subproblems efficient solvers are needed. GAMS provides interfaces to different solvers like the GRG code CONOPT for NLP problems or CPLEX for MILP problems.

Global Optimization

So far, nothing has been said about convergence properties or multiple local optimal solutions. In contrast to linear problems, in general nonlinear optimization problems have multiple solutions, i.e. multiple local minima. Consider for example the simple optimization problem

$$\min_{x} \quad f(x) = \cos(x)$$
$$x \in I\!R$$

(1.6)

This simple problem has infinitely many optimal solutions for

$$x^{*} = (2\,k - 1)\,\pi\,, \qquad k \in \mathbb{Z}$$

Any of the above mentioned NLP solvers will find that solution nearest to the starting point given to the algorithm. Thus they are only able to find local optimal solutions with no guarantee that the optimal point found corresponds to the global optimal solution. For convex optimization problems there is only one local solution which is also the global one, but these cases are rare in chemical engineering problems.

Global optimization algorithms have been developed during the last decades, reviewed by Floudas [26] recently. There are two main classes of algorithms:

- deterministic approaches like
  - Branch and Bound methods,
  - Cutting Plane methods,
  - Interval methods, and

- probabilistic approaches like

    - Simulated Annealing,
    - Evolutionary or Genetic algorithms,
    - random search methods.

To each method many examples are reported where it has been succesfully applied. However, most of these examples are fairly small concerning their numbers of variables and equations. For most of the approaches the computational burden increases with the problem size. This means that for problems like those faced in the remainder of this thesis, the computation times become prohibitively large. Furthermore, probabilistic or heuristic search methods often find the global optimal solutions but they are not guaranteed to do so. To sum up, global optimization approaches are very promising. But up to now, there exists no software implementation of such an algorithm that could be applied to the problems faced in the following chapters.

Software Tools

The development of solution algorithms and methods is out of the scope of this thesis. Thus, in order to solve the problems encountered, suitable model formulations have to be found that are solvable with state-of-the-art solvers described above. Most of the following problems were modelled and solved in the *General Algebraic Modeling System* GAMS [9]. Due to its powerful indexing concept, chemical engineering systems like distillation columns can be modelled in a very compact way. The disadvantage is that there is no possibility to distinguish between intermediate help variables and real state variables, leading to a large set of variables, equalities and inequality constraints. GAMS provides interfaces to LP, MILP, NLP and MINLP solvers.

Some examples were also investigated with the process modeling and simulation environment DIVA [39, 45, 42]. In DIVA only continuous variables are allowed, thus it is not possible to solve MILP or MINLP problems. On the other hand, due to the distinction of state variables and help variables, the size of the problem can be reduced. DIVA was originally developed to solve dynamic problems. Thus, with its interface to the SQP methods E04UCF and NLPQL mentioned above, it is able to solve NLP problems as well as optimal control or dynamic optimization problems.

Besides these complementary simulation and optimization tools, MATLAB [71] is used for the solution of smaller optimization problems and to visualize the results obtained from DIVA and GAMS.

Chapter 2

Physico-chemical fundamentals

Design and synthesis of reactive distillation processes are based on the knowledge of basic physico-chemical properties of the reaction system under consideration. This chapter provides the necessary information about attainable products depending on the interaction of separation and reaction. Probably the most important tool to check the feasibility of nonreactive as well as reactive processes are *residue curve maps*. Their use is directly related to the concept of *kinetic azeotropy*. As Chadda et al. [13] pointed out recently, these well established methods are only part of the truth for kinetically controlled reaction-separation systems. They propose the concept of *reactive flash cascades* to close the gap and to provide better estimates of attainable distillation top product regions. All of these concepts will be revisited briefly in this chapter. Detailed discussions on those topics are found in textbooks like those of Stichlmair and Fair [64], Doherty and Malone [20] or Sundmacher and Kienle [66]. As will be demonstrated later on, the physico-chemical basics are necessary informations for a proper process design. Without them, the optimization of mathematical process models is like looking for a needle in a haystack.

2.1 Nonreactive distillation

2.1.1 Residue curve maps

Consider the open evaporation process shown in Fig. 2.1. In a first step, a nonreactive system is considered. A liquid mixture of holdup n and composition $\mathbf{x}$ is heated in a still such that a vapor stream V with composition $\mathbf{y}$ emerges. Equilibrium is assumed between
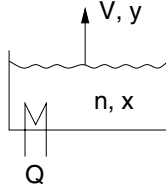
Figure 2.1: Open evaporation.

the liquid and the vapor leaving the still. The lighter boiling components of the mixture enrich in the vapor whereas the heavier boiling components remain in the liquid phase. Thus the last droplet in the still is the heaviest species which might be the heaviest pure component or an azeotrope. The resulting variation of the liquid holdup and composition with time is described by the component material balance

$$\frac{d(n\,x_i)}{dt} = -V\,y_i, \qquad i = 1(1)nc - 1 \tag{2.1}$$

and the total material balance

$$\frac{dn}{dt} = -V. \tag{2.2}$$

Here, x_i and y_i denote the liquid and vapor mole fractions, respectively. nc corresponds to the number of components. Combining Eqs. (2.1) and (2.2) leads to

$$\frac{dx_i}{dt} = \frac{V}{n}\,(x_i - y_i) \tag{2.3}$$

where V and n are time-dependent as dictated by an energy balance including the heating policy $Q(t)$. Introducing a new transformed time τ defined by

$$d\tau = \frac{V}{n}\,dt \tag{2.4}$$

and the vapor-liquid equilibrium relationship

$$y_i = f_i(\mathbf{x}) \tag{2.5}$$

leads to the final equations defining the residue curves for the open evaporation, also termed as *simple distillation*

$$\frac{dx_i}{d\tau} = x_i - f_i(\mathbf{x}), \qquad i = 1(1)nc - 1. \tag{2.6}$$

Fig. 2.2 shows the residue curve maps of two example systems. On the left hand side an ideal ternary mixture of substances A, B and C is considered, where A and C are

16

the lightest and the heaviest boiling components, respectively. All trajectories start at
the pure component A, reach a maximum of B and end at the pure component C. On
the right hand side the nonideal system isobutene/methanol/MTBE is considered. This
system exhibits two binary azeotropes. The first consists mainly of isobutene and a small
amount of methanol. This is an unstable node and therefore can be regarded as the lightest
pseudo-component of this system. The second azeotrope consist of methanol and MTBE.
It is a saddle and can be viewed as an intermediate boiling pseudo-component. These two
azeotropes divide the composition space into two distillation regions. All trajectories in
the upper region ① end up in pure methanol, whereas all trajectories in the lower region
② end up in pure MTBE. All trajectories start from the isobutene/methanol azeotrope as
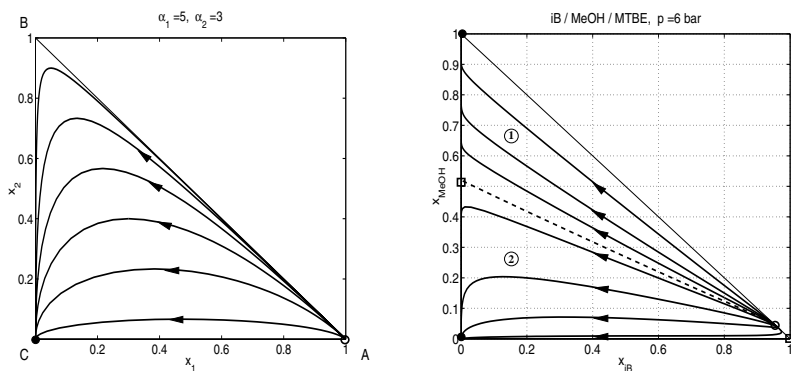the lightest pseudo-component.

Figure 2.2: Residue curve maps of nonreactive ternary systems. Ideal system (left) and
isobutene/methanol/MTBE (right).

2.1.2 Packed column profiles

So far, an open evaporation process has been investigated. To demonstrate the significance
of informations drawn from residue curve maps, consider a section of a packed distillation
column. The steady state equations for such a column section are derived from Eqs.
(A.12) to

$$\frac{\partial x_i}{\partial z^*} = j_{ai}^*(\mathbf{x}, \mathbf{y}), \qquad i = 1(1)nc - 1 \tag{2.7}$$

$$\frac{1}{A}\frac{\partial y_i}{\partial z^*} = j_{ai}^*(\mathbf{x}, \mathbf{y}), \qquad i = 1(1)nc - 1 \tag{2.8}$$

$$j_{ai}^*(\mathbf{x}, \mathbf{y}) = \frac{B_i(\mathbf{x}, \mathbf{y})}{A}\left(f_i(\mathbf{x}) - y_i\right) \tag{2.9}$$

where the star ($*$) denotes dimensionless variables. The basic assumptions and the full derivation is given in the appendix. Subtracting Eq. (2.8) from Eq. (2.7) and integrating from $\zeta = 0$ to $\zeta = z^*$ yields

$$0 = x_i(z^*) - x_{i0} - \frac{1}{A}\left(y_i(z^*) - y_{i0}\right).$$

Assuming total reflux means

$$A = 1 \quad \text{and} \quad x_{i0} = y_{i0}$$

leading to

$$y_i(z^*) = x_i(z^*). \tag{2.10}$$

Combining Eqs. (2.10), (2.9) and (2.7) leads to the final equation for packed column profiles at total reflux

$$\frac{dx_i}{dz^*} = B_i\left(f_i(\mathbf{x}) - x_i\right), \qquad i = 1(1)nc - 1. \tag{2.11}$$

This equation is identical to that of the nonreactive residue curves, Eq. (2.6), except for scaling and orientation. The same orientation would have been obtained if the packed column equation were derived for the stripping section instead of the rectifying section, depending on the orientation of the spatial coordinate. Thus the concentration profiles of a packed column at infinite reflux are identical to the residue curves. A real column will not be operated at total reflux of course, but possible product regions of a packed distillation column operated at finite reflux can be estimated from residue curves.

2.1.3 Staged column profiles

In the previous section the analogy between residue curves and composition profiles in a packed distillation column was shown. In this section, a staged column section is considered as shown in Fig. 2.3. Under the assumptions of constant molar flow rates and
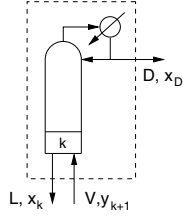
18
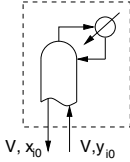
Figure 2.3: Rectifying section of a staged column.

holdups the following steady state model is derived for the rectifying section including the condenser.

Component material balances

$$0 = V\,\mathbf{y}_{k+1} - L\,\mathbf{x}_k - D\,\mathbf{x}_D \qquad (2.12)$$

Total material balance

$$0 = V - L - D \qquad (2.13)$$

Definition of reflux ratio

$$r = L/D \qquad (2.14)$$

Note that r can also be written as a function of the parameter A of the previous section:

$$r = \frac{L}{D} = \frac{L}{V-L} = \frac{A}{1-A}$$

Vapor-liquid equilibrium

$$\mathbf{y} = \mathbf{f}(\mathbf{x}) \qquad (2.15)$$

Combining Eqs. (2.15), (2.14), (2.13) and (2.12) leads to

$$\mathbf{f}(\mathbf{x}_{k+1}) = \left(\frac{r}{r+1}\right)\mathbf{x}_k + \left(\frac{1}{r+1}\right)\mathbf{x}_D \qquad (2.16)$$

or

$$\mathbf{f}(\mathbf{x}_{k+1}) = A\,\mathbf{x}_k + (1-A)\,\mathbf{x}_D. \qquad (2.17)$$

In the limit of total reflux ($r \to \infty$ or $A = 1$) this equation reduces to the *distillation lines* which are discussed in the following in more detail

$$f_i(\mathbf{x}_{k+1}) = x_{ik}, \qquad i = 1(1)nc - 1. \qquad (2.18)$$

19

2.1.4   Distillation lines

Under the assumption of total reflux and vapor-liquid equilibrium on each column tray, the concentration profiles of a staged distillation column are determined as follows. Starting from a liquid composition $\mathbf{x}_0$ its corresponding equilibrium vapor composition $\mathbf{y}_0^{eq}$ is calculated. If this vapor is completely condensed, a new liquid composition $\mathbf{x}_1$ is obtained.

$$\mathbf{x}_0 \rightarrow \mathbf{y}_0^{eq} = \mathbf{x}_1 \rightarrow \mathbf{y}_1^{eq} = \mathbf{x}_2 \rightarrow \mathbf{y}_2^{eq} \ldots \tag{2.19}$$

This procedure leads to concentration profiles indicated by circles in Fig. 2.4. For ideal
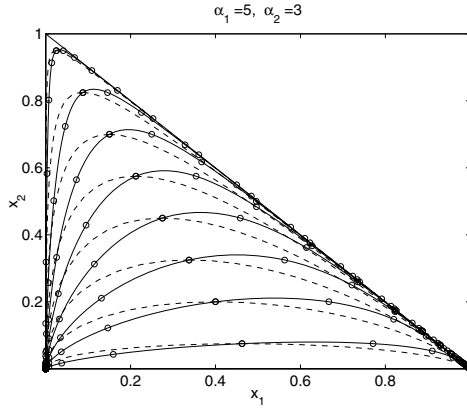

Figure 2.4: Comparison of residue curves (- - -) and distillation lines (—). Circles denote equilibrium stages of a column.

mixtures assuming constant relative volatilities, these liquid composition profiles can be calculated directly starting from $\mathbf{x}_0$ with the following equation (Stichlmair and Fair [64])

$$x_{i,n} = \frac{\alpha_i^n \, x_{i0}}{1 + \sum_{k=1}^{nc-1} (\alpha_k^n - 1) \, x_{k0}} \qquad i = 1(1)nc - 1. \tag{2.20}$$

Fig. 2.4 shows a comparison of residue curves (- - -) and distillation lines (—) for an ideal ternary system A, B, C with $\alpha_1 = 5$ and $\alpha_2 = 3$. The profiles differ quantitatively but their qualitative behavior is the same.

Distillation lines can be calculated for packed columns, too. But in that case, the equilibrium assumption no longer holds and a mass transfer model has to be used. Vogelpohl [78] compares residue curves with distillation lines and states that the latter are better suited to represent concentration profiles along the height of a column. This is especially true for nonideal systems where distillation boundaries are predicted more accurately. However, since the information about the qualitative behavior, especially singular points or fixed points of the system, is identical, residue curves are used in the remainder of this thesis. Distillation lines are not considered any further.

2.1.5 Design methods

Residue curve maps (RCM) are a valuable tool in the early process design stage as they indicate possible top and bottom product regions of a distillation column. As an example consider the isobutene/methanol/MTBE system. Its RCM is given on the right hand side of Fig. 2.2. In order to construct and visualize the regions of possible top and bottom products, one has to keep in mind that the component mass balances around the column have to be fulfilled. Thus, the top, feed and bottom concentrations must lie on a straight line in a two-dimensional diagram for a ternary system.
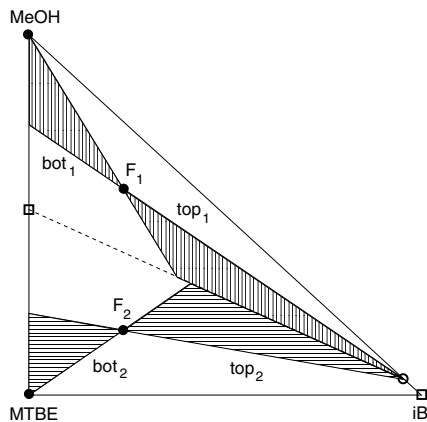

Figure 2.5: Simplified top and bottom product regions for the system isobutene/-methanol/MTBE.

This is illustrated in Fig. 2.5. Consider a feed F_1 with its composition in the distillation region 1. If the distillate consists of the lowest boiling pseudo-component, the binary azeotrope iB-MeOH, the corresponding bottom concentration lies on the straight line through this azeotrope and the feed point. On the other hand, if pure methanol shall be obtained in the bottom outlet, the corresponding distillate concentration lies on the straight line through methanol and F_1. These two lines together with the binary edge methanol-MTBE and the distillation boundary (dashed line) span two triangles: the region of possible distillate (top_1) and bottom (bot_1) compositions. For a feed point in the distillation region 2, F_2, analogous regions are obtained. These regions are shaded in Fig. 2.5. Note that these are simplified considerations, as the boundaries are curved for the real system due to the highly nonlinear vapor-liquid equilibria. This example shows that from the investigation of a RCM important informations are obtained without the necessity of solving a rigorous distillation column model.

2.2 Reactive distillation

So far, only nonreactive systems have been considered. If reaction occurs simultaneously in the liquid phase of the still or in a column, an additional term has to be included in the corresponding mathematical model. For equilibrium limited reactions, which are of major interest in reactive distillation, this term reads

$$r_j(\mathbf{x}) = k_{f,j} \left(\prod_{\substack{i=1 \\ \nu_{ij}<0}}^{nc} a_i^{(-\nu_{ij})} - \frac{1}{K_{eq,j}} \prod_{\substack{k=1 \\ \nu_{kj}>0}}^{nc} a_k^{\nu_{kj}} \right), \quad j = 1(1)nr \qquad (2.21)$$

where nr represents the number of reactions and the stoichiometric coefficients are given by

$$\nu_{ij} \begin{cases} < 0 & \text{for reactants} \\ > 0 & \text{for products} \\ = 0 & \text{for inerts} \end{cases}$$

In general, the reaction rate is formulated in liquid phase activities $a_i = \gamma_i x_i$. For ideal mixtures these are identical to the liquid phase mole fractions x_i as in that case the activity coefficients γ_i are equal to one. K_{eq} represents the chemical equilibrium constant which in general is a function of temperature. The forward reaction rate typically follows an Arrhenius temperature dependence of the form

$$k_f = k_{f0} \exp(-E/I\!RT) \qquad (2.22)$$

where the reaction rate constant k_{f0} and the activation energy E are usually obtained from experimental data regression.

2.2.1 Reactive residue curves

Assumed that a single chemical reaction occurs in the still shown in Fig. 2.1, the extended mathematical model reads

$$\frac{n}{V} \frac{dx_i}{dt} = (x_i - y_i) + \frac{n}{V} \left(\nu_i - \nu_T x_i \right) r(\mathbf{x}) \qquad (2.23)$$

with the total molar change of the reaction ν_T. To investigate the system, the definition of the transformed time τ of Eq. (2.4) and the *Damköhler number* are introduced

$$Da = \frac{t_{process}}{t_{reaction}} = \frac{n/V}{1/r_0}. \qquad (2.24)$$

The Damköhler number is defined as the ratio of a characteristic process time (liquid residence time) to a characteristic reaction time [17]. The choice of the reference reaction rate is arbitrary, but a common choice is the rate r_0 itself or the forward reaction rate constant k_{f0} at a standard temperature such as the lowest boiling point among the pure components and azeotropes. $Da = 0$ means no reaction, whereas $Da \to \infty$ represents the limit of chemical equilibrium. With these definitions and the vapor-liquid equilibrium relationship $y_i = f_i(\mathbf{x})$ the final equation describing the reactive residue curve is obtained

$$\frac{dx_i}{d\tau} = x_i - f_i(\mathbf{x}) + Da \, (\nu_i - \nu_T \, x_i) \, \frac{r(\mathbf{x})}{r_0}, \qquad i = 1(1)nc - 1. \qquad (2.25)$$

In contrast to the nonreactive case the time dependency of V and n relative to $r(\mathbf{x})$ is important. Depending on the heating policy, Da varies differently with time. A common assumption is that Da is constant over time. The corresponding heating policy reduces V according to the decrease of n over time. If Da is not constant, Eqs. (2.25) become nonautonomous and the system behavior is substantially different. (See [77] for a more profound discussion on that issue.)

2.2.2 Transformed coordinates

For the limiting case of chemical equilibrium ($Da \to \infty$) Ung and Doherty [74] propose transformed coordinates

$$X_i = \frac{x_i - \boldsymbol{\nu}_i^T \, \mathcal{V}^{-1} \, \mathbf{x}_{ref}}{1 - \boldsymbol{\nu}_T^T \, \mathcal{V}^{-1} \, \mathbf{x}_{ref}}, \qquad i = 1(1)nc - nr, \qquad (2.26)$$

where nc is the number of components and nr the number of independent chemical reactions. $\mathbf{x}_{ref}$ is the vector of nr reference components which are chosen in such a way that the matrix of stoichiometric coefficients for the reference components $\mathcal{V}$ is nonsingular. Without loss of generality the indices of the reference components are assumed to be $i = (nc - nr + 1)(1)nc$. $\boldsymbol{\nu}_i^T$ is the vector of stoichiometric coefficients of component i for all reactions and $\boldsymbol{\nu}_T^T$ represents the vector of the sum of stoichiometric coefficients per reaction. For inert components $\boldsymbol{\nu}_i^T = \mathbf{0}$ holds. Analogous to Eq. (2.26) transformed coordinates of the vapor phase are defined

$$Y_i = \frac{y_i - \boldsymbol{\nu}_i^T \, \mathcal{V}^{-1} \, \mathbf{y}_{ref}}{1 - \boldsymbol{\nu}_T^T \, \mathcal{V}^{-1} \, \mathbf{y}_{ref}}, \qquad i = 1(1)nc - nr. \qquad (2.27)$$

These transformed coordinates have some basic properties:

- They are reaction invariant, i.e. they do not depend on the extent of reaction ξ,

$$X_i(0) = X_i(\xi), \quad \forall \xi, \quad i = 1(1)nc - nr.$$

- They sum up to unity,

$$\sum_{i=1}^{nc-nr} X_i = 1.$$

- The necessary and sufficient condition for reactive azeotropy is

$$X_i = Y_i, \qquad i = 1(1)nc - nr. \tag{2.28}$$

(This issue will be discussed in a forthcoming section.)

In the case of a single equilibrium chemical reaction the transformations reduce to

$$X_i = \frac{x_i - \frac{\nu_i}{\nu_k} x_k}{1 - \frac{\nu_T}{\nu_k} x_k}, \qquad i = 1(1)nc,\ i \neq k \tag{2.29}$$

$$Y_i = \frac{y_i - \frac{\nu_i}{\nu_k} y_k}{1 - \frac{\nu_T}{\nu_k} y_k}, \qquad i = 1(1)nc,\ i \neq k \tag{2.30}$$

where k is the index of the reference component. If $\nu_T = 0$, any non-inert component can be chosen as the reference component, otherwise k has to be chosen in such a way that the denominator in the above equations is never zero. Therefore, a reactant should be chosen if $\nu_T > 0$, a product if $\nu_T < 0$.

For the example of an ideal ternary system $A + B \rightleftharpoons C$ the transformations are

$$X_1 = \frac{x_1 + x_3}{1 + x_3} \qquad \text{and} \qquad X_2 = \frac{x_2 + x_3}{1 + x_3} \tag{2.31}$$

where the indices 1 to 3 denote the components A to C, respectively. C is chosen as the reference component.

Residue curves in transformed coordinates

As Barbosa and Doherty [5] showed, the residue curve equation (2.25) can be transformed to

$$\frac{dX_i}{d\tau} = X_i - Y_i, \qquad i = 1(1)nc - 2 \tag{2.32}$$

using the transformations shown above, including a suitable time transformation. This equation exhibits exactly the same structure as that of the nonreactive residue curve,

Eq. (2.6). Thus the design methods developed for nonreactive distillation columns on the basis of residue curve maps can be applied to the reactive system as well. X_i and Y_i are related by the vapor-liquid equilibrium of their original components

$$\mathbf{Y} = \mathbf{Y}(\mathbf{y}), \qquad \mathbf{y} = \mathbf{y}(\mathbf{x}), \qquad \mathbf{x} = \mathbf{x}(\mathbf{X}).$$

For the example shown in Eq. (2.31) the transformed vapor phase composition reads

$$Y_1 = \frac{y_1(\mathbf{x}) + y_3(\mathbf{x})}{1 + y_3(\mathbf{x})} \qquad \text{and} \qquad Y_2 = \frac{y_2(\mathbf{x}) + y_3(\mathbf{x})}{1 + y_3(\mathbf{x})}$$

Thus, $\mathbf{Y}$ is only an implicit function of $\mathbf{X}$ according to Eq. (2.27)

$$Y_i = \frac{y_i(\mathbf{x}(\mathbf{X})) - \boldsymbol{\nu}_i^T \, \mathcal{V}^{-1} \, \mathbf{y}_{ref}(\mathbf{x}(\mathbf{X}))}{1 - \boldsymbol{\nu}_T^T \, \mathcal{V}^{-1} \, \mathbf{y}_{ref}(\mathbf{x}(\mathbf{X}))}, \qquad i = 1(1)nc - nr. \tag{2.33}$$

To evaluate this function, the backward transformation $\mathbf{x}(\mathbf{X})$ has to be determined. As will be shown in a forthcoming section, this is only possible for the chemical equilibrium case but not for the case of a kinetically controlled reaction, even though the transformations themselves can be applied.

2.2.3 Packed reactive column profiles

The relationship between residue curve maps and packed column profiles is illustrated for a single equimolar reaction. However, it should be noted that similar arguments apply for the nonequimolar multi-reaction system. If a single equimolar reaction takes place in the liquid phase of a packed column the equation for the liquid phase, Eq. (2.7), changes to

$$\frac{\partial x_i}{\partial z} = j_{ai}(\mathbf{x}, \mathbf{y}) + \nu_i \, r(\mathbf{x}), \qquad i = 1(1)nc - 1. \tag{2.34}$$

Writing this equation for two different components i and k and eliminating $r(\mathbf{x})$ yields

$$\frac{\partial}{\partial z} \left(\frac{x_i}{\nu_i} - \frac{x_k}{\nu_k} \right) = \frac{j_{ai}(\mathbf{x}, \mathbf{y})}{\nu_i} - \frac{j_{ak}(\mathbf{x}, \mathbf{y})}{\nu_k} \tag{2.35}$$

Substituting the intra-phase flow $j_{ai}(\mathbf{x}, \mathbf{y})$ by Eq. (2.9) gives

$$\frac{\partial}{\partial z} \left(\frac{x_i}{\nu_i} - \frac{x_k}{\nu_k} \right) = \frac{1}{A} \left(\left(\frac{B_i}{\nu_i} \, f_i(\mathbf{x}) - \frac{B_k}{\nu_k} \, f_k(\mathbf{x}) \right) - \left(\frac{B_i}{\nu_i} \, y_i - \frac{B_k}{\nu_k} \, y_k \right) \right) \tag{2.36}$$

Assuming that $B_i = B_k = B$ and introducing transformed coordinates of the following form (k is the reference coordinate)

$$
\begin{aligned}
X_i &= \frac{x_i}{\nu_i} - \frac{x_k}{\nu_k} \\
Y_i &= \frac{y_i}{\nu_i} - \frac{y_k}{\nu_k} \\
F_i(\mathbf{x}) &= \frac{f_i(\mathbf{x})}{\nu_i} - \frac{f_k(\mathbf{x})}{\nu_k}
\end{aligned}
\tag{2.37}
$$

leads to

$$
\frac{\partial X_i}{\partial z} = \frac{B}{A}\left(F_i(\mathbf{x}) - Y_i\right), \qquad i = 1(1)nc - 2
\tag{2.38}
$$

where the influence of the reaction has been eliminated by the transformation.

On the other hand, combining Eq. (2.35) with Eq. (2.8) gives

$$
\frac{\partial}{\partial z}\left(\frac{x_i}{\nu_i} - \frac{x_k}{\nu_k}\right) = \frac{1}{A}\frac{\partial}{\partial z}\left(\frac{y_i}{\nu_i} - \frac{y_k}{\nu_k}\right)
\tag{2.39}
$$

or

$$
\frac{\partial}{\partial z}\left(X_i - \frac{1}{A}Y_i\right) = 0.
\tag{2.40}
$$

This means that

$$
X_i(z) - \frac{1}{A}Y_i(z) = const.
\tag{2.41}
$$

For total reflux with

$$
A = 1 \quad \text{and} \quad X_{i0} = Y_{i0}
$$

the following equation holds

$$
Y_i(z) = X_i(z).
\tag{2.42}
$$

Combining Eqs. (2.42) and (2.38) leads to the final equation for packed reactive column profiles at total reflux

$$
\frac{dX_i}{dz} = B\left(F_i(\mathbf{x}) - X_i\right), \qquad i = 1(1)nc - 2.
\tag{2.43}
$$

This set of equations corresponds to that of the simple distillation residue curves for an equilibrium chemical reaction, Eq. (2.32). Hence, residue curves and the concentration profiles in a packed column at total reflux are identical in that case.

Backward transformation

As was shown previously, the calculation of the transformed vapor phase coordinates $\mathbf{Y}$ requires the existence of the backward transformation

$$x_i = x_i(\mathbf{X}).$$

In the case of a single chemical equilibrium reaction the corresponding equations read

$$X_i = \frac{x_i}{\nu_i} - \frac{x_k}{\nu_k}, \qquad i = 1(1)nc - 2 \tag{2.44-a}$$

$$K_{eq} = \prod_{i=1}^{nc} x_i^{\nu_i} \tag{2.44-b}$$

$$0 = 1 - \sum_{i=1}^{nc} x_i \tag{2.44-c}$$

If the reaction is kinetically controlled, Eq. (2.44-b) does not hold which means that one equation is missing and x_i can not be calculated from $\mathbf{X}$. Therefore, the transformation of a reactive distillation problem to a nonreactive one only makes sense for the limiting case of chemical equilibrium.

2.2.4 Staged reactive column profiles

Like in the case of packed reactive columns, a single equimolar reaction is considered as an example, but again the following argumenation is valid for the general case of multiple nonequimolar reactions. Assuming that a single equimolar reaction takes place on each tray of a staged column, Eq. (2.12) is extended to

$$0 = V\,\mathbf{y}_{k+1} - L\,\mathbf{x}_k - D\,\mathbf{x}_D + \boldsymbol{\nu}\sum_{m=1}^{k} n_m\,r_m(\mathbf{x}_m). \tag{2.45}$$

With $\nu_T = 0$ as assumed, the component material balances can be transformed to

$$\mathbf{f}(\mathbf{x}_{k+1}) = \left(\frac{r}{r+1}\right)\mathbf{x}_k + \left(\frac{1}{r+1}\right)\mathbf{x}_D + \frac{\boldsymbol{\nu}}{D}\sum_{m=1}^{k} n_m\,r_m(\mathbf{x}_m). \tag{2.46}$$

Writing this equation for component i and a reference component j and eliminating the sum of reaction terms leads to

$$\underbrace{\frac{f_{i,k+1}(\mathbf{x}_{k+1})}{\nu_i} - \frac{f_{j,k+1}(\mathbf{x}_{k+1})}{\nu_j}}_{F_{i,k+1}(\mathbf{x}_{k+1})} = \left(\frac{r}{r+1}\right)\underbrace{\left(\frac{x_{i,k}}{\nu_i} - \frac{x_{j,k}}{\nu_j}\right)}_{X_{i,k}} + \left(\frac{1}{r+1}\right)\underbrace{\left(\frac{x_{i,D}}{\nu_i} - \frac{x_{j,D}}{\nu_j}\right)}_{X_{i,D}}$$

$$\tag{2.47}$$

28

Introducing transformed variables as indicated above, for total reflux ($r \rightarrow \infty$) an equation is obtained that is equivalent to the distillation lines in the nonreactive case

$$F_{i,k+1}(\mathbf{x}_{k+1}) = X_{i,k}, \qquad i = 1(1)nc - 1, \quad i \neq j. \tag{2.48}$$

Like in the previous cases, the vapor phase composition is a function of the liquid phase composition in original coordinates. Thus, the backward transformation is only possible for the limiting case of chemical equilibrium.

2.2.5 Reactive azeotropy

The combination of reaction and separation in a single device like a simple distillation still or a distillation column may lead to completely new phenomena. Probably the most important among them are kinetic or reactive azeotropes. Rév [54] introduced the term *kinetic azeotropy* for reactions which are not near the chemical equilibrium in contrast to the term *reactive azeotropy* defined by Barbosa and Doherty [4, 5] related to chemical equilibrium reactions. The notation in this thesis will follow these terms with *kinetic reactive azeotropes* and *equilibrium reactive azeotropes*. Nonreactive kinetic azeotropes due to finite mass transfer kinetics are not taken into account here [57].

Before turning to azeotropes, *stoichiometric lines* have to be explained. Consider a chemical reaction starting with an initial molar amount n_0 and mole fractions x_{i0}. Due to the reaction these values change to n and x_i

$$\Delta n \;=\; n - n_0 = \nu_T\,\xi \tag{2.49}$$

$$\Delta n_i \;=\; x_i\,n - x_{i0}\,n_0 = \nu_i\,\xi \tag{2.50}$$

with

$$\xi = \frac{\Delta n_i}{\nu_i} = \frac{\Delta n_k}{\nu_k} = \frac{\Delta n}{\nu_T} \tag{2.51}$$

and

$$\nu_T = \sum_{k=1}^{nc} \nu_k. \tag{2.52}$$

Combining Eqs. (2.49) to (2.51) leads to

$$\frac{n_0}{\xi} = \frac{\nu_i - \nu_T\,x_i}{x_i - x_{i0}} = \frac{\nu_k - \nu_T\,x_k}{x_k - x_{k0}} \tag{2.53}$$

which can be solved for x_i to

$$x_i = \frac{x_{i0}(\nu_k - \nu_T\,x_k) + \nu_i(x_k - x_{k0})}{\nu_k - \nu_T\,x_{k0}} \tag{2.54}$$

This equation describes the stoichiometric lines and determines the mole fraction x_i depending on a reference component x_k for a given initial point $\mathbf{x}_0$. For nonequimolar reactions, thus $\nu_T \neq 0$, all these lines have a common pole

$$x_i^{pole} = \frac{\nu_i}{\nu_T}, \qquad i = 1(1)nc - 1. \tag{2.55}$$

For $\nu_T = 0$ Eq. (2.54) simplifies to

$$x_i = x_{i0} + \frac{\nu_i}{\nu_k}(x_k - x_{k0}). \tag{2.56}$$

In this case there exists no pole but all stoichiometric lines are parallel. Examples of both kinds will be shown in the sequel.

Like in the nonreactive case, azeotropy means that the composition of the mixture does not change any more with time (simple distillation) or space (along the column height). An intuitive graphical explanation is possible with the vector concept proposed by Hauan et al. [34]. Fig. 2.6 shows a residue curve (—) together with a stoichiometric line (- - -).
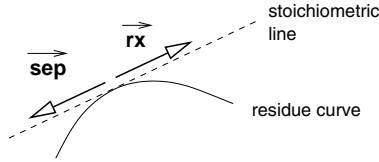
Figure 2.6: Visualization of kinetic azeotropy.

At a kinetic azeotrope both lines are tangent, the separation vector $\overrightarrow{sep}$ and the reaction vector $\overrightarrow{rx}$ having the same length but opposite direction. Thus the change in composition due to separation and to reaction cancel each other. Eq. (2.25) rewritten in vector form for all components exemplifies this concept

$$\underbrace{\frac{d\mathbf{x}}{d\tau}}_{=0} = \underbrace{\mathbf{x} - \mathbf{f}(\mathbf{x})}_{\overrightarrow{sep}} + \underbrace{Da\left(\boldsymbol{\nu} - \nu_T\,\mathbf{x}\right)\frac{r(\mathbf{x})}{r_0}}_{\overrightarrow{rx}}. \tag{2.57}$$

Following the notation of Rév [54], the loci of potential kinetic azeotropes can be derived by solving Eq. (2.25) for $Da \cdot r(\mathbf{x})/r_0$ and considering two components i and j

$$\frac{f_i(\mathbf{x}) - x_i}{\nu_i - \nu_T\,x_i} = \frac{f_j(\mathbf{x}) - x_j}{\nu_j - \nu_T\,x_j}, \qquad i, j = 1(1)nc. \tag{2.58}$$

For a ternary mixture this represents a line in the two-dimensional phase plane, the *extended line of kinetic azeotropy* (*elka*).

Fig. 2.7 presents the same ideal ternary system as in Fig. 2.2 (left) but with a simultaneous reaction

$$A + B \rightleftharpoons C$$

in the liquid phase. In addition to the residue curves of the nonreactive system, the chemical equilibrium line (-··-) and the stoichiometric lines (- - -) are plotted. In this case, they have a common pole $\mathbf{x}^{pole}$ where they all start. Connecting all points where the stoichiometric lines are tangent to the residue curves yields the extended line of kinetic azeotropy (-·--). The solution of Eq. (2.58) gives the same result and additionally a second branch outside the physically meaningful composition triangle (-··--).
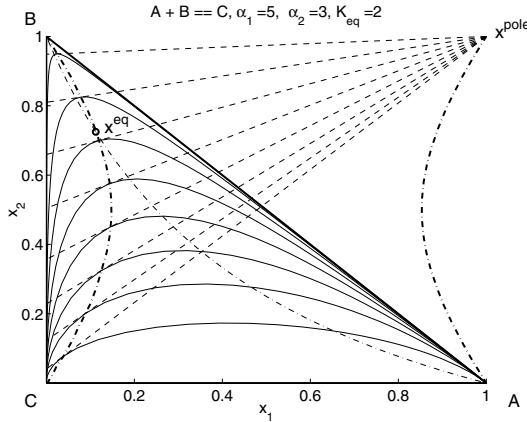
Figure 2.7: Simple distillation residue curves (—) and stoichiometric lines (- - -). Chemical equilibrium curve (-··-) and extended line of kinetic azeotropy (-·--).

At the intersection of the *elka* with the chemical equilibrium curve the *equilibrium reactive azeotrope* $\mathbf{x}^{eq}$ is obtained. As Rév pointed out, only a part of the *elka* provides real kinetic azeotropes. This becomes clear by considering the separation and reaction vectors along that line. The reaction vector always points towards the chemical equilibrium line. For $x_2 > x_2^{eq}$ both vectors point in the same direction and can not cancel each other. Thus in this example, kinetic azeotropes are only possible on that part of the *elka* starting

from pure component C for $Da = 0$ towards the reactive azeotrope for $Da \to \infty$. Fig. 2.8 shows component B of the kinetic azeotrope as a function of the scaled Damköhler number Da^* which is more convenient than Da

$$Da^* = \frac{Da}{1 + Da}, \qquad Da \in [0, +\infty), \qquad Da^* \in [0, 1).$$

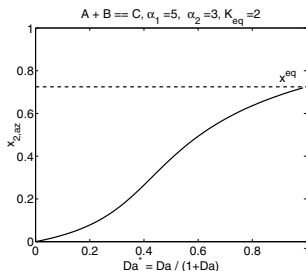According to Barbosa and Doherty [4] kinetic azeotropes are possible for ideal systems

Figure 2.8: Kinetic azeotrope $x_{2,az}$ as a function of the scaled Damköhler number Da^*.

only if all reactants are lighter boiling or heavier boiling than all products. Following this argumentation, the systems $A + B \rightleftharpoons C$ and $B + C \rightleftharpoons A$ exhibit kinetic azeotropes, but the system $A + C \rightleftharpoons B$ does not. As will be seen in chapter 3.2, the existence of kinetic reactive azeotropes has strong implications on attainable products and the column design.

Only a single reaction is taken into account in Eq. (2.25). However, for reaction systems with multiple reactions, the occurence of kinetic azeotropes is even more likely. In that case, the overall reaction vector, defined as the sum of single reaction vectors, must be colinear with the separation vector. Therefore, kinetic azeotropes may even occur in a system of two reactions where each of them on its own shows no kinetic azeotropes. As a first example consider an ideal ternary mixture with the reactions

$$2\,B \rightleftharpoons A + C \quad \text{combined with} \quad B \rightleftharpoons A + C.$$

This example is fictitious as the stoichiometry is not possible. But it is very instructive and can be visualized easily as it is an ideal ternary system. Fig. 2.9 shows the chemical equilibrium curves of the two reactions together with the resulting extended line of kinetic azeotropy. Even though these curves do not intersect, there exists a equilibrium reactive azeotrope for $Da \to \infty$.
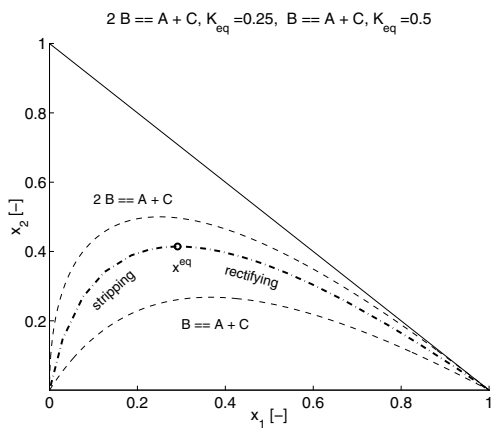
Figure 2.9: Chemical equilibrium curves (- - -) and fixed points of the rectifying and stripping cascade (-·-·-) for a combined reaction system.
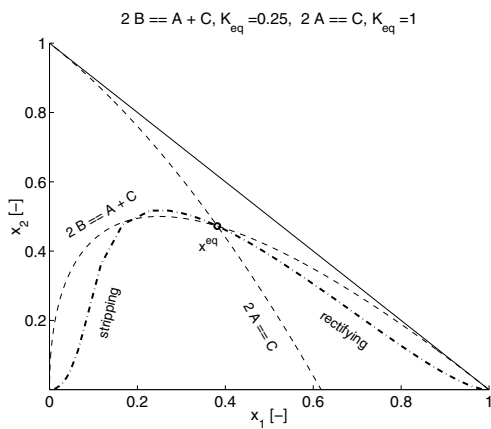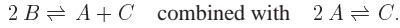

Figure 2.10: Chemical equilibrium curves (- - -) and fixed points of the rectifying and stripping cascade (-·-·-) for a combined reaction system.

Probably a more realistic example is provided by the reaction scheme

$$2\,B \rightleftharpoons A + C \quad \text{combined with} \quad 2\,A \rightleftharpoons C.$$

This could be a metathesis reaction followed by a dimerization reaction for instance. The resulting chemical equilibrium curves and the extended line of kinetic azeotropy are shown in Fig. 2.10. In this case, the point of intersection of the chemical equilibrium curves is identical to the reactive equilibrium azeotrope.

2.2.6 Flash cascades

In view of process synthesis it is important to know the possible products of nonreactive as well as reactive distillation columns. These informations are provided by residue curves or distillation lines for example. But as Chadda et al. [13] pointed out recently, these tools are only sufficient in the nonreactive case ($Da = 0$) and in the limiting case of chemical equilibrium ($Da \rightarrow \infty$). To determine the possible products for kinetically controlled reactions, they propose to calculate the fixed points of flash cascades as illustrated in Fig. 2.11.
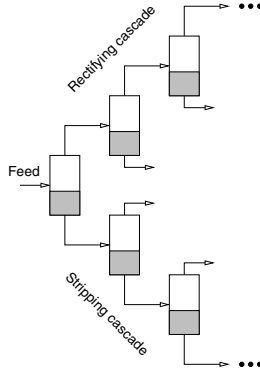
Figure 2.11: Flash cascades according to Chadda et al. [13].

Solutions to Eq. (2.59) are the fixed points of the stripping cascade and thus correspond to possible bottom products.

$$0 = x_i - y_i + \nu_i \frac{k_f}{k_{f,ref}} \frac{Da}{\phi} r^*(\mathbf{x}), \qquad i = 1(1)nc - 1, \qquad (2.59)$$

where $r^*(\mathbf{x}) = r(\mathbf{x})/k_f$. The fraction of feed vaporized in each flash unit is assumed to be constant for all units and is arbitrarily chosen to $\phi = 0.5$. Apart from scaling, this equation is identical to the fixed points of the reactive residue curves, Eq. (2.25) for equimolar reactions ($\nu_T = 0$).

The fixed points of the rectifying cascade are obtained as solutions to Eq. (2.60) and correspond to possible top products.

$$0 = x_i - y_i - \nu_i \frac{k_f}{k_{f,ref}} \frac{Da}{1 - \phi} r_0^*(\mathbf{x}), \qquad i = 1(1)nc - 1. \tag{2.60}$$

The only difference between the two fixed point equations above lies in the sign of the reaction term. But this small difference has an important impact on the possible products to be withdrawn at the top of a reactive distillation column, as will be shown in chapter 3.2.

The above equations are valid for equimolar reactions. For nonequimolar reactions,

$$\nu_T = \sum_{k=1}^{nc} \nu_k \neq 0,$$

the influence of molar masses has to be taken into account. In that case, the fixed point equation for the stripping section reads

$$0 = \frac{M(\mathbf{x})}{M(\mathbf{y})} (x_i - y_i) + (\nu_i - \nu_T x_i) \frac{k_f}{k_{f,ref}} \frac{Da}{\phi} r^*(\mathbf{x}), \qquad i = 1(1)nc - 1, \tag{2.61}$$

and the corresponding equation of the rectifying section

$$0 = \frac{M(\mathbf{x})}{M(\mathbf{y})} (x_i - y_i) - (\nu_i - \nu_T x_i) \frac{k_f}{k_{f,ref}} \frac{Da}{1 - \phi} r^*(\mathbf{x}), \qquad i = 1(1)nc - 1. \tag{2.62}$$

These equations were used to calculate the reactive kinetic azeotropes in the last two examples, Figs. 2.9 and 2.10. The different locations of the azeotropes in the rectifying and the stripping cascades are indicated.

2.2.7 Conclusions

Similar informations are obtained from residue curves, packed column profiles at total reflux as well as staged column profiles at total reflux (distillation lines). Among these informations the knowledge of singular points or fixed points are of special interest for

the column design, as they refer to possible top or bottom products of a (reactive) distillation column. As Doherty and Malone [20] pointed out, the fixed points and their stability are the same for all three models. This is true for nonreactive distillation and for reactive distillation in the limiting case of chemical equilibrium. For kinetically controlled reactions, only the possible bottom product is predicted correctly by these models. For a correct prediction of possible top products as well, the concept of reactive flash cascades has to be applied [13]. The knowledge of attainable products is indispensable for a proper process design. Hence, the concept of residue curve maps extended by flash cascade considerations is a valuable tool in the early design stage.

Chapter 3

Applications

In this chapter, optimal process configurations are developed for different reaction-separation systems. These optimal solutions are based on the fundamental concepts explained in detail in the previous chapter. The first example is an ideal binary system where an isomerization reaction transforms substance A to substance B and vice versa. Starting from the properties of this system like relative volatilities and reaction kinetics different processes are developed and compared. This example demonstrates the relevance of simple basic considerations for the actual process design.

In a second part ideal ternary systems are considered. The focus in this section is on the influence of physico-chemical properties of the system on the optimal process design. It will be shown why reactive distillation has a paramount effect on the profit for some systems and why it is not worth considering for others.

Finally, the separation of closely boiling components using a selective reaction is investigated. The first application of this type is an ideal quaternary system, an extension of the previous part. After that, two real physical systems are considered. The closely boiling isomers isobutene and 1-butene are to be separated. In one case methanol is used as the reaction partner leading to the well known system isobutene/methanol/MTBE. In the second case, isobutene reacts with water to *tert*-butyl alcohol (TBA) resulting in a system with an additional liquid phase. These examinations demonstrate that the application of mathematical optimization methods for the process design is limited due to the complexity and nonlinearity of the underlying systems. Therefore, this chapter ends with considerations on suitable model simplifications that might enable the profitable usage of mathematical optimization tools to solve real-world design problems.

3.1 Isomerization reaction

3.1.1 Fundamentals

According to Barbosa and Doherty [4], reactive azeotropes may occur for ideal constant volatility systems only if all products of a chemical reaction are either lighter or heavier than the reactants. In the binary system of an isomerization reaction this necessary condition is always fulfilled as it is for any binary reaction system, e.g. dimerization or trimerization reactions. This is easily verified by considering the condition of the extended line of kinetic azeotropy, Eq. (2.58), for the special case considered here

$$A \rightleftharpoons B, \qquad \nu_1 = -1, \; \nu_2 = 1, \; \nu_T = 0$$
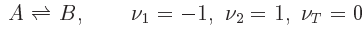
with

$$x_2 = 1 - x_1, \quad y_1 = f_1(x_1) \quad \text{and} \quad y_2 = 1 - y_1.$$

Singular points

In the previous chapter, the recent work of Chadda et al. [13] was cited, demonstrating that there exist different fixed points of this reactive system for the rectifying and the stripping section of a reactive distillation column. Those can be determined as the solution of the corresponding fixed point equations. Writing Eq. (2.59) for component A ($i = 1$, $\nu_1 = -1$) and chosing $k_f = k_{f,ref}$ results in

$$0 = x - y - \frac{Da}{\phi} \left(x - \frac{1-x}{K_{eq}} \right) \tag{3.1}$$

where the component index has been neglected. Da is the Damköhler number, introduced in section 2.2, and provides a measure for the extent of reaction. $Da = 0$ means no reaction whereas for $Da \to \infty$ the chemical equilibrium is reached. The vapor-to-feed fraction ϕ is a parameter in the range of $[0 \ldots 1]$ which only scales the Damköhler number and may be set to 0.5 without loss of generality. The vapor mole fraction y is a function of x. For the ideal binary mixture considered here, a constant relative volatility α is used to calculate the vapor-liquid equilibrium

$$y = \frac{\alpha \, x}{1 + (\alpha - 1) \, x}$$

The corresponding fixed point equation for the rectifying cascade reads

$$0 = x - y + \frac{Da}{1 - \phi} \left(x - \frac{1-x}{K_{eq}} \right). \tag{3.2}$$

Solving Eqs. (3.1) and (3.2) for x leads to quadratic equations. It can be shown that there exists a single kinetic azeotrope for every Damköhler number Da in each case which depends on α and K_{eq} only. Fig. 3.1 shows the fixed points for the rectifying (- - -) and the stripping (—) section. As can be seen, the second solution of the quadratic equation has no physical meaning. The fixed points for the limiting cases $Da = 0$ and $Da \to \infty$ are identical whereas those for finite Damköhler numbers differ significantly. The implication of these fixed points on the column design will be demonstrated in forthcoming sections.
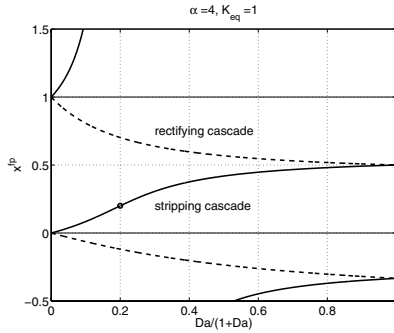
Figure 3.1: Fixed points for the rectifying (- - -) and the stripping (—) cascade for an ideal binary system with an isomerization reaction.

3.1.2 Homogeneously catalyzed reactive distillation

In the following, a homogeneously catalyzed reactive distillation column is considered as shown on the right hand side. Reaction is indicated by the shaded parts in the remainder. Hence, in Fig. 3.2 reaction is taking place in the total condenser (stage 1), along the whole column and in the partial reboiler (stage N). One single feed of pure component A is provided. A constant pressure and constant molar holdups on each stage are assumed. The column is operated at total reflux, thus the single product stream is withdrawn from the reboiler. The isomerization reaction $A \rightleftharpoons B$ takes place in the liquid phase with constant reaction parameters k_f and K_{eq} and the reaction rate

$$r_0 = k_f \left(x_1 - \frac{1 - x_1}{K_{eq}} \right).$$
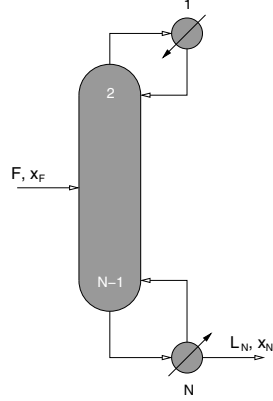
Figure 3.2: Homogeneously catalyzed reactive distillation column.

The overall molar amount is not changed by the reaction as $\nu_T = 0$. Thus, substituting the total material balances

$$0 = F_k + L_{k-1} - L_k + V_{k+1} - V_k, \qquad k = 2(1)N - 1$$

into the component material balances for the first component A (component index ignored, $\nu_1 = -1$)

$$0 = F_k \, x_{F,k} + L_{k-1} \, x_{k-1} - L_k \, x_k + V_{k+1} \, y_{k+1} - V_k \, y_k - m_k \, r_{0,k}, \qquad k = 2(1)N - 1,$$

the complete set of equations reads

$$
\begin{aligned}
0 &= V \left(y_2 - x_1 \right) - m_1 \, r_{0,1} & \text{(3.3-a)} \\
0 &= F_k \left(x_{F,k} - x_k \right) + L_{k-1} \left(x_{k-1} - x_k \right) + V \left(y_{k+1} - y_k \right) - m_k \, r_{0,k}, \\
& \quad k = 2(1)N - 1 & \text{(3.3-b)} \\
0 &= L_{N-1} \left(x_{N-1} - x_N \right) - V \left(y_N - x_N \right) - m_N \, r_{0,N} & \text{(3.3-c)}
\end{aligned}
$$

Furthermore, the overall component and total material balance have to be fulfilled

$$0 \;=\; \sum_{k=2}^{N-1} F_k\, x_{F,k} - L_N\, x_N + \underbrace{\nu_1}_{=-1} \sum_{k=1}^{N} m_k\, r_{0,k} \tag{3.4}$$

$$0 \;=\; \sum_{k=2}^{N-1} F_k - L_N + \underbrace{\nu_T}_{=0} \sum_{k=1}^{N} m_k\, r_{0,k} \tag{3.5}$$

Optimal feed stage location

Solving Eq. (3.3-b) for x_{k-1} and assuming that pure A is fed to the column ($x_{F,k} = 1$), it is obvious that x_{k-1} is larger if no feed is introduced to stage k than otherwise. Assuming further that B is produced on stage k, i.e. $x_{k-1} > x^{eq}$ it follows that $r_{0,k-1}$ is larger if k is not a feed stage. Taking Eq. (3.4) into account, it turns out that the uppermost tray ($k = 2$) is the best choice for a homogeneously catalyzed reaction with respect to a minimum number of stages for a fixed reboil ratio ($s = V/L_N$).

Critical Damköhler number

Kinetic azeotropy in the steady state case means that liquid compositions on subsequent stages of a reactive distillation column do not change any more. Considering the reboiler, Eq. (3.3-c), this is equivalent to

$$x_{N-1} = x_N$$

Defining the Damköhler number $Da_N = \frac{m_N/V}{1/k_f}$, the modified reaction rate $r_{0,N}^* = r_{0,N}/k_f$ and the reboil ratio $s = V/L_N$ the condition of kinetic azeotropy for the reboiler is given by

$$0 = x_N - y_N - Da_N\, r_{0,N}^*$$

which is exactly the same equation as the condition of kinetic azeotropy for the stripping section, Eq. (3.1), except for the scaling by ϕ. For a fixed value of x_N, corresponding to a certain product specification for B, a *critical Damköhler number*

$$(Da_N)_{crit} = \frac{x_N - y_N}{r_{0,N}^*}$$

is obtained as an upper bound for the actual Damköhler number of the reboiler. Note that $r_{0,N}^* < 0$ as $x_N < x^{eq}$. From this critical value either a maximum amount of catalyst in

the reboiler

$$m_N < \frac{s\,L_N}{k_f}\,(Da_N)_{crit} \quad = m_{N,max}$$

or a minimum reboil ratio

$$s > \frac{m_N\,k_f}{L_N}\,\frac{1}{(Da_N)_{crit}} \quad = s_{min}$$

is determined.

Following the same argumentation as above for the lowermost column stage ($k = N - 1$) and assuming a constant amount of catalyst for every stage, a different critical Damköhler number is obtained from Eq. (3.3-b)

$$(Da_k)_{crit} = \frac{y_N - y_{N-1}}{r^*_{0,N-1}}.$$

Note that the feed is assumed to be introduced at the top of the column. As the reboil ratio s is already fixed, the maximal value of the amount of catalyst per stage results to

$$m_{k,max} = \frac{s\,L_N}{k_f}\,(Da_k)_{crit}.$$

But this is only a necessary condition. For large values near $m_{k,max}$ the composition profile is concave, i.e. the influence of the reaction is stronger than that of the separation. Therefore a further condition must hold taking into account the shape of the composition profile for the first two stages counting from the bottom

$$(x_{N-2} - x_{N-1}) \geq (x_{N-1} - x_N).$$

This results in a tighter limit for the maximal amount of catalyst per stage

$$m_{k,max} = \frac{s\,L_N}{k_f\,r^*_{0,N-1}}\,\left((y_N - y_{N-1}) + (y_N - x_N) + Da_N\,r^*_{0,N}\right).$$

Hence, the critical Damköhler number of the stripping cascade (scaled by ϕ) is a lower bound for that of the reactive distillation column with a single bottom product!

Column design

Having chosen an appropriate reboil ratio s, amount of catalyst of the reboiler m_N and of the column trays m_k, the number of stages for a homogeneously catalyzed reactive

distillation column can be determined. The fact that the feed should be introduced to the top stage (cf. above section) and the information about the total extent of reaction needed, Eq. (3.4), is included in the design procedure. The amount of catalyst in the condenser is assumed to be less or equal to that of the column stages. Fig. 3.3 shows the dependence of the number of column stages on the amount of catalyst per stage for the following data.

physical properties				stream data				design parameters			
k_f	=	1.0	[mol/(kg s)]	F	=	1.0	[mol/s]	s	=	50.0	[–]
K_{eq}	=	1.0	[–]	x_F	=	1.0	[–]	m_N	=	0.1	[kg]
α	=	4.0	[–]	L_N	=	1.0	[mol/s]				
				x_N	=	0.001	[–]				
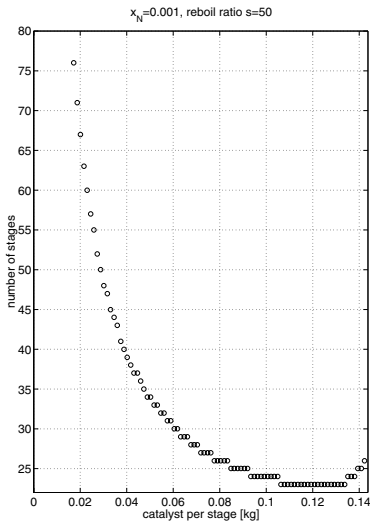
Figure 3.3: Number of stages as a function of the amount of catalyst per column tray m_k.
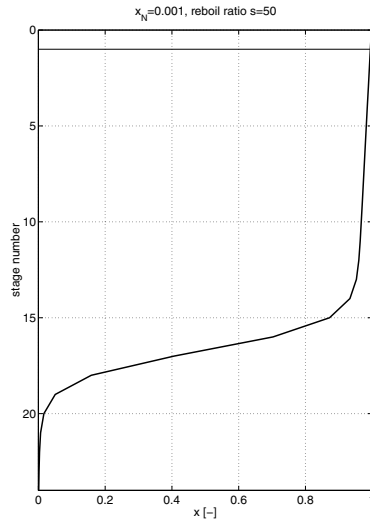
Figure 3.4: Concentration profile of component A over the height of the column.

As can be seen, there exists a certain region of the amount of catalyst per tray resulting in the minimum number of stages. Fig. 3.4 shows the liquid mole fraction of component A over the height of the column for a design with the minimum number of stages. The

amount of catalyst of each tray is chosen to $m_k = 0.12$ [kg], resulting in 23 inner column stages or 25 stages including the condenser and the reboiler. As expected, for lower values of the reboil ratio s the number of stages increases and the minimum number of stages is obtained in a smaller region, e.g. $m_k \in [0.048, 0.055]$ for $s = 40.0$.

3.1.3 Comparison of process configurations

During the development of a reactive distillation process the question has to be answered if the RDC process is advantageous compared to other reaction/separation schemes. In the following, four different processes are investigated for the isomerization reaction $A \rightleftharpoons B$ with A the more volative component.

1. Homogeneously catalyzed reactive distillation column (rdc_hom)
2. Heterogeneously catalyzed reactive distillation column (rdc_het)
3. Nonreactive distillation column with a reactor at the top (rplusc)
4. Reactor coupled with a nonreactive distillation column (rplusrecy)

As the desired product is the heavy component, the RDC processes are both operated at total reflux. To enable a fair comparison, all processes are optimized with the optimization tool GAMS [9]. Process 3 is formulated as a Nonlinear Programming (NLP) problem wheras the remaining processes 1, 2 and 4 are formulated as Mixed-Integer Nonlinear Programming (MINLP) problems. The discrete variable in the latter models is the feed position for the fresh feed or the feed from the reactor, respectively. The reaction zone of the heterogeneously catalyzed column is not formulated by binary variables but in a continuous way $m_k < m_{max}$, reducing the number of binary variables of this MINLP problem. The data used for the optimization studies are given below.

physical properties			stream data			design parameters		
k_f	= 1.0	[mol/(kg s)]	F	= 1.0	[mol/s]	N	= 29	[–]
K_{eq}	= 1.0	[–]	x_F	= 1.0	[–]	L_{max}	= 10^5	[mol/s]
α	= 4.0	[–]	$x_{N,max}$	= 0.001	[–]	m_{max}	= 5.0	[kg]

The concentrations x_F and $x_{N,max}$ refer to the mole fraction of component A in the feed and in the bottom product stream, respectively. N denotes the fixed number of column

stages where the condenser is stage 1 and the reboiler is stage N. One exception is the process configuration 3 where stage 1 corresponds to the uppermost column tray. In this configuration, the reactor serves as the condenser, see Fig. 3.5. m_{max} denotes the maximum allowed amount of catalyst on each column tray. The objective function to be minimized is the vapor stream V leaving the reboiler in every case, thus the energy demand is to be minimized.
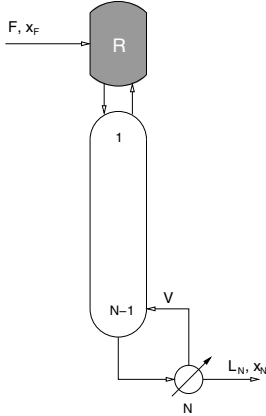

Figure 3.5: Reactor on top of a nonreactive distillation column (rplusc).
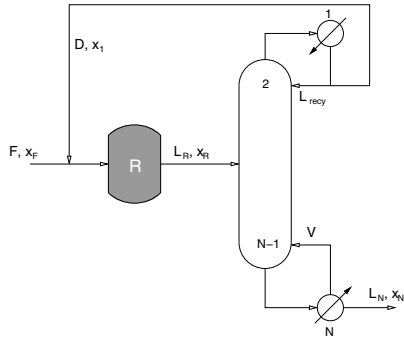
Figure 3.6: Conventional reactor/separator scheme with recycle of the reactant (rplusrecy).

Results

1. *Homogeneously catalyzed reactive distillation column*

   As expected from the considerations in the previous section, the uppermost column tray turns out to be the optimal feed position. Depending on the model assumptions wrto. where the reaction takes place, the following cases are considered:

   (a) The amount of catalyst in the condenser ($m_1 \leq 1.0$) is independent on that of each tray (m_k), the reboiler is nonreactive ($m_N = 0$).

   (b) Condenser and reboiler are both nonreactive ($m_1 = m_N = 0$).

(c) The amount of catalyst in the condenser ($m_1 \leq 1.0$) is independent on that of each tray (m_k), the reboiler is reactive ($m_N = m_k$).

(d) The condenser is nonreactive ($m_1 = 0$), the reboiler is reactive ($m_N = m_k$).

The following table summarizes the results for the different assumptions.

	1a	1b	1c	1d
m_1 [kg]	1.0	0.0	1.0	infeas.
m_k [kg]	0.0389	0.0897	0.0210	infeas.
m_N [kg]	0.0	0.0	0.0210	infeas.
V [mol/s]	6.682	13.147	11.282	infeas.

The last case (1d) is infeasible as the required bottom specification $x_N \leq 0.001$ can not be reached for this combination. As discussed in the previous section, the Damköhler number must be very small for a reactive reboiler. A similar result is obtained from case (1c) where $m_k = m_N$ is small. The main conversion from A to B takes place in the reactive condenser in that case. This is not possible in case (1d), thus there is not enough catalyst in the column to reach the desired conversion and the required product purity simultaneously.

2. *Heterogeneously catalyzed reactive distillation column*

The main difference between homogeneously and heterogeneously catalyzed RDC processes is that in the latter case the reaction zone can be specified, e.g. by providing a catalytic packing in the column. From a practical point of view it is difficult to realize a reactive condenser. Thus the condenser is assumed to be nonreactive ($m_1 = 0$) in the present process configuration. The optimal configuration for this case is shown below.

$$V = 1.663$$
$$m_k = \begin{cases} 5.0 & \text{[kg]} \quad \text{for} \quad k = 2(1)9 \\ 0.0 & \text{[kg]} \quad \text{for} \quad k = 10(1)29 \end{cases}$$

In a second scenario, the total amount of catalyst in the column is limited to the total amount of the homogeneously catalyzed case (1b), $m_{tot} = 2.42$. The optimal solution for this scenario provides 17 reactive stages, as can be seen from Fig. 3.7. The value of the objective function is
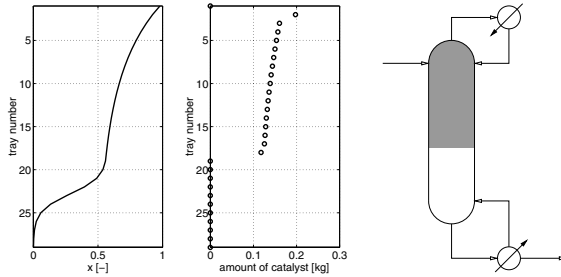
$$V = 2.101$$

Figure 3.7: Heterogeneously catalyzed RDC with limited total amount of catalyst $m_{tot} = 2.42$. Concentration profile – catalyst profile – column configuration.

The amount of catalyst continuously decreases from stage 2 to stage 18, as does the mole fraction of reactant A. This means that the optimizer provides the largest amount of catalyst at the uppermost tray of the column where x and the reaction rate

$$r_0 = k_f \left(x \left(1 + \frac{1}{K_{eq}} \right) - \frac{1}{K_{eq}} \right)$$

have their largest values. The condenser is defined to be nonreactive.

3. *Reactor at the top of a nonreactive distillation column*

   The feed is introduced into the reactor which also serves as the total condenser of the column. As the structure is fixed for this process, no binary variables are needed, resulting in a NLP formulation. The main degree of freedom for the design of this process is the amount of catalyst in the reactor m_R. For different upper bounds on this variable $m_{R,max}$, the following results are obtained.

$m_{R,max}$ [kg]	2.42	10.0	40.0	100.0
m_R [kg]	2.42	10.0	40.0	100.0
V [mol/s]	3.536	1.959	1.732	1.690

4. *Reactor coupled with a nonreactive distillation column*

   This process configuration is again modelled as a MINLP problem as the position of the feed tray shall be determined by the optimization. Further design variables are the amount of catalyst in the reactor, the recycle rate and the vapor flow rate. The table below summarizes the results for different upper bounds on the catalyst in the reactor. N_F denotes the feed tray location.

$m_{R,max}$ [kg]	2.42	10.0	40.0	100.0
m_R [kg]	2.42	10.0	40.0	100.0
N_F [–]	16	16	16	16
V [mol/s]	3.537	1.961	1.733	1.692

It should be noted that all optimal solutions obtained are local optimal solution as for nonlinear optimization problems (NLP or MINLP) the global optimal solution can not be guaranteed. But at least for the homogeneously catalyzed RDC it can be shown with the considerations of the previous section that the optimization in GAMS gives the global optimal solution in this case.

Table 3.1 summarizes the optimal process configurations for different total amounts of catalyst. As can be seen, the heterogeneously catalyzed RDC is the best process configuration wrto. energy consumption. For the homogeneously catalyzed RDC, the optimal

$m_{R,max}$	2.42	10.0	40.0	100.0
V(rdc_hom)	13.147	13.147	13.147	13.147
V(rdc_het)	2.101	1.666	1.663	1.663
V(rplusc)	3.536	1.959	1.732	1.690
V(rplusrecy)	3.537	1.961	1.733	1.692

Table 3.1: Optimal process configurations.

solution is found for $m_{tot} = 2.42$ in all cases. All other processes make use of the maximal allowed amount of catalyst $m_{R,max}$ in every case. The optimal process configurations rplusc and rplusrecy are nearly identical. This is due to the similarity in the general process configuration. Comparing Figs. 3.5 and 3.6 the only differences are the feed position of the reactor outlet and the liquid or vapor recycle to the reactor.

Sundmacher and Qi [67] recently published similar results for the "inverse problem": A light product is produced from a heavy reactant, the distillation columns are operated with a total reboiler and the product is withdrawn as the column distillate stream.

Dynamic behavior

So far, the investigations and optimizations have been related to the steady state case. But for process operation the time-dependent dynamic behavior of the systems is crucial. To enable dynamic simulation studies, Eqs. (3.3-a) to (3.3-c) are rewritten in the following form

$$n_1 \frac{dx_1}{dt} = V(y_2 - x_1) - m_1 r_{0,1} \tag{3.6-a}$$

$$n_k \frac{dx_k}{dt} = F_k(x_{F,k} - x_k) + L_{k-1}(x_{k-1} - x_k) + V(y_{k+1} - y_k) - m_k r_{0,k},$$
$$k = 2(1)N - 1 \tag{3.6-b}$$

$$n_N \frac{dx_N}{dt} = L_{N-1}(x_{N-1} - x_N) - V(y_N - x_N) - m_N r_{0,N} \tag{3.6-c}$$

where the molar holdups n_k are assumed to be time-independent.

As a first example, the optimal configurations for $m_{R,max} = 2.42$ are compared. A feed flow rate disturbance from $F = 1.0$ to $F = 0.5$ [mol/s] at time $t = 1$ [s] is considered while reflux and reboil ratios are kept constant. Fig. 3.8 shows the profiles of the concentration of A in the bottom product for the different processes. All profiles start at the
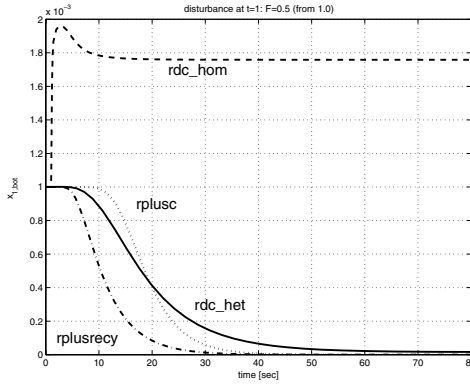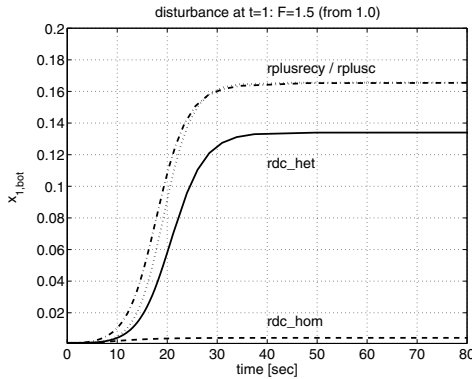

Figure 3.8: Step responses of the four different systems to a disturbance in the feed flow rate at $t = 1$ [s] from 1.0 to 0.5 [mol/s]. Process designs for $m_{R,max} = 2.42$ [kg].

nominal steady state, $x_{1,bot} = 0.001$. Immediately after the disturbance, the concentration x_1 increases to a value of 0.0018 for the homogeneously catalyzed RDC. All other processes are characterized by a slower response to that disturbance and a decrease in $x_{1,bot}$

49

towards zero. The reason for the fast dynamic response of rdc_hom is the high internal flow rate of V or L_k, respectively. The molar holdups n_k are identical for all processes, but the essential time constant "holdup / flow rate" is much smaller for the homogeneous RDC process than for the other three processes. Accordingly, the heterogeneously catalyzed column with its lowest internal flow rate among all processes exhibits the slowest dynamic response. Interestingly, the dynamic behavior of the two reactor-column processes is different even though their steady state design is nearly identical. In that case, the difference is contributed to the fact that the feed for rplusc enters the column at the top whereas the feed stage for rplusrecy is stage 16, which is closer to the bottom. Thus a disturbance in the feed flow rate influences the bottom product of rplusrecy faster than that of rplusc. The increase in the bottom product concentration $x_{1,bot}$ for the homogeneously catalyzed RDC can be explained by the increase in the Damköhler number due to the decrease of the internal flow rate. The bottom concentration cannot be lower than the fixed point of the stripping section and the latter depends on the Damköhler number according to Fig. 3.1.

If the feed flow rate is increased at $t = 1$ [s] from $F = 1.0$ to $F = 1.5$ [mol/s] completely different results are obtained as shown in Fig. 3.9. Again, the initial bottom concentration

Figure 3.9: Step responses of the four different systems to a disturbance in the feed flow rate at $t = 1$ [s] from 1.0 to 1.5 [mol/s]. Process designs for $m_{R,max} = 2.42$ [kg].

of A is $x_{1,bot} = 0.001$ for all processes. In the case of the homogeneously catalyzed RDC, $x_{1,bot}$ increases to 0.004, more than double the amount of the previous example. Following the argumentation of the first example, a decrease of $x_{1,bot}$ is expected for

rdc_hom because of the reduced Damköhler number. But the fixed point is only a lower bound. In the actual case, a different effect is more important.
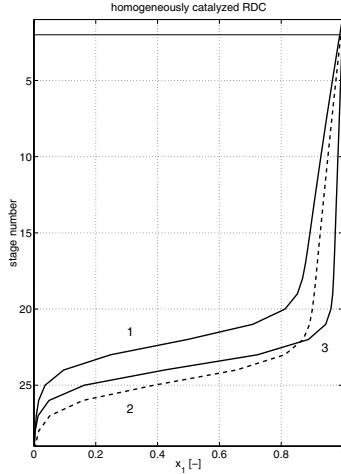

Figure 3.10: Concentration profile of component A in the homogeneously catalyzed RDC. 1 ... initial profile, 2 ... after the disturbance, 3 ... reboil ratio increased.

The higher flow rate after the disturbance drives the concentration profile towards the bottom of the column as illustrated in Fig. 3.10 ($1 \rightarrow 2$). Hence, more A leaves the column in the bottom product. Increasing the reboil ratio and thus the vapor flow rate pushes the concentration profile back towards the top of the column ($2 \rightarrow 3$). But to achieve the original specification of $x_{1,bot} = 0.001$, the amount of vapor and along with that the energy consumption rise considerably from initial values of the reboil ratio $s_1 = 13.2$ and the vapor flow rate $V_1 = 13.2$ to the final values $s_3 = 43.0$ and $V_3 = 64.5$.

In case of the heterogeneously catalyzed RDC the new steady state concentration of A after the disturbance is $x_{1,bot} = 0.134$, roughly 30 times the value of the homogeneously catalyzed RDC! The deviation for the processes with reactor and nonreactive column is even larger, $x_{1,bot} = 0.165$. The reason for this dramatic increase is the same as for the homogeneously catalyzed RDC, a shift of the concentration profile towards the bottom of the column. But in contrast to that process, the energetic effort needed to achieve the initial specification for $x_{1,bot}$ is much smaller. Table 3.2 summarizes the results.

	V_1	V_2	$(x_{1,bot})_2$	V_3
$V(\text{rdc\_hom})$	13.15	19.72	0.004	65.00
$V(\text{rdc\_het})$	2.10	3.15	0.134	4.94
$V(\text{rplusc})$	3.54	5.30	0.166	8.99
$V(\text{rplusrecy})$	3.54	5.31	0.166	9.00

Table 3.2: Comparison of different processes after a feed flow rate disturbance. Indices: 1 ... initial value, 2 ... after the disturbance, 3 ... reboil ratio increased.

Comparing the vapor flow rates of rdc_het with rdc_hom and rplusc shows that the savings by using a heterogeneously catalyzed RDC increase from initially 84% and 41% to final values of 92% and 45%, respectively.

Finally, the influence of the amount of catalyst is investigated. In Fig. 3.11, the same feed disturbance as above is considered for the process configurations with $m_{R,max} = 10.0$. The deviations from the nominal steady state are drastically reduced. The new steady state for the heterogeneous RDC is nearly identical to that of the homogeneous RDC. To obtain the original value for $x_{1,bot} = 0.001$ only a slight enlargement of the reboil ratio from $s_2 = 1.666$ ($V_2 = 2.50$) to $s_3 = 1.678$ ($V_3 = 2.52$) is necessary. It should be noted that the process design for rdc_hom in this case is the same as in the previous case as this is the optimal design for any $m_{R,max} \geq 2.42$.
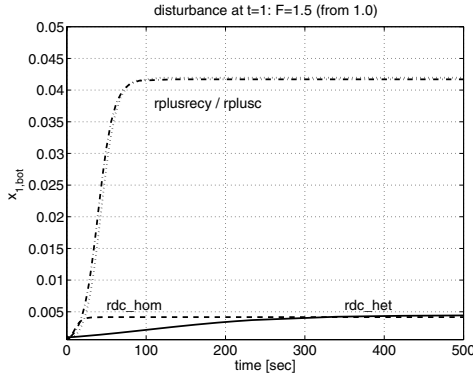
Figure 3.11: Step responses of the four different systems to a disturbance in the feed flow rate at $t = 1$ [s] from 1.0 to 1.5 [mol/s]. Process designs for $m_{R,max} = 10.0$ [kg].

52

The dynamic behavior for the optimal processes with the total amount of catalyst increased to $m_{R,max} = 40.0$ is shown in Fig. 3.12. In this case, the bottom concentration of rdc_het merely changes at all. The deviations for the reactor/column configurations are further reduced.
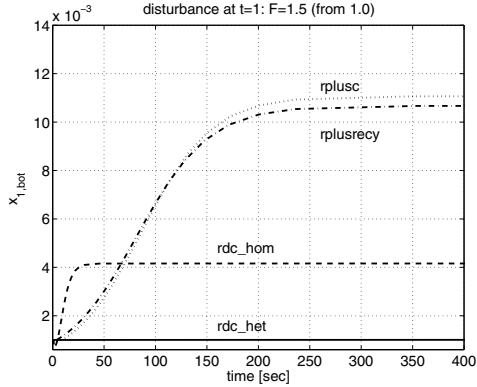
Figure 3.12: Step responses of the four different systems to a disturbance in the feed flow rate at $t = 1$ [s] from 1.0 to 1.5 [mol/s]. Process designs for $m_{R,max} = 40.0$ [kg].

Increasing the amount of catalyst means that the reactor outlet concentration or the composition of the liquid phase leaving the lowermost reactive stage in a RDC approaches the chemical equilibrium composition. In the limiting case of an infinitely large reactor (rplusc and rplusrecy), $x_{1,bot}$ would not change for any finite augmentation of the flow rate.

In summary, these studies demonstrate the necessity for investigations of the dynamic behavior of the different systems in the early process design stage. One possibility to optimize the structure of the process and its dynamic behavior simultaneously is the formulation of general mixed-integer dynamic optimization (MIDO) problems. But up to now, the solution of those problems is a rather challenging task. Alternatively, the consideration of different typical szenarios like disturbances or product changeover policies could be incorporated in the process design step.

3.2 Ideal ternary systems

With the experience of process design for binary systems, documented in section 3.1, ideal ternary systems are considered in detail in the following. Constant relative volatilities α_i are assumed to represent the ideal vapor-liquid equilibrium

$$y_i = \frac{\alpha_i \, x_i}{1 + \sum\limits_{k=1}^{nc-1} (\alpha_k - 1) \, x_k} \qquad\qquad i = 1(1)nc - 1, \qquad\qquad (3.7)$$

where $nc = 3$ is the number of components. In the remainder, A describes the lightest, B the intermediate and C the heaviest boiling component. Their mole fractions are denoted by x_1, x_2 and x_3, respectively. The reaction rate depends on the reaction scheme according to Eq. (2.21). For the ideal mixtures considered in the following, K_{eq} and k_f are assumed to be constant. With the knowledge of fixed points from flash cascade calculations basic process configurations can be derived. To design the processes and to compare them, different mathematical models are used. Details are provided in Appendix B. All variables and equations are given in dimensionless forms throughout this section.

- For all design studies, feed specifications are given and certain product purities are required in the form $x_{i,P} \geq x_{i,P,min}$.

- Nonreactive distillation columns are designed on the basis of the Fenske and Underwood equations to estimate their minimum number of stages and the minimum reflux. The nonreactive separation tasks involved are fairly easy such that the influence of the concrete design of these columns is small in comparative studies.

- In some cases, flash cascade calculations according to Chadda et al. [13] are used to estimate the number of stages for a reactive distillation column. Component and total material balances, vapor-liquid equilibrium relations, and an expression for the reaction rate are needed for these calculations.

- For a fixed number of stages simulation and optimization studies are performed with equilibrium stage column models, again on the basis of material balances, as well as expressions for the VLE and the chemical reaction. The optimization tool GAMS [9] is used for the design of feasible process configuration, especially if binary decision variables are involved. Examples for such mixed-integer problems are positions of feed or side withdrawls. The basic design configurations are further examined in simulation studies in the process simulation tool DIVA [39, 45, 42].

3.2.1 Ideal ternary system $2\,B \iff A + C$

Fundamentals

Following the argumentation of Barbosa and Doherty [4], kinetic azeotropes are not possible for this reaction system. Fig. 3.13 shows the phase portrait of this system with the chemical equilibrium curve (-·-·-), stoichiometric lines (- - -) and nonreactive residue curves (—). As can be seen, there are no tangent points of the stoichiometric lines to the residue curves, indicating that no kinetic azeotropes are possible.
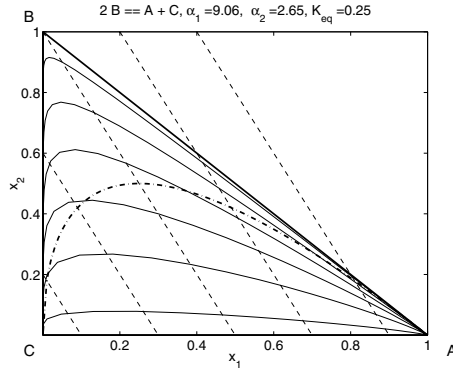

Figure 3.13: Phase portrait for the reactive system $2\,B \iff A + C$ with stoichiometric lines (- - -), nonreactive residue curves (—) and the reaction equilibrium line (-·-·-).

In the following, the metathesis of 2-pentene is considered as an example with data taken from Chen et al. [14].

$$
\begin{array}{llll}
A & C_4H_8 & \text{2-butene} & \rightsquigarrow x_1 \\
B & C_5H_{10} & \text{2-pentene} & \rightsquigarrow x_2 \\
C & C_6H_{12} & \text{3-hexene} & \rightsquigarrow x_3
\end{array}
$$

Chen et al. used a model with temperature dependent nonlinear relations for the forward reaction rate $r_0(\mathbf{x}, T)$ and the VLE calculation. However, as this reaction system is nearly ideal, the temperature effect can be neglected for a given constant pressure. Eqs. (3.7) and (2.21) are used in the following with parameters fitted to the reference model

$$
\boldsymbol{\alpha} = [9.06,\ 2.65,\ 1.0] \quad \text{and} \quad k_f = 2.9.
$$

55

$K_{eq} = 0.25$ is taken from the literature reference. The reaction rate for this system reads

$$r_0(\mathbf{x}) = k_f \left(x_2^2 - \frac{x_1 \, x_3}{K_{eq}} \right). \qquad (3.8)$$

Solving Eqs. (2.59) and (2.60) for this system leads to pure component A ($x_1 = 1$) and pure component C ($x_3 = 1$) as the only fixed points of the rectifying and stripping flash cascade. Their stability behavior is indicated in Table 3.3. Thus, pure A can be obtained

	rectifying cascade	stripping cascade
A	unstable node	unstable node for $0 \leq Da^* \leq 0.273$, saddle otherwise
B	no fixed point	no fixed point
C	stable node for $0 \leq Da^* \leq 0.6$, saddle otherwise	stable node

Table 3.3: Fixed points for the reaction system $2\,B \Longleftrightarrow A + C$ depending on the scaled Damköhler number $Da^* = Da/(1 + Da)$.

as the column's top product for any D (unstable node of the rectifying cascade) and pure C as the bottom product (stable node of the stripping cascade), provided that there is enough catalyst in the column or that the reaction is fast enough to reach full conversion of B.

Conventional process for the decomposition of B

The conventional process consists of a single phase CSTR followed by two nonreactive distillation columns. The whole system is fed by a pure stream of component B at a dimensionless flow rate of $F = 100$. Two variants are considered, the direct split and the indirect split case. Figs. 3.14 and 3.15 show the corresponding flowsheets. The design of these two processes is based on material balances together with the Fenske equation for the minimum number of stages and the Underwood equation for minimum reflux for the two columns (see appendix B.1). This design model is solved with the optimization tool GAMS. With an upper bound on the number of stages of $N_{max} = 50$ and on the amount of catalyst in the reactor of $n_{R,max} = 200$ optimal values for the design parameters are obtained. These are the actual amount of catalyst in the reactor n_R, the total numbers of stages N_k, feed stage locations $N_{F,k}$, reflux ratios r_k and reboil

ratios s_k. The index $k \in \{1, 2\}$ represents the column number. On the basis of these design parameters, the conventional process is simulated and optimized in DIVA. As DIVA is only capable of solving continuous optimization problems, the discrete decision variables ($N_{F,k}$) are fixed, and the reflux and reboil ratios remain as degrees of freedom. As objective function to be minimized the sum of internal vapor flow rates V_k is used, corresponding to a minimization of the energy consumption of the overall process. Table 3.4 summarizes the optimal configuration for the direct split conventional process.
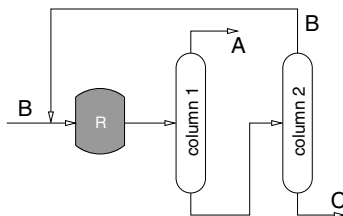
Figure 3.14: Conventional process flowsheet – direct split.

	n_R	N	N_F	r	s	V
column 1		25	15	1.91	0.60	145.66
column 2		10	5	0.91	7.31	365.49
reactor	200.0					

Table 3.4: Design parameters for the direct split conventional process.

Table 3.5 shows the corresponding values for the optimal configuration of the indirect split conventional process. As can be seen, the overall energy consumption of the two processes are comparable with a slightly lower value for the direct split configuration. This is mainly due to the large relative volatility of component A.
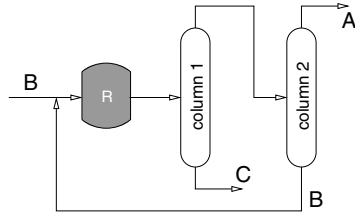
Figure 3.15: Conventional process flowsheet – indirect split.

	n_R	N	N_F	r	s	V
column 1		10	5	0.67	8.13	406.27
column 2		25	15	1.82	0.73	141.06
reactor	200.0					

Table 3.5: Design parameters for indirect split conventional process.

Design of RD processes for the decomposition of B

In the sequel, four different reactive distillation processes are proposed. The basis for all investigations is a column with 25 stages and a total amount of catalyst of $n_{tot} = 200$ to be comparable to the conventional processes. Accordingly, pure B is fed at $F = 100$ and the required product purities are $x_{1,1} = x_{3,25} = 0.99$. The processes differ in the catalyst distribution along the height of the column, the feed position and the operating conditions (reflux and reboil ratio). The optimal solutions are obtained from optimizations with GAMS where the vapor flow rate in the column is minimized. For all configurations the total condenser and the partial reboiler are assumed to be nonreactive. Furthermore, only one single feed of pure component B is allowed.

Fig. 3.16 shows the optimal design of an homogeneously catalyzed RDC. The optimal feed stage turns out to be stage 11, thus the middle of the column. The amount of catalyst on each of the 23 reactive stages is 8.7 resulting in a total amount of catalyst of the maximal allowed value. With this configuration, a vapor flow rate of $V = 118.2$ is obtained.

For the heterogeneously catalyzed RDC it is assumed that the same amount of catalyst is provided at all reactive stages. The decision whether a column stage is reactive or not is
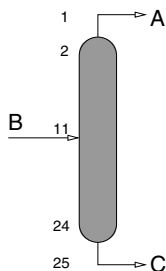
Figure 3.16: Homogeneously catalyzed reactive distillation column.
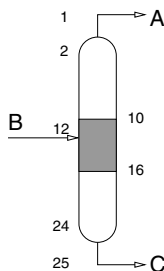
Figure 3.17: Heterogeneously catalyzed reactive distillation column.

made by binary variables in the MINLP model. Fig. 3.17 shows the optimal solution with 7 reactive stages with an amount of catalyst of 28.57 each, summing up to the maximum of 200. The vapor flow rate is $V = 113.3$ in this case.

The vapor flow rate can be further decreased if the amount of catalyst is allowed to vary from stage to stage. The optimal configuration is shown in Fig. 3.18 along with the catalyst distribution along the column. This catalyst profile corresponds to the concentration profile of component B inside the column. The stage with the highest concentration of B and thus with the highest reaction rate according to Eq. (3.8) is provided with the largest amount of catalyst. Again, the total amount sums up to 200. The value of the vapor flow rate is $V = 107.6$.
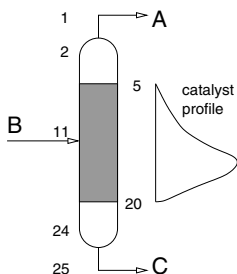
Figure 3.18: Heterogeneously catalyzed reactive distillation column with individual amounts of catalyst per reactive stage.
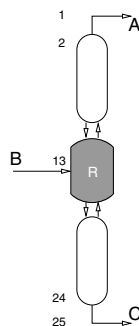
Figure 3.19: Nonreactive distillation column with a middle vessel.

The last concept investigated consists of two nonreactive distillation columns with a reactor in between, the so called *middle vessel distillation*. In this configuration, the feed is defined to be introduced to the reactor. The position of the middle vessel is determined by the optimization algorithm. This configuration is a special case of the heterogeneously catalyzed RDC with only one reactive stage. The optimal values found are 200 for the amount of catalyst in the reactor and $V = 166.3$ for the vapor flow rate.

Comparison

One criterion to compare the different reactive distillation processes is the energy consumption in the optimum steady state. As can be seen from Table 3.6 the homogeneously, the heterogeneously and the individually catalyzed columns are characterized by the lowest energy consumption, roughly 20% of the best conventional process.

	conv1	conv2	hom	het	indiv	mv
V	512.2	548.3	118.2	113.3	107.6	166.3
dyn. behav.	1	1	3	4	2	5

Table 3.6: Comparison of different processes.

But steady state considerations are not sufficient to compare design alternatives thouroughly. Therefore, the dynamic behavior of the processes is also compared. Fig. 3.20 shows the time transients of the product purities after a step disturbance in the feed flow rate of $\pm$ 50%. It is obvious that the conventional processes are the most robust processes wrto. this kind of disturbances. The middle vessel column performes worst. Among the different types of reactive distillation columns the individually catalyzed column shows the best performance. A further interesting criterion for the comparison and evaluation of the different processes is controllability. But this investigation is beyond the scope of this thesis.
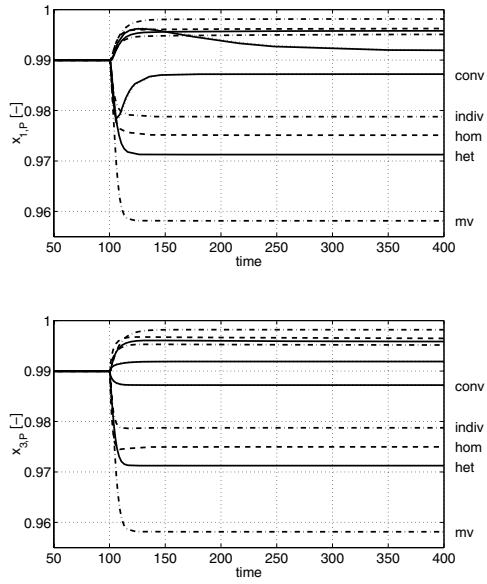
Figure 3.20: Time transients of product purities after a step disturbance in the feed flow rate of $\pm$ 50%. Upper figure: component A, lower figure: component C in the corresponding product streams.

Conventional process for the synthesis of B

In the following, the synthesis of B from A and C is considered. Like in the decomposition problem, a direct split as well as an indirect split process is possible. Again, the direct split process is favorable with respect to the overall energy consumption. The resulting flowsheet is shown in Fig. 3.21.
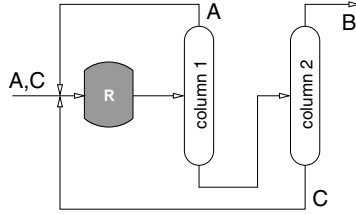
Figure 3.21: Conventional process flowsheet for the production of B.

Following the same procedure as for the decomposition of B, optimization of the FUGK model in GAMS and optimization of the resulting rigorous model in DIVA, optimal design parameters are obtained as shown in Table 3.7. A stoichiometric mixture of A and C ($x_{F,1} = x_{F,3} = 0.5$) with a total flow rate of $F = 100$ is fed to the system. The upper bound for the amount of catalyst in the reactor is $n_{R,max} = 500.0$ in this case. A product purity of $x_{2,P} \geq 0.99$ is required. The total energy consumption is measured by the sum of the vapor flow rates, $V = V_1 + V_2 = 336.7$.

	n_R	N	N_F	r	s	V
column 1		20	8	1.38	0.66	117.5
column 2		20	14	1.19	2.82	219.2
reactor	500.0					

Table 3.7: Design parameters for the conventional process for the production of B.

Design of RD processes for the synthesis of B

To understand the main difference between the design of a RD process for the synthesis and the decomposition of B, consider the phase portrait of this reaction system, Fig. 3.13, and the fixed points in Table 3.3. The pure component B can not be obtained as a top or bottom product of a distillation column as long as a ternary mixture is present in the column. In column 2 of the conventional process, Fig. 3.21, it is possible to obtain pure B at the top because there is no component A present in that column.

One possible process implementing the RD technology is shown in Fig. 3.22. It results from combining the reactor and the first nonreactive column from the conventional scheme in one RDC. The nonreactive column separating B and C is essentially the same as in the conventional process. This configuration is not considered any further.
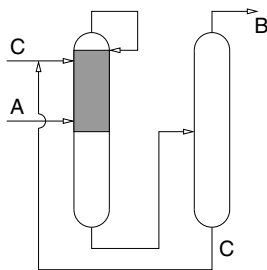
Figure 3.22: RDC with nonreactive column for the production of B.

An RD process like in the B decomposition case is not possible for the reasons given above. Nonetheless, there exist some reactive distillation configurations where pure B is obtained as a product. One configuration is shown in Fig. 3.23 which may be interpreted as a combination of the two columns in Fig. 3.22. Components A and C are converted to B in the reactive rectifying section. The product B is obtained in a side stream below the reactive zone with a purity of $x_{2,sd} = 0.99$. Even though the production of B from A and C is feasible in a single RDC, with an internal vapor flow rate of $V = 5000$ the energy consumption is prohibitively large compared to that of the conventional process.

An alternative process scheme is shown in Fig. 3.24, a RDC with dividing wall. This RDC consists of a total condenser, a common rectifying section, two middle sections divided by a vertical wall, a common stripping section and a partial reboiler.
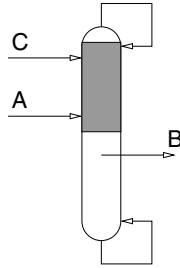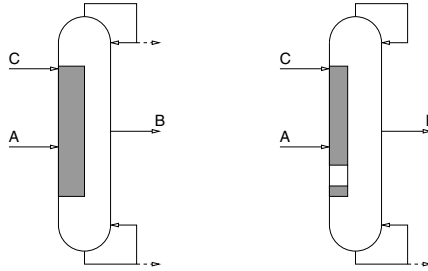
Figure 3.23: RDC with side draw for the production of B.

Figure 3.24: RDC with dividing wall for the production of B. Two different process configurations.

For the simulation and optimization studies, 10 theoretical trays in the nonreactive rectifying and stripping sections each are used, whereas the inner column sections have 40 trays each. For the design of the left column, the inner sections are assumed to be of the same size. Thus, the ratio of liquid flowing into the left inner section from the rectifying section is $L_{il}/L_{re} = 0.5$, as is the ratio of vapor entering the left inner section from the stripping section $V_{il}/V_{st} = 0.5$. The subscripts denote the inner left (il), rectifying (re) and stripping (st) section, respectively. In the optimal solution, pure component C is fed to the uppermost tray of the left inner section at a flow rate of $F_C = 50$ and pure C to tray 25 of the left inner section at $F_A = 50$. The left inner section is fully reactive with an amount of catalyst per stage of $n_k = 21.25$, summing up to a total amount of 850. The product B is withdrawn from stage 20 of the right inner section as a side draw at a flow rate of $L_{sd} = 99.3$ with a purity of $x_{2,sd} = 0.993$. The remaining outlet streams are withdrawn at the top and the bottom at a flow rate of $Dist = Bot = 0.35$ each consisting

of pure A and C, respectively. The flow rate of the vapor produced by the reboiler is $V_{st} = 3500$ in this case.

A different design is shown on the right hand side of Fig. 3.24. The optimization algorithm found the best solution wrto. vapor flow rate minimization if the inner sections are of different size: $L_{il}/L_{re} = 0.337$, $V_{il}/V_{st} = 0.334$. Some lower stages in the left inner section are nonreactive and the amount of catalyst per stage is $n_k = 20$. The feed and side draw positions are identical to the previous case, only the product purity decreases slightly: $L_{sd} = 99.3$, $x_{2,sd} = 0.986$. There is no top product, $Dist = 0$, the bottom product consists of pure C with a flow rate of $Bot = 0.7$. The vapor flow rate is considerably reduced to $V_{st} = 1813$. Compared to the single RDC process in Fig. 3.23 this is a considerable improvement, but compared to the conventional process, the arguments in favor of a RDC realization are rather weak.

But coming back to the principles of the dividing wall column, these processes can be regarded as two separate columns with direct liquid and vapor coupling, equivalent to the Petlyuk column [49]. If one allows the optimization algorithm to vary the position of these liquid and vapor connections, a very interesting process configuration is found, shown in Fig. 3.25.
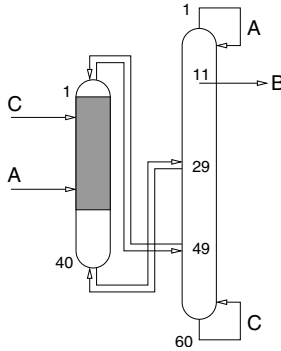
Figure 3.25: Nonreactive column with reactive prefractionator for the production of B – column configuration.

A nonreactive column is coupled to a reactive prefractionator, but compared to the classical prefractionator scheme, the coupling is "inversed". Looking at the main column,

liquid is withdrawn from tray 49 and is fed to the top of the prefractionator. The vapor leaving the latter is fed to the main column on stage 49, too. The liquid leaving the prefractionator is fed to the main column on stage 29, i.e. at a position above the liquid withdrawal. Accordingly, a vapor stream is withdrawn from the main column on stage 29 and fed to the bottom of the prefractionator. The overall feed of pure A and C respectively is introduced to the reactive section of the prefractionator in a countercurrent manner like in the previous processes. The inverse coupling leads to an inverse column profile in the prefractionator as can be seen on the left hand side of Fig. 3.26. The heavy component C is enriched at the top, B and C leave the bottom and A is nearly completely consumed by the reaction. The most astonishing feature of this process is its energy consumption, measured by the vapor flow rate leaving the reboiler. With $V = 217.13$ it is even considerably lower than that of the conventional process ($V_1 + V_2 = 336.7$)!
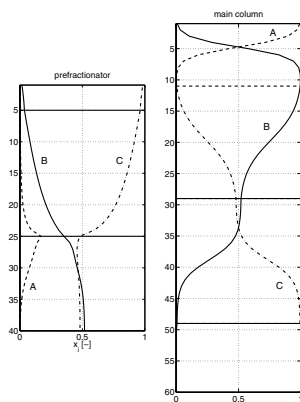
Figure 3.26: Nonreactive column with reactive prefractionator for the production of B – liquid mole fraction profiles.

The investigation of this first ideal ternary system demonstrates that the knowledge of principal properties like reactive azeotropes and attainable product regions is necessary but not sufficient for a proper process design. The usage of mathematical programming techniques leads to non-intuitive process variants with large performance improvements.

3.2.2 Ideal ternary system $2\,A \Longleftrightarrow B + C$

Fundamentals

The only difference between the reaction system considered in this section and that of the previous section is the order of relative volatilities. Here, the lightest boiling component A is decomposed to (or produced from) the intermediate and the heavy boiling species B and C. As pointed out by Barbosa and Doherty [4] and by Rév [54], kinetic azeotropes may occur for ideal systems if all reactants are either lighter or heavier than all products. This condition is fulfilled for this system. Fig. 3.27 shows the phase portrait with the chemical equilibrium line (**- - -**), nonreactive residue curves (—) and stoichiometric lines (- - -). Connecting the points where the latter two are tangent leads to the extended line of kinetic azeotropy (**-·--·-**) (*elka*).
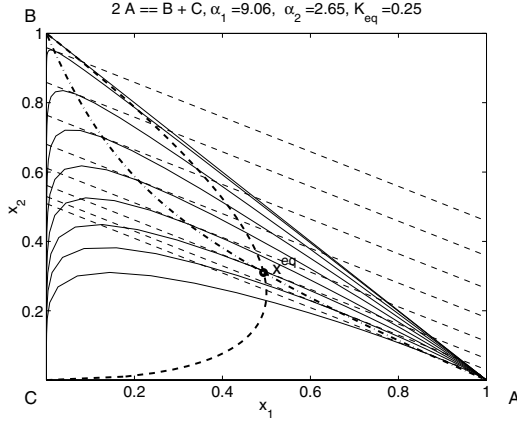
Figure 3.27: Phase portrait for the reactive system $2\,A \Longleftrightarrow B + C$ with stoichiometric lines (- - -), nonreactive residue curves (—), reaction equilibrium line (**- - -**) and the extended line of kinetic azeotropy (**-·--·-**).

The extended line of kinetic azeotropy can also be determined analytically. Writing Eq. (2.58) with $y_i = f_i(\mathbf{x})$ for $\boldsymbol{\nu} = [-2, 1, 1]$, $\nu_T = 0$, $i = 1$ and $j = 2$ results in

$$\frac{y_1 - x_1}{-2} = \frac{y_2 - x_2}{1} \tag{3.9}$$

Substituting $y_i = \alpha_i \, x_i / (1 + \sum_{k=1}^{nc-1} (\alpha_k - 1) \, x_k)$ leads to a quadratic equation for $x_2(x_1)$. The intersection of the extended line of kinetic azeotropy with the chemical equilibrium curve gives the chemical equilibrium reactive azeotrope $\mathbf{x}^{eq}$.

For subsequent studies the same data as in the previous example are used

$$\boldsymbol{\alpha} = [9.06, \ 2.65, \ 1.0], \quad k_f = 2.9 \quad \text{and} \quad K_{eq} = 0.25.$$

The reaction rate for this system reads

$$r_0(\mathbf{x}) = k_f \left(x_1^2 - \frac{x_2 \, x_3}{K_{eq}} \right). \tag{3.10}$$

The solution of Eqs. (2.59) and (2.60) with the reaction rate according to Eq. (3.10) delivers the fixed points of the rectifying and the flash cascade and thus possible top and bottom products of a reactive distillation column. Table 3.8 summarizes the fixed points and shows their stability behavior. As can be seen, the pure component A is not

	rectifying cascade	stripping cascade
elka	unstable node	no fixed point for $0 \le Da^* \le 0.072$, saddle otherwise
A	no fixed point	no fixed point
B	saddle	saddle for $0 \le Da^* \le 0.072$, stable node otherwise
C	stable node for $0 \le Da^* \le 0.171$, saddle otherwise	stable node

Table 3.8: Fixed points for the reaction system $2\,A \Longleftrightarrow B + C$ depending on the scaled Damköhler number $Da^* = Da/(1 + Da)$.

a fixed point of this system for any value of $Da^* > 0$, in contrast to the nonreactive system, where A is a possible top product. Instead, the only possible top product of a RDC is the kinetic azeotrope as it is the unstable node of the rectifying cascade. This kinetic azeotrope, which must be located on the extended line of kinetic azeotropy, does not influence the bottom product. Possible bottom products are pure component C for all Damköhler numbers and pure component B for scaled Damköhler numbers $Da^* > 0.072$ (stable nodes of the stripping cascade). Fig. 3.28 shows the fixed points along the extended line of kinetic azeotropy. The fixed point of the rectifying cascade is an unstable node, that of the stripping cascade is a saddle.
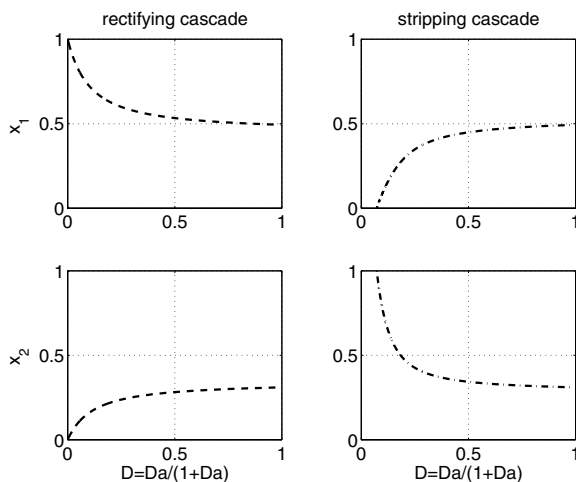
Figure 3.28: Fixed points for the reaction system $2\,A \Longleftrightarrow B + C$ along the extended line of kinetic azeotropy. Unstable node (- - -) in the rectifying, saddle (-·--·-) in the stripping cascade.

Conventional process for the decomposition of A

The conventional process for the production of B and C from A consists of a reactor followed by a nonreactive distillation column where the reactant A is separated and recycled to the reactor. The bottom product of this column is fed to a second nonreactive column where pure B is obtained as the top product and pure C as the bottom product. Fig. 3.29 shows this configuration.

As in the previous example a basic design is obtained on the basis of the Fenske and Underwood equations, optimized in GAMS. For the resulting structure a tray-by-tray model is optimized in DIVA to obtain an energetically optimal process. Pure A is fed at $F = 100$. For the product specifications $x_{2,P} \geq 0.99$ and $x_{3,P} \geq 0.99$ the optimal solution is shown in Table 3.9 where n_R, N, N_F, r, s denote the amount of catalyst in the reactor, total number of stages, feed stage location, reflux ratio and reboil ratio, respectively. The total amount of vapor produced in the reboilers sums up to $V_1 + V_2 = 293$.

69
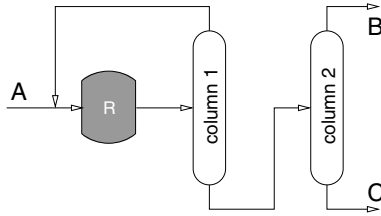
Figure 3.29: Conventional process flowsheet for the decomposition of A.

	n_R	N	N_F	r	s	V
column 1		20	5	0.02	1.77	176.98
column 2		25	12	1.32	2.32	116.02
reactor	200.0					

Table 3.9: Design parameters for the conventional process.

Design of RD processes for the decomposition of A

As this reaction system exhibits a kinetic azeotrope and product B is the intermediate boiling component, it is not possible to obtain the products from a RDC configuration as in the case $2\,B \rightleftharpoons A + C$. However, there exist different RD processes which will be explained in more detail in the following.

Having a closer look on the conventional process, it turns out that nearly the whole amount of the condenser outlet of the first column is recycled to the reactor, whereas only a small portion serves as the column reflux ($s_1 = 0.02$). Thus, a configuration with direct coupling of the reactor to the top of the first column should give results similar to the conventional process. Fig. 3.30 shows this configuration. As expected, an optimization in DIVA yields the same result with an overall amount of vapor of $V_1 + V_2 = 293$.

In a next step, the reactor and the first column are combined. The resulting heterogeneously catalyzed RDC followed by a nonreactive column is shown in Fig. 3.31. Assuming that condensers and reboilers are nonreactive, an optimal configuration is found where the uppermost six stages of the first column are reactive with an amount of catalyst of $n_k = 33.3$ each. Thus the total amount equals the maximal allowed $n_{max} = 200$. The optimal feed position is the uppermost column tray. With this configuration, the total vapor flow rate can be reduced to $V_1 + V_2 = 271$.
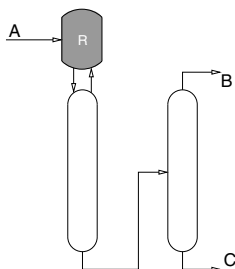
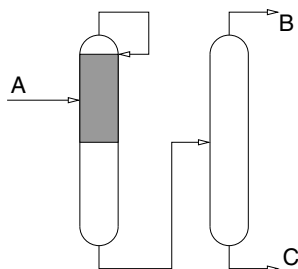Figure 3.30: Reactor on top of a nonreactive distillation column.

Figure 3.31: RDC with nonreactive column.

Both processes described so far require two distillation columns. To study the feasibility of the reaction/separation task in a single column, a heterogeneously catalyzed RDC with a side draw is considered, as depicted in Fig. 3.32. In a first design study, a column
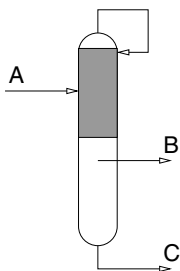

Figure 3.32: Heterogeneously catalyzed RDC with side draw.

with 40 stages is investigated. Stage 1 represents the total condenser, stage 40 the partial reboiler. The feed of pure A is introduced at the uppermost column stage and the product B is withdrawn from stage 20. Stages 2 to 15 are reactive with $n_k = 14.28$ each, i.e. $n_{tot} = n_{max} = 200$. Even though this process is feasible, it can not be regarded as an alternative to the above proposed processes as the required vapor flow rate increases to $V = 7900$.

Looking at the fixed points for this system given in Table 3.8, two stable nodes for the stripping section are found for a scaled Damköhler number of $Da^* > 0.072$. This means that for a sufficiently high Damköhler number two distinct bottom products are possible,

pure B or pure C. Pure C is always a stable node, independent on Da, and can therefore be obtained in a nonreactive stripping section. Thus, a RD process in a single column can be realized with a divided stripping section, as shown in Fig. 3.33. In contrast to the dividing wall column configuration in the previous section, only the rectifying section is used commonly, whereas each stripping section has its own reboiler and no contact of the two bottom products is allowed.
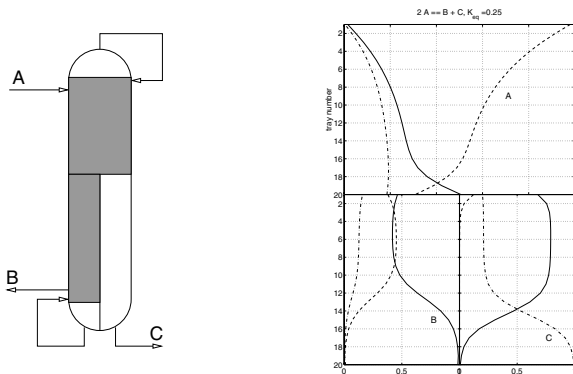

Figure 3.33: Heterogeneously catalyzed RDC with divided stripping section. Column configuration and liquid mole fraction profiles.

In a first design, the number of stages for the rectifying and each stripping section is set to 20. The rectifying section and the left stripping section are completely reactive, the total condenser and partial reboilers are assumed to be nonreactive. The fresh feed of pure A is introduced to the uppermost column tray. Product B is withdrawn as a liquid side draw from the lowermost tray of the left stripping section and product C as the bottom stream from the reboiler of the right stripping section. An optimization study in DIVA provided the optimal amount of catalyst per stage for the rectifying section to be $n_{re} = 8.55$ and for the left stripping section $n_{ls} = 20.0$, the maximal allowed value. With this configuration, the vapor flow rate in the rectifying section is $V_{re} = 666$. The energy consumption of this process is much smaller than that of the RDC with sidedraw, but it is still more than twice the amount of energy needed in the conventional system. Thus, the best configuration with respect to energy consumption is the heterogeneously catalyzed RDC with a downstream separation column as shown in Fig. 3.31. The MINLP optimizations showed that there exists no better solution among those configurations considered here.

Conventional process for the synthesis of A

The conventional process flowsheet for the production of A from B and C is shown in Fig. 3.34. It consists of a reactor followed by a nonreactive distillation column where the pure product A is removed at the top and the reactants are recycled to the reactor.
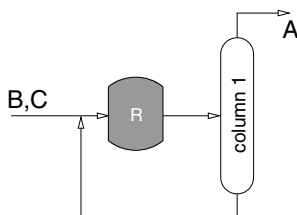

Figure 3.34: Conventional process flowsheet.

Design of RD processes for the synthesis of A

In contrast to the decomposition of A in a reactive distillation column, the synthesis of A from B and C is an easy task. The main requirement for the design of a RD process is the nonreactive rectifying section as this is the only way to obtain pure A as a product.

This information is given by the fixed points of the rectifying flash cascade in Table 3.8. Pure A is a fixed point for the nonreactive system only, whereas the kinetic azeotrope on the extended line of kinetic azeotropy is the fixed point for the reactive system. This implicates that a homogenously catalyzed RDC is not suitable. Fig. 3.35 proposes a feasible process design. In a one-product column the reactants B and C are fed to the stripping section which is filled with catalyst. In a nonreactive rectifying section the product A is separated from the reacting mixture and is obtained as the column top product.
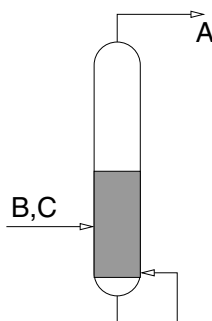

Figure 3.35: Heterogeneously catalyzed RDC for the production of A.

3.2.3 Ideal ternary system $2\,C \Longleftrightarrow A + B$

Fundamentals

Once again, only the volatilities of the ideal ternary mixture are changed such that the heaviest boiling component C is decomposed to (or produced from) the lightest and the intermediate boiling components A and B. Like in the previous case the products are all lighter or heavier boiling than the reactants, and thus kinetic azeotropes will occur in this system. Fig. 3.36 shows the phase portrait with the chemical equilibrium line (**- - -**), nonreactive residue curves (—) and stoichiometric lines (- - -). Connecting the points where the latter two are tangent leads to the extended line of kinetic azeotropy (**-·--·-**) (*elka*).
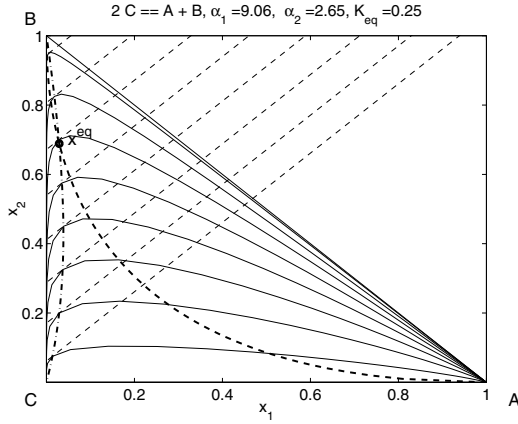
Figure 3.36: Phase portrait for the reactive system $2\,C \Longleftrightarrow A + B$ with stoichiometric lines (- - -), nonreactive residue curves (—), reaction equilibrium line (**- - -**) and the extended line of kinetic azeotropy (**-·--·-**).

The same data as in the previous examples are used

$$\boldsymbol{\alpha} = [9.06,\ 2.65,\ 1.0], \quad k_f = 2.9 \quad \text{and} \quad K_{eq} = 0.25,$$

with the reaction rate

$$r_0(\mathbf{x}) = k_f \left(x_3^2 - \frac{x_1\,x_2}{K_{eq}} \right). \tag{3.11}$$

74

Table 3.10 shows the fixed points of the rectifying and flash cascade as the solution of Eqs. (2.59) and (2.60) with the reaction rate according to Eq. (3.11). The pure component A is

	rectifying cascade	stripping cascade
elka	no fixed point for $0 \leq Da^* \leq 0.232$, saddle otherwise	stable node
A	unstable node	unstable node for $0 \leq Da^* \leq 0.081$, saddle otherwise
B	saddle for $0 \leq Da^* \leq 0.232$, unstable node otherwise	saddle
C	no fixed point	no fixed point

Table 3.10: Fixed points for the reaction system $2C \Longleftrightarrow A + B$ depending on the scaled Damköhler number $Da^* = Da/(1 + Da)$.

always obtainable as a top product of a RDC, whereas component B becomes a possible top product for scaled Damköhler numbers higher than $Da^* > 0.232$ (unstable nodes of the rectifying cascade). Apart from the nonreactive case, the pure component C is no potential product. The stable node of the stripping cascade and thus a possible bottom product of a RDC is the kinetic azeotrope located on the extended line of kinetic azeotropy for any Damköhler number. For the limit of no reaction ($Da^* \to 0$), the kinetic azeotrope approaches the pure component C. Fig. 3.37 shows the fixed points along the extended line of kinetic azeotropy.

Conventional process for the decomposition of C

The conventional process for the decomposition of C consists of a reactor and two nonreactive distillation columns, Fig. 3.38. The reactor outlet is fed to the first column where the reactant C is completely separated and recycled to the reactor. The remaining binary mixture of A and B is separated in the second column. Like in the previous example an optimal design is obtained from the optimization of the Fenske and Underwood equations. The resulting design is used as a basis for further optimizations with a tray-by-tray model. For a feed of pure C with $F = 100$ and the product specifications $x_{1,P} \geq 0.99$ and $x_{2,P} \geq 0.99$ the optimal solution is shown in Table 3.11 where n_R, N, N_F, r, s denote the amount of catalyst in the reactor, total number of stages, feed stage location, reflux ratio and reboil ratio, respectively. The total amount of vapor produced in the reboilers sums up to $V_1 + V_2 = 279.9$.
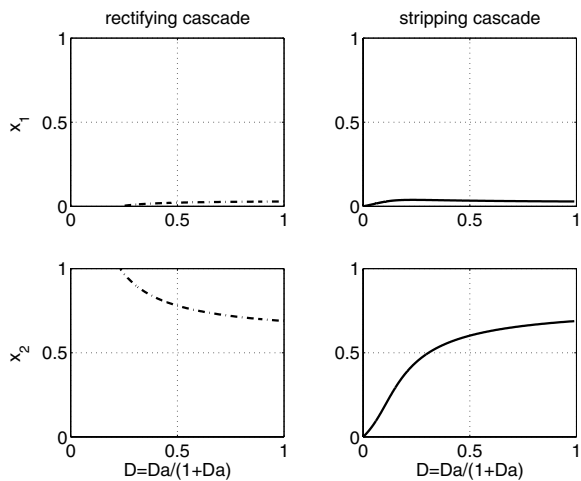
Figure 3.37: Fixed points for the reaction system $2\,C \iff A + B$ along the extended line of kinetic azeotropy. Saddle (-·-·-) in the rectifying, stable node (—) in the stripping cascade.

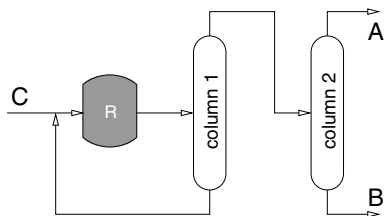Figure 3.38: Conventional process flowsheet for the decomposition of C.

	n_R	N	N_F	r	s	V
column 1		25	12	1.21	0.40	182.68
column 2		20	10	1.07	1.95	97.22
reactor	200.0					

Table 3.11: Design parameters for the conventional process.

Design of RD processes for the decomposition of C

The reaction system $2\,C \Longleftrightarrow A + B$ is very similar to the previously considered system $2\,A \Longleftrightarrow B + C$, including the problem of kinetic azeotropy and the resulting difficulties to obtain the pure products from a RDC configuration. Not surprisingly, the RD process solutions proposed are mirror images of those in the previous section. Simply spoken, the terms *rectifying* and *stripping* are exchanged.

Fig. 3.39 shows a heterogeneously catalyzed RDC coupled with a nonreactive distillation column. The reactor and the first column of the conventional process are combined in this RDC. Using the same number of stages as in the conventional process, the optimal solution is found with four reactive stages (21–24) with an amount of catalyst of $n_k = 50$ each and the feed of pure C to the lowermost column tray. The overall amount of vapor needed to assure the product purities sums up to $V_1 + V_2 = 259$.
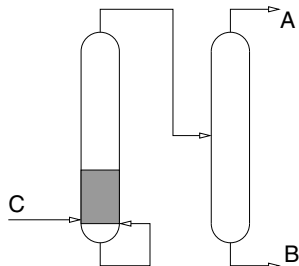
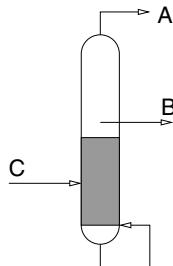Figure 3.39: RDC with nonreactive column.

Figure 3.40: Heterogeneously catalyzed RDC with side draw.

In Fig. 3.40 the first realization in a single RDC is shown. The column consists of 40 stages, the total condenser and the partial reboiler representing stages 1 and 40, respectively. Pure reactant C is fed to the lowermost stage and the product B is withdrawn from stage 20 as a liquid side draw. Stages 25 to 39 are reactive with an amount of catalyst of $n_k = 13.3$ each, summing up to the maximal total amount of $n_{tot} = n_{max} = 200$. To guarantee the product specifications, a vapor flow rate of $V = 2103$ has to be produced in the reboiler. Due to this high energy consumption this process has to be seen as a feasibility study only.

The same is valid for the heterogeneously catalyzed RDC with divided rectifying sections, presented in Fig. 3.41. Each rectifying section as well as the common stripping section

consist of 20 stages. The left rectifying section is fully reactive with an amount of catalyst of $n_k = 110$, the maximal allowed value in this optimization study. The stripping section is also completely reactive with $n_k = 4.66$ and the pure reactant C fed to the lower part (stage 15). From the mole fraction profiles it can be seen that pure products A and B are obtained, at a cost of a vapor flow rate in the stripping section of $V_{st} = 1438$, which is still prohibitive for a real process.
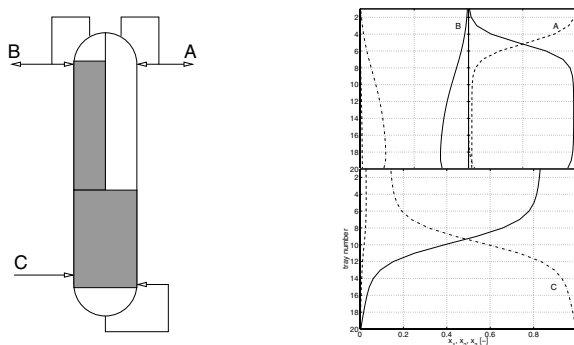

Figure 3.41: Heterogeneously catalyzed RDC with divided rectifying section. Column configuration and liquid mole fraction profiles.

In principle, the RDC with divided rectifying sections is identical to a RDC with a side column, presuming that the heat effects across the dividing wall are negligible. Fig. 3.42 shows such a configuration as it was returned from the optimization tool GAMS for the current reaction/separation problem. The main column has 30 trays, stage 1 and stage 30 representing the total condenser and the partial reboiler, respectively. At the lowermost column stage pure reactant C is fed. At the same stage a side column with 20 trays is coupled via a vapor stream to and a liquid stream from the side column. This column has a total condenser at the top but no own reboiler. In the main column the reactive section is placed in the middle (stages 12 to 16) with $n_k = 110$, whereas in the side column only the last stage is reactive, $n = 110$. As can be seen from the composition profiles in Fig. 3.42, pure product B is obtained as the main column's distillate, and pure A as the distillate of the side column. Interestingly enough, the intermediate boiling component B is obtained from a nonreactive rectifying section even though it is no unstable node but a saddle point in the nonreactive case (Table 3.10). Compared to the previous process configuration, only half the amount of vapor is needed, $V = 732$.
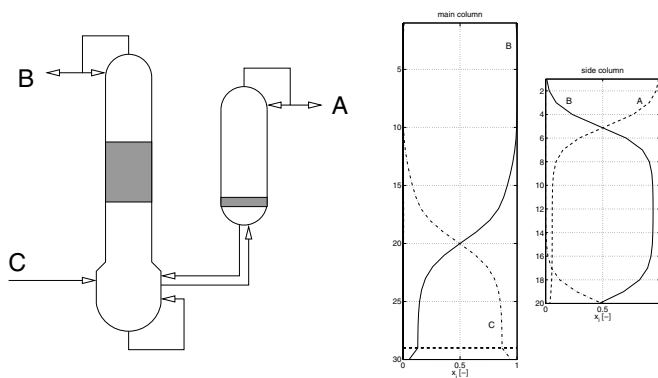
Figure 3.42: Heterogeneously catalyzed RDC with side column. Column configuration and liquid mole fraction profiles.

The last configuration tested is a nonreactive distillation column with a reactive prefractionator. Fig. 3.43 shows the design found by optimization studies in GAMS. The main
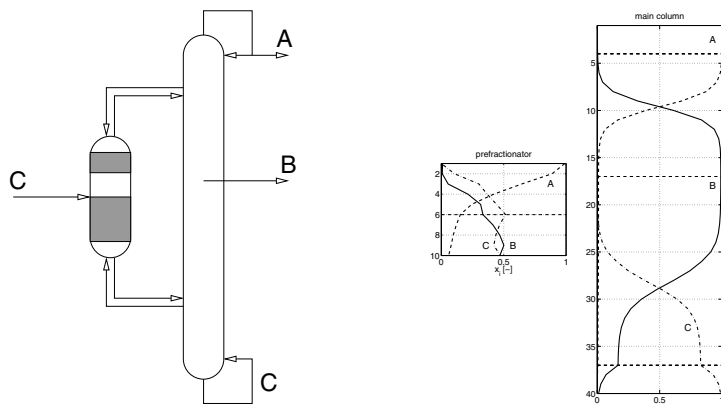

Figure 3.43: Heterogeneously catalyzed RDC with reactive prefractionator. Column configuration and liquid mole fraction profiles.

column consists of 40 stages including condenser and reboiler. A prefractionator with 10 stages is coupled to it via liquid and vapor streams on stages 4 and 37 of the main column. Pure reactant C is fed to stage 6 of the prefractionator. Stages 2, 3 and 6–10 of the latter

are reactive. Pure product A is obtained as the main column distillate, whereas pure B is withdrawn from stage 17. With this configuration the energy demand can be further reduced, $V = 437$. This is still more than in the conventional process or in the two-column configurations, but these studies clearly demonstrate the important role of mathematical models and optimization tools for process design. It should be noted that the MINLP model for the optimization studies turned out to be difficult to solve. One should keep in mind that the optimization algorithms in GAMS can provide local optimal solutions only. No statement can be made how far away this solution is from the global optimum.

Conventional process for the synthesis of C

In contrast to the decomposition of C, its synthesis is an easy task, in the conventional process as well as in a RDC. Fig. 3.44 shows the conventional process flowsheet with a reactor followed by a single nonreactive distillation collumn. Pure product C is obtained as the column bottom product and the reactants A and B are recycled to the reactor.

Design of RD processes for the synthesis of C

Like in the previous example for the production of a single light component, a heterogeneously catalyzed RDC is suitable for the current reaction/separation task. Again, a one-product column is proposed with a reactive rectifying section and a nonreactive stripping section. The latter is important to overcome the reactive azeotrope. Fig. 3.45 shows the principle design.
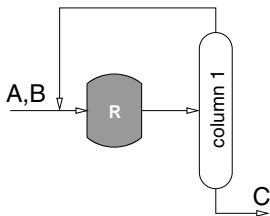

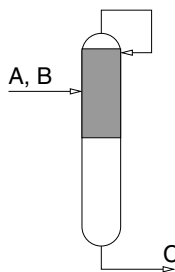Figure 3.44: Conventional process flowsheet.

Figure 3.45: Heterogeneously catalyzed RDC for the production of C.

3.2.4   Ideal ternary system $2\,A + B \Longleftrightarrow C$

Fundamentals

This ideal reaction system is similar to the previous case, but there exists one important difference: the existence of kinetic azeotropes and thus the reachable product regions not only depend on the reaction stoichiometry but also on the actual values of the chemical equilibrium constant and the relative volatilities. The following data are used for numerical studies

$$\boldsymbol{\alpha} = [4,\ 2,\ 1], \quad k_f = 1.0 \quad \text{and} \quad K_{eq} \in \{1,\ 10,\ 25\}$$

with the reaction rate

$$r_0(\mathbf{x}) = k_f\ \left(x_1^2\, x_2 - \frac{x_3}{K_{eq}} \right). \tag{3.12}$$

Fig. 3.46 shows the phase portrait with the chemical equilibrium line (- - -), nonreactive residue curves (—) and stoichiometric lines (- - -) for a chemical equilibrium constant of $K_{eq} = 1$. Connecting the points where the latter two are tangent leads to the extended line of kinetic azeotropy (-·-·-) (*elka*).
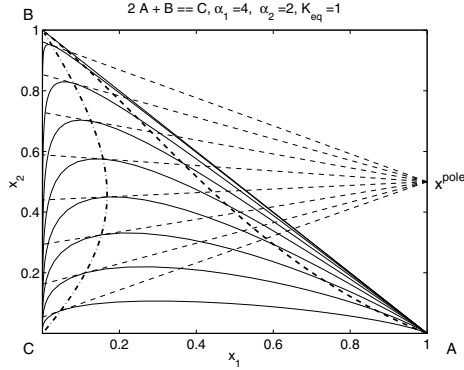

Figure 3.46: Phase portrait for the reactive system $2\,A + B \Longleftrightarrow C$ with stoichiometric lines (- - -), nonreactive residue curves (—), reaction equilibrium line (- - -) and the extended line of kinetic azeotropy (-·-·-) for $K_{eq} = 1$.

The main difference between this reaction system and the previously treated $A + B \Longleftrightarrow 2\,C$ is the curvature of the chemical equilibrium curve near the pure compo-

nent B. In the actual system the chemical equilibrium curve is tangent to the $A - B$ edge which means that the curve does not intersect with the extended line of kinetic azeotropy. Thus, there is no chemical equilibrium reactive azeotrope in this system, at least not for low chemical equilibrium constants K_{eq}. Table 3.12 lists the fixed points of this reaction system for $K_{eq} = 1$, the fixed points along the *elka* are shown in Fig. 3.47.

$K_{eq} = 1$	rectifying cascade	stripping cascade
elka	no fixed point	stable node for $0 \leq Da^* \leq 0.202$, saddle for $0.2 \leq Da^* \leq 0.202$ (MSS)
A	unstable node	unstable node for $0 \leq Da^* \leq 0.13$, saddle otherwise
B	saddle	saddle for $0 \leq Da^* \leq 0.2$, stable node otherwise
C	no fixed point	no fixed point

Table 3.12: Fixed points for the reaction system $2\,A + B \Longleftrightarrow C$ for $K_{eq} = 1$ depending on the scaled Damköhler number $Da^* = Da/(1 + Da)$.

As this reaction system is nonequimolar, the fixed points are the solutions of Eq. (2.61) for the stripping cascade and Eq. (2.62) for the rectifying cascade. In accordance to the stoichiometry the molar masses are arbitrarily chosen to

$$\mathbf{M} = [28,\ 56,\ 112].$$

For $K_{eq} = 1$ the pure component A is the unstable node of the rectifying cascade, corresponding to the top product of a reactive distillation column. The pure component B is the stable node for the stripping cascade for $Da^* > 0.2$ and a saddle otherwise. The extended line of kinetic azeotropy (*elka*) is a stable node for $0 \leq Da^* \leq 0.202$ and additionally a saddle for $0.2 \leq Da^* \leq 0.202$. This means that there exist multiple steady states for the same value of the scaled Damköhler number Da^*, corresponding to different fixed points. According to these results, the bottom product of a reactive distillation column corresponds to the kinetic azeotrope on the extended line of kinetic azeotropy for Damköhler numbers which are smaller than the critical one ($Da^*_{crit} = 0.202$ in this case). For the small region of $0.2 \leq Da^* \leq 0.202$ there are two possible product concentrations and for $Da^* > Da^*_{crit}$ the pure component B is the bottom product.

If the chemical equilibrium constant K_{eq} increases, the chemical equilibrium line approaches the extended line of kinetic azeotropy. This situation is shown in Fig. 3.48 for a
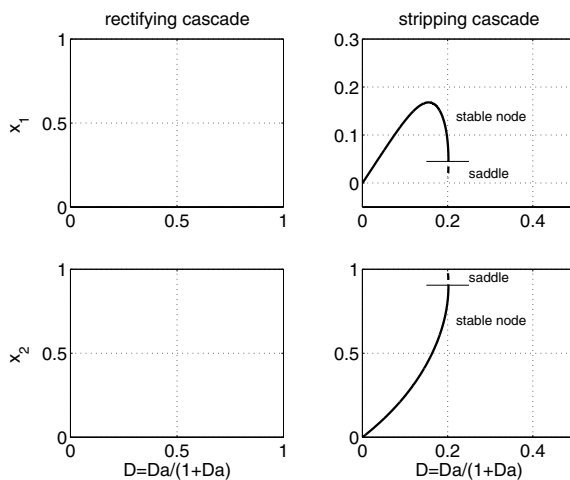
Figure 3.47: Fixed points for the reaction system $2\,A + B \Longleftrightarrow C$ along the extended line of kinetic azeotropy for $K_{eq} = 1$.
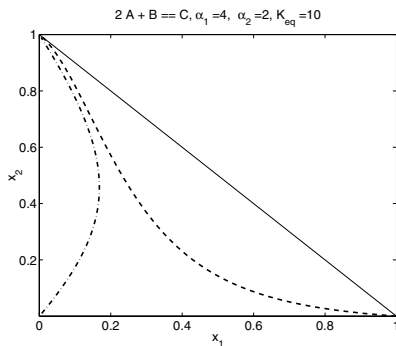
value of $K_{eq} = 10$.

Figure 3.48: Reactive system $2\,A + B \Longleftrightarrow C$ with reaction equilibrium line (- - -) and the extended line of kinetic azeotropy (-·--·-) for $K_{eq} = 10$.

Table 3.13 shows the fixed point and their stability. The properties of the system are

similar to those in the case of $K_{eq} = 1$ but the critical Damköhler number to obtain pure product B increases considerably to $Da^*_{crit} = 0.865$. The region of multiple steady states is also significantly enlarged to $0.714 \leq Da^* \leq 0.865$. This is illustrated on the right hand side of Fig. 3.49.

$K_{eq} = 10$	rectifying cascade	stripping cascade
elka	no fixed point	stable node for $0 \leq Da^* \leq 0.865$, saddle for $0.714 \leq Da^* \leq 0.865$ (MSS)
A	unstable node	unstable node for $0 \leq Da^* \leq 0.19$, saddle otherwise
B	saddle	saddle for $0 \leq Da^* \leq 0.714$, stable node otherwise
C	no fixed point	no fixed point

Table 3.13: Fixed points for the reaction system $2\,A + B \Longleftrightarrow C$ for $K_{eq} = 10$ depending on the scaled Damköhler number $Da^* = Da/(1 + Da)$.
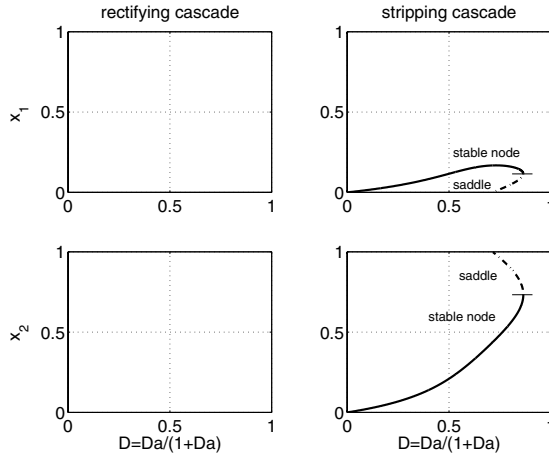

Figure 3.49: Fixed points for the reaction system $2\,A + B \Longleftrightarrow C$ along the extended line of kinetic azeotropy for $K_{eq} = 10$.

Increasing the chemical equilibrium constant any further to $K_{eq} = 25$ leads to an inter-

section of the chemical equilibrium curve with the extended line of kinetic azeotropy at two points. Thus in this case, there exist two equilibrium reactive azeotropes as can be seen in Fig. 3.50. In Table 3.14 the fixed points are indicated together with their stability properties. In contrast to the previous cases of lower values of K_{eq}, there are fixed points on the extended line of kinetic azeotropy for the rectifying cascade, too.
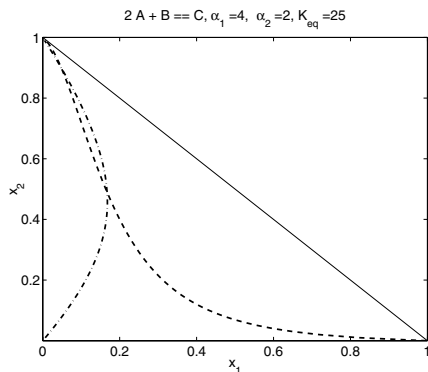

Figure 3.50: Reactive system $2\,A + B \iff C$ with reaction equilibrium line (- - -) and the extended line of kinetic azeotropy (-·--·-) for $K_{eq} = 25$.

$K_{eq} = 25$	rectifying cascade	stripping cascade
elka	no fixed point for $0 \leq Da^* \leq 0.9$, saddle and unstable node for $Da^* > 0.9$ (MSS)	stable node for $0 \leq Da^* \leq 1$, saddle for $0.862 \leq Da^* \leq 1$ (MSS)
A	unstable node	unstable node for $0 \leq Da^* \leq 0.196$, saddle otherwise
B	saddle	saddle for $0 \leq Da^* \leq 0.862$, stable node otherwise
C	no fixed point	no fixed point

Table 3.14: Fixed points for the reaction system $2\,A + B \iff C$ for $K_{eq} = 25$ depending on the scaled Damköhler number $Da^* = Da/(1 + Da)$.

In this example, multiple kinetic azeotropes exist in the rectifying section for $Da^* > 0.9$

as can be seen on the left hand side of Fig. 3.51. For the stripping cascade, kinetic azeotropes now exist for every value of the scaled Damköhler number Da^* with multiplicity for $Da^* > 0.862$. In that case, it is not possible to obtain pure B as the bottom product by simply providing a sufficiently large residence time (catalyst or holdup).
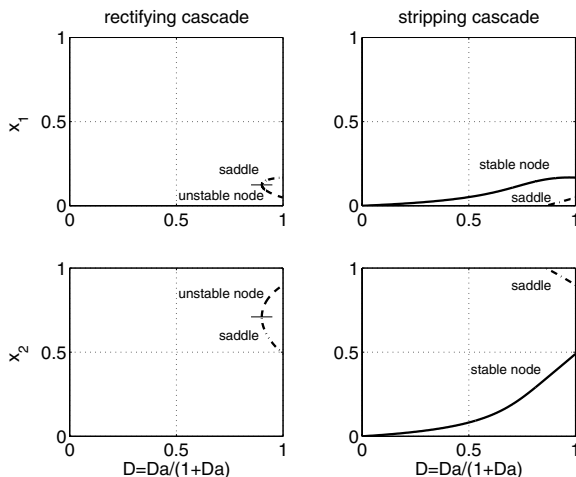

Figure 3.51: Fixed points for the reaction system $2\,A + B \Longleftrightarrow C$ along the extended line of kinetic azeotropy for $K_{eq} = 25$.

To sum up, the reaction system $2\,A + B \Longleftrightarrow C$ is an interesting example to demonstrate that not only the reaction scheme but also concrete values of reaction parameters decide whether kinetic azeotropes exist or not.

Process design

The conventional process for this system is identical to that of the reaction system $2\,C \rightleftharpoons A + B$, for the synthesis of C as well as for its decomposition. The reactive distillation process for the synthesis of C is identical to that of the system $2\,C \rightleftharpoons A + B$ as shown in Fig. 3.45. For the decomposition of C the processes proposed in the previous section should work as well. However, for small values of the chemical equilibrium

constant K_{eq} there exists a more attractive configuration. In that case pure products A and B can be obtained as top and bottom products from a single homogeneously catalyzed RDC as shown in Fig. 3.52. As K_{eq} increases the separation becomes more and
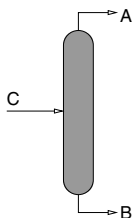

Figure 3.52: Homogeneously catalyzed RDC for the decomposition of C.

more difficult until a critical value of the equilibrium constant is reached. At that point kinetic azeotropes occur for all values of the Damköhler number Da and the single RDC configuration becomes infeasible.

This example shows that key properties like reactive azeotropes not only depend on structures like stoichiometry but also on actual values like the chemical equilibrium constant or relative volatilities. As a consequence, these dependencies directly influence the process design and hence economics.

3.2.5 Ideal ternary system $A + B \Longleftrightarrow C$

Fundamentals

The last ideal reaction system considered in this thesis is similar to the examples in sections 3.2.3 and 3.2.4 with slight changes in the stoichiometry. But again, a different behavior is observed wrto. the existence of azeotropes depending on the actual values of the chemical equilibrium constant and the relative volatilities. The data chosen are

$$\boldsymbol{\alpha} = [5, \ 3, \ 1], \quad k_f = 1.0 \quad \text{and} \quad K_{eq} \in \{0.5, \ 1, \ 4\}$$

with the reaction rate

$$r_0(\mathbf{x}) = k_f \left(x_1 \, x_2 - \frac{x_3}{K_{eq}} \right). \tag{3.13}$$

Fig. 3.53 shows the chemical equilibrium line (- - -), and the extended line of kinetic azeotropy (-·-·-) (*elka*) for a chemical equilibrium constant of $K_{eq} = 0.5$. Both lines
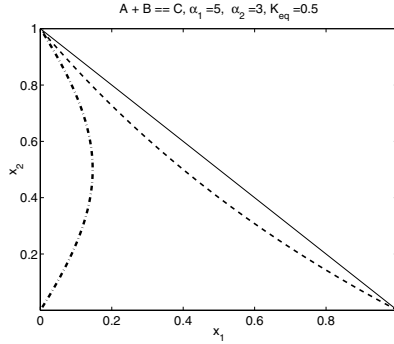

Figure 3.53: Phase portrait for the reactive system $A+B \Longleftrightarrow C$ with reaction equilibrium line (- - -) and the extended line of kinetic azeotropy (-·-·-) for $K_{eq} = 0.5$.

intersect at pure B ($x_2 = 1$) only, there exists no equilibrium reactive azeotrope inside the composition triangle. Thus, the decomposition of C to A and B is possible in a single RDC as shown in the previous section in Fig. 3.52. But as can be seen from the fixed points in Fig. 3.54, this is only true for higher Damköhler numbers. For values of $Da^* < 0.25$, the stable node of the stripping cascade lies on the extended line of kinetic azeotropy. Thus, there exist reactive kinetic azeotropes even though no equilibrium reactive azeotropes appear in this system.
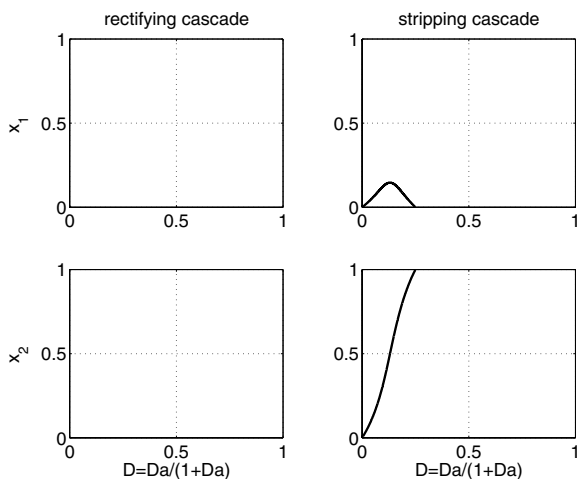
Figure 3.54: Fixed points for the reaction system $A + B \Longleftrightarrow C$ along the extended line of kinetic azeotropy for $K_{eq} = 0.5$.

For a higher value of the chemical equilibrium constant of $K_{eq} = 1$ similar results are obtained, Figs. 3.55 and 3.56. In this case it is possible to obtain A and B as decomposition products as well, but only for the limiting case of chemical equilibrium ($Da^* \to 1$). For even higher values of K_{eq} an equilibrium reactive azeotrope appears as the chemical equilibrium line and the extended line of kinetic azeotropy intersect inside the composition triangle. This situation is shown in Figs. 3.57 and 3.58 for $K_{eq} = 4$.

The selected examples presented above clearly demonstrate the need of detailed investigations of the reaction system under consideration. Residue curve maps have proven to be indespensable tools for a preliminary process design. They give important insights about attainable products in either configuration. On the other hand they are necessary but not sufficient for a successful process design. Mathematical programming and MINLP optimization turned out to be promising techniques for the development of innovative and cost optimal processes.
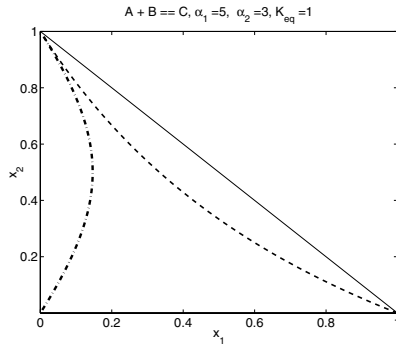
Figure 3.55: Phase portrait for the reactive system $A+B \Longleftrightarrow C$ with reaction equilibrium line (- - -) and the extended line of kinetic azeotropy (-·--·-) for $K_{eq} = 1$.
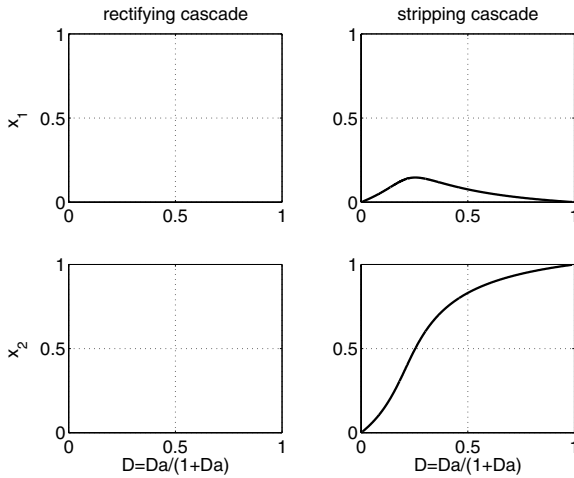

Figure 3.56: Fixed points for the reaction system $A + B \Longleftrightarrow C$ along the extended line of kinetic azeotropy for $K_{eq} = 1$.
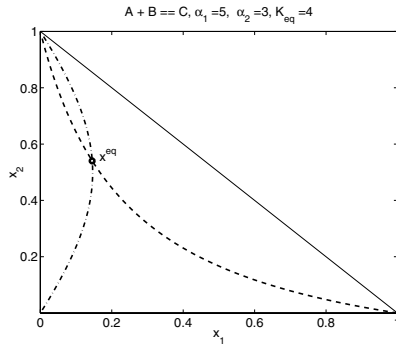
Figure 3.57: Phase portrait for the reactive system $A+B \Longleftrightarrow C$ with reaction equilibrium line (- - -) and the extended line of kinetic azeotropy (-·-·-) for $K_{eq} = 4$.
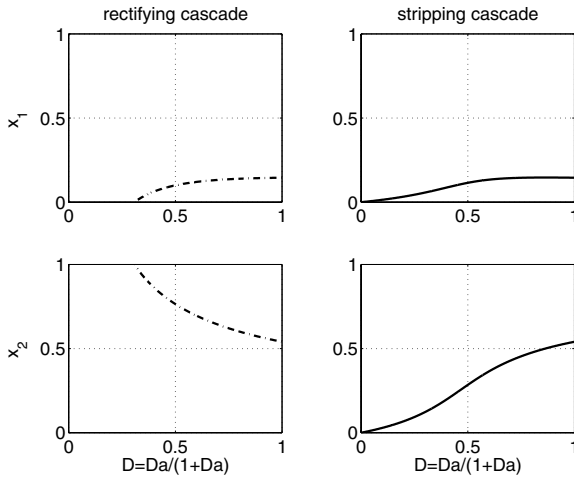

Figure 3.58: Fixed points for the reaction system $A + B \Longleftrightarrow C$ along the extended line of kinetic azeotropy for $K_{eq} = 4$.

3.3 Reactive separation

3.3.1 Fundamentals

Introduction

One of the major problems in the chemical process industries is the separation of fluid mixtures into its pure components. The standard techniques to tackle this problem are distillation or rectification. Unfortunately these techniques fail if the boiling points of the components to be separated are very close. However, if these closely boiling components differ considerably in their chemical properties, especially their reactivity, it is possible to separate at least the reactive components from the mixture by applying a suitable chemical reaction. In the following, this principle will be explored in more detail, first considering the separation of an ideal mixture A/B and second the separation of isobutene from a C_4 hydrocarbon mixture in coupled reactive distillation columns as case studies.

Reactive separation

Fig. 3.59 shows the general process scheme of a reactive separation process.

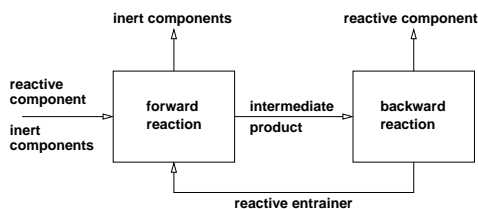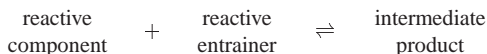Figure 3.59: General process scheme of reactive separation.

A mixture of reactive and inert closely boiling components is fed to a first reaction/separation device where the reactive components react with a suitable reactive entrainer to form an intermediate product.

$$\text{reactive component} \quad + \quad \text{reactive entrainer} \quad \rightleftharpoons \quad \text{intermediate product}$$

This intermediate product should be easily separated from the inert components which are withdrawn from the first device. The pure intermediate product enters a second reaction/separation device where it is decomposed into the original reactive components and the reactive entrainer. The latter is recycled to the first device whereas the light boiling reactive components leave the plant as products.

In general, the reaction/separation devices may be any kind of single units and combinations thereof. However, recent research on reactive distillation processes opens new ways of performing reactive separations very efficiently [50]. In this process both the forward reaction to form the intermediate product and the backward reaction to decompose it are performed in reactive distillation columns (RDC).

3.3.2 Ideal System

In the following, the separation of components A and B in an ideal mixture is considered. Their boiling points are very close with a relative volatility of $\alpha = 1.1$. It is assumed that component B reacts with the higher boiling substance C to form the highest boiling component D. Component A is nonreactive wrto. substances C and D, resulting in the reaction system

$$B + C \rightleftharpoons D, \quad A \text{ inert.}$$
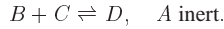
According to Eq. (2.21), the reaction scheme

$$r_0 = k_f \left(x_2\, x_3 - \frac{x_4}{K_{eq}} \right) \tag{3.14}$$

is assumed with parameters

$$k_f = 1, \quad K_{eq} = 4$$

where the indices 1 to 4 denote the components A to D, respectively. The boiling point differences of the reaction partners should be sufficiently large to enable an easy separation of the ideal quaternary system. The relative volatilities are chosen to

$$\boldsymbol{\alpha} = [4.4,\ 4.0,\ 2.0,\ 1.0].$$

This system is very similar to that of section 3.2.3 even though the parameters differ and the reaction is nonequimolar in this case. The main characteristics are identical enabling to use those previous results for the optimal design of the system under consideration. In

the following, a conventional process and a RDC process are developed for a mixture of 60% A / 40% B with a normalized dimensionless flow rate of 1

$$F = 1.0, \ \mathbf{x}_F = [0.6, 0.4, 0, 0].$$

Conventional process

In order to develop a flowsheet consisting of reactors (CSTRs) and distillation columns, several tasks must be reflected:

1. Convert B with C to D.
2. Remove A from the system.
3. Decompose D to B and C.
4. Remove B from the system.
5. Recycle C and D appropriately.

Figs. 3.44 and 3.38 in section 3.2.3 are prototypes of conventional process for the synthesis and decomposition of the heaviest boiling component in an ideal ternary mixture. The same problems are to be solved in the actual quaternary mixture, D is synthesized (tasks 1, 5 above) and decomposed (tasks 3, 4, 5). But there exists one important difference between the two systems: in the actual case, the light boiling inert component A has to be removed (task 2). This implies that virtually no B is allowed to be present in the column where A is separated. Hence, full or at least very high conversion of B is necessary in the reactor, depending on the product purity requirements. As the highest achievable conversion in a CSTR is limited by the chemical equilibrium, the only way to reduce the amount of B in the reactor outlet is a high C to B ratio in the feed. On the other hand the feed flow rate is limited by the reactor holdup if an operating point near the equilibrium is chosen. This means that for a given reactor holdup the outlet concentration of B has a lower limit. A reduction of x_B beyond that point is only possible for a cascade of reactors and distillation columns where the product D is withdrawn before the next reaction stage.

This configuration is shown in Fig. 3.60. In order to obtain the components A and B with a purity of at least 96%, two reactors (R1 and R2) are necessary with an upper limit on each reactor holdup of 200. Reactor R1 is fed with the fresh A/B mixture to be separated and with pure C from recycle streams. In column C1 the product D is removed and fed to the decomposition reactor R3. The remaining mixture $A/B/C$ flows to reactor R2 where
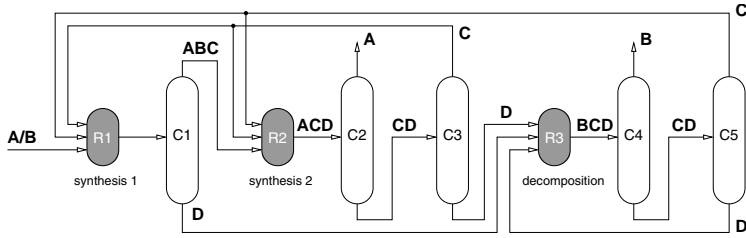
Figure 3.60: Conventional process for the reactive separation of the closely boiling components A and B.

it is further diluted with C. Only a small amount of B is present in the reactor outlet enabling the removal of product A in column C2 with the required purity. Column C3 separates C and D, the former recycled to R1, the latter fed to R3. The configuration R3/C4/C5 is similar to that of the ternary system in Fig. 3.38. Here, D is decomposed, C is recycled to the synthesis section and pure B is obtained as the second product.

A simple model consisting of total and component material balances was implemented in MATLAB. Sharp splits are assumed for the columns and the extend of reaction is calculated according to Eq. (3.14). A first basic design was obtained and used as initial guess for the optimization in GAMS. The optimization model extends the MATLAB model with calculations of the number of stages and minimum reflux according to the FUGK design method (see appendix B.1 for details). The objective function to be minimized reads

$$\min \left(w_1 \sum_{k=1}^{5} N_k + w_2 \sum_{k=1}^{5} r_k \right)$$

with the number of stages N_k and the reflux ratios r_k for all columns. Choosing the weights $w_1 = 1$, $w_2 = 10$ and thus focusing on operating costs rather than investment costs, delivers the results shown in Tables 3.15 and 3.16.

It should be mentioned that the optimal solution was rather difficult to find, several subsystems had to be solved creating new initial conditions before the final solution was obtained. Furthermore, one should keep in mind that the result is a local optimal solution as the optimization algorithm cannot guarantee the global optimum to a nonlinear programming (NLP) problem. In this optimal solution all available amount of C is fed to the first reactor R1 and none to R2, even though the initial values distributed this feed. Thus, reactor R2 is used for "fine tuning" after the removal of D in column C1. In or-

	N_{min}	N	r	V	F	D	B
C1	30	56	1.6	12.1	4.97	4.67 $(x_3 = 0.85)$	0.30 $(x_4 = 1)$
C2	30	61	8.8	6.1	4.60	0.63 $(x_1 = 0.96)$	3.97 $(x_3 = 0.98)$
C3	29	54	1.5	9.8	3.97	3.89 $(x_3 = 1)$	0.08 $(x_4 = 1)$
C4	30	53	4.9	2.2	1.33	0.38 $(x_2 = 1)$	0.96 $(x_4 = 0.53)$
C5	10	21	2.6	1.4	0.96	0.38 $(x_3 = 0.99)$	0.58 $(x_4 = 0.88)$

Table 3.15: Design parameters and operating conditions for the conventional process. N_{min}...minimum number of stages, N...actual number of stages, r...reflux ratio, V...internal vapor flow rate, F...feed flow rates, D...distillate flow rates, B...bottom flow rates.

	n_R	F_1		F_2		F_3		P	
R1	200	1.00	(F_{in})	3.89	(D_3)	0.38	(D_5)	4.97	$(x_2 = 0.021)$
R2	200	4.67	(D_1)	0	(D_3)	0	(D_5)	4.60	$(x_2 = 0.006)$
R3	200	0.30	(B_1)	0.08	(B_3)	0.58	(B_5)	1.33	$(x_2 = 0.281)$

Table 3.16: Design parameters and operating conditions for the conventional process. n_R...reactor holdup, F_k...feed flow rates, P...reactor product flow rate.

der to increase the conversion of B, more than ten times its amount is provided by the recycles of C. This leads to large column loadings and the overall total vapor produced in the column reboilers sums up to 31.6, compared to product flow rates of 0.6 of A and 0.4 of B. A detailed simulation with tray-by-tray models might result in smaller columns and reduced flow rates. But high investment and operating costs will remain the essential characteristics of this process scheme.

RDC process

As an alternative to the expensive conventional process, a realization with reactive distillation columns is considered in this section. Fig. 3.45 in section 3.2.3 shows the optimal design for the production of a heavy boiling component from lighter ones. The ability of RDC processes to overcome chemical equilibrium limitations is a big advantage in the current quaternary system. With a suitable configuration it is possible to obtain both pure intermediate D as well as pure product A from a single RDC, fed with the fresh feed A/B and the recycle of C. For the decomposition of D a suitable configuration is shown in Fig. 3.39. In contrast to the synthesis of D, two columns are necessary for its decomposition

due to the reactive azeotrope as discussed in detail in section 3.2.3. Coupling these two parts results in the process scheme shown in Fig. 3.61. A rigorous tray-by-tray model of this process was implemented in GAMS with binary decision variables indicating the feed trays. Like in the ternary examples, the reaction zones are modeled by continuous variables, in order to reduce the number of binary variables.
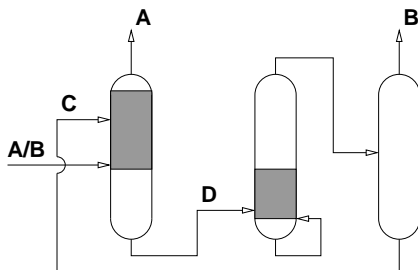

Figure 3.61: RDC process for the reactive separation of the closely boiling components A and B.

The resulting mixed-integer nonlinear programming (MINLP) problem was solved in several stages minimizing the amount of vapor as a measure for the energy consumption. Fig. 3.62 shows the mole fraction profiles of the three columns. The operating conditions are summarized in Table 3.17.
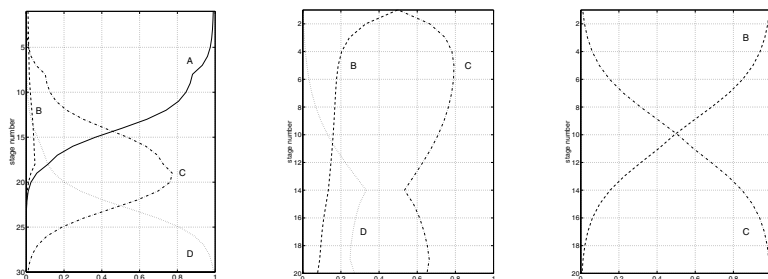

Figure 3.62: RDC process for the reactive separation of the closely boiling components A and B – liquid mole fraction profiles.

It is easily seen that B and C are fully converted in the first RDC, i.e. they are fed in a stoichiometric ratio. The large C to B ratio, which is necessary in the RDC process as

97

column	r	V	N	N_{rx}	N_F	component	purity
formation	8.5	8.5	30	2–18	8 / 18	A	0.99
decomposition	1.6	2.1	20	14–20	14		
separation	4.6	2.2	20	—	11	B	0.99

Table 3.17: Operating conditions for the coupled RDC system with nonreactive separation column. r...reflux ratio, V...vapor flow rate N...number of stages, N_{rx}...reactive section (counting from the top), N_F...feed stage.

well, is produced by an internal recycling stream ($V = 8.5$). The overall energy consumption in terms of vapor flow rates of the RDC process sums up to roughly a third of that of the conventional process. The savings in investment costs are even more impressive: two reactors (R1, R2) and three distillation columns (C1, C2, C3) are replaced by a single RDC! Being well aware of the limitations of a single case study, the potential of RDC processes to solve difficult separation problems is clearly demonstrated. In the following, the applicability of RDC process to real world problems is considered.

3.3.3   Reactive Separation by Etherification

As an example, consider the task of separating the reactive component isobutene (iB) from a mixture of inert C_4 hydrocarbons, represented by 1-butene (nB). Among the various possible reaction systems the etherification of isobutene with methanol (MeOH) to form methyl *tert*-butyl ether (MTBE) is chosen,

$$iB + MeOH \rightleftharpoons MTBE.$$

This system has been well investigated and is one of the industrially established reactive distillation processes (see [50] and references therein). Several process configurations for MTBE synthesis in a RDC are reported in literature [61, 65]. For the decomposition of MTBE in a RDC only two process descriptions are available in the patent literature. However, neither of these two processes matches the requirements of a coupled process scheme as proposed in Fig. 3.59.

Gabel et al. [27] describe the decomposition of MTBE in a RDC. The reaction zone is located in the lower part of the column. Very high purity isobutene is only obtained if water is used as an extracting agent, otherwise the isobutene/methanol azeotrope is obtained as the top product. This corresponds to the computational results of the residue

curves for the ternary system isobutene/methanol/MTBE (Figs. 2.2 and 3.63). Methanol leaves the system together with water in a side draw and together with MTBE in the bottom product stream. The authors claim that in the presence of water and the given operating conditions no byproducts (diisobutene or dimethyl ether) are produced. The experiments were performed in a pilot scale column at a pressure of 5 bar with a pure MTBE feed (> 99.9% wt).

Smith [60] had patented a different process for the decomposition of MTBE in a RDC. The reaction zone is located in the lower portion of the column with the feed at the upper end of the reaction zone. Data for different MTBE feed stocks and different pressures (4.8 and 5.5 bar) are given. The top product isobutene concentrations vary in the range of 96.5 to 99.6%. It is not clear from the description how the isobutene/methanol azeotrope can be broken under the given operating conditions to achieve such high purity isobutene products. A mixture of methanol and MTBE leaves the column in the bottom product stream. Thus there is no complete conversion of MTBE. No byproduct formation is reported.

Up to now there was no need to decompose MTBE in large quantities as it was sold as a fuel additive due to its octane enhancing property. But having in mind the current discussion on the environmental impacts of MTBE and its ban in the U.S.A., the question of MTBE decomposition in an economical way is arising. Furthermore, the separation of isobutene from a C_4 cut is an important issue. Both isobutene as well as 1-butene are valuable starting materials for further syntheses like polymerizations or copolymerizations, e.g. the formation of butyl rubber. Accordingly, an efficient process for the separation of these isomers is of high practical interest.

The following case study is to be seen as a feasibility study based on numerical simulations rather than a design for direct application. The mathematical model used for simulation is taken from Mohl [43] and includes the following assumptions:

- tray column with equilibrium stages
- vapor-liquid equilibrium according to UNIQUAC and UNIFAC (For those binary pairs of components where UNIQUAC parameters are not available the activity coefficients are estimated by the UNIFAC approach [30, 35].)
- reaction in the liquid phase only
- quasihomogeneous reaction kinetics [52] with modifications for low methanol concentrations according to [44]
- constant pressure over the column
- fluid dynamics ignored

Basic physico-chemical behavior

To develop a feasible column configuration the physico-chemical behavior of the system (isobutene/1-butene)/methanol/MTBE is considered. *Residue curve maps* (RCM) or phase portraits provide a valuable tool to determine possible column product regions. These concepts are explained in section 2.2 in more detail. RCM for a simple distillation process are the solutions to the following initial value problem

$$\frac{dx_i}{d\tau} = x_i - y_i, \quad x_i(0) = x_{i0}, \quad i = 1(1)nc - 1 \tag{3.15}$$

and thus the trajectories of the liquid compositions in an open evaporation process. In the following figures filled and non-filled circles denote the stable and unstable nodes of the trajectories, corresponding to possible bottom and top products for a distillation column. Squares denote saddle points. Fig. 3.63 shows the RCM at a pressure of 6 bar for the nonreactive system. A distillation boundary, connecting the two nonreactive binary azeotropes isobutene/methanol (unstable node) and methanol/MTBE (saddle), devides the concentration diagram into two distinct distillation regions. The possible bottom product of a distillation column with a feed in the lower distillation region is pure MTBE (stable node) whereas a possible bottom product with a feed in the upper region is pure methanol (stable node). In both cases the single unstable node and thus a possible top product is the isobutene/methanol azeotrope. Pure isobutene (saddle) can not be obtained as a product in a nonreactive distillation column.

The behavior of the system changes considerably if the chemical reaction takes place simultaneously to the vapor-liquid separation. Eq. (3.15) is extended by the reaction term leading to

$$\frac{dx_i}{d\tau} = (x_i - y_i) + Da \frac{k_f(T)}{k_{f,ref}} \nu_i r_0^*(\mathbf{x}, T). \tag{3.16}$$

The Damköhler number

$$Da = \frac{m_{cat} \, q/V}{1/k_{f,ref}}$$

is used to measure the extent of reaction. Considering a simple batch distillation, m_{cat} denotes the amount of catalyst in the still, q is the amount of acid groups on the resin, V corresponds to the vapor flow rate and $k_{f,ref}$ is a reference forward reaction rate calculated at $T = 333$ K. m_{cat} and V are held constant, resulting in an autonomous model as discussed in Venimadhavan et al. [77]. Thiel et al. [72] demonstrated the importance of a suitable reaction representation by comparing the homogeneous with the heterogeneous reaction kinetics. The qualitative behavior is the same for both cases but quantitatively the results
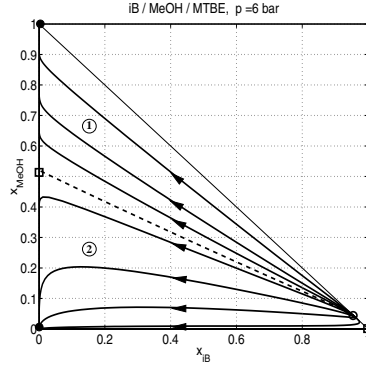
Figure 3.63: Residue curve map for the nonreactive system isobutene/methanol/MTBE at a pressure of 6 bar.

differ significantly, influencing also the fixed points obtained for a certain Damköhler number.

As shown in section 2.2.6, the fixed points of the rectifying section of an RDC have to be calculated by the rectifying flash cascade.

$$\frac{dx_i}{d\tau} = (x_i - y_i) - Da \, \frac{k_f(T)}{k_{f,ref}} \, \nu_i \, r_0^*(\mathbf{x}, T). \tag{3.17}$$

Eqs. (3.16) and (3.17) only differ in the sign in front of the reaction term. But this distinction allows to obtain physically meaningful fixed points for the top and bottom products for all extents of reaction.

Fig. 3.64 shows the phase portrait for the reactive system with a Damköhler number $Da = 0.002$ at a pressure of 6 bar. The starting points are given at $x_{iB} = 0.4$ with different values of x_{MeOH}. The trajectories are calculated with different flash cascade equations. For the rectifying section, Eq. 3.17 is used with negative time τ, whereas for the stripping section, Eq. 3.16 is used with positive time τ.

For this relatively low Damköhler number there exist two stable nodes, two unstable nodes and two saddles, giving rise to three different distillation regions:

- Starting with a feed in the upper region, pure methanol is a possible bottom product whereas a ternary mixture of mainly isobutene is a possible top product. This *kinetic*
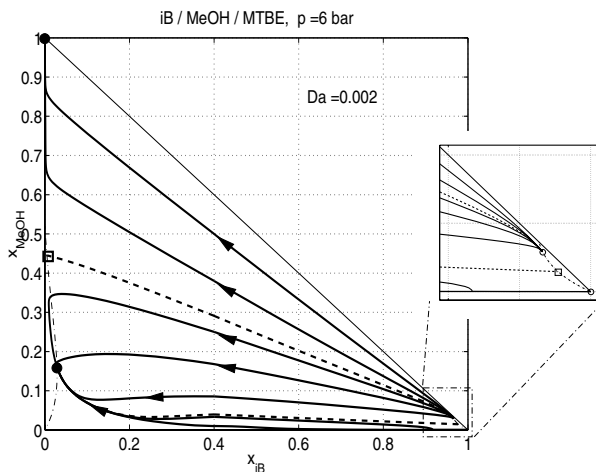
101

Figure 3.64: Residue curve map for the reactive system isobutene/methanol/MTBE at a pressure of 6 bar and a Damköhler number of $Da = 0.002$.

    azeotrope results from the movement of the nonreactive binary azeotrope into the composition triangle as the Damköhler number is increased. Figs. 3.65 and 3.66 show this behavior in more detail.

- The top product of the middle region is the same as for the top region. However, the bottom product changes from pure MTBE in the nonreactive case to a *kinetic azeotrope* consisting of mainly MTBE and methanol (• in Fig. 3.64).

- The lowest distillation region has the same possible bottom product as in the previous case but the top product changes to pure isobutene. In contrast to the nonreactive case a pure isobutene product is possible here as the saddle point moves into the composition triangle.

As expected from Figs. 3.65 and 3.66 the behavior of the system changes for higher Damköhler numbers. For $0 < Da \leq 0.00258$ the phase diagram is qualitatively the same as shown in Fig. 3.64. For $0.00258 < Da \leq 0.00435$ the kinetic azeotrope near pure isobutene vanishes leading to a single unstable node of pure isobutene.
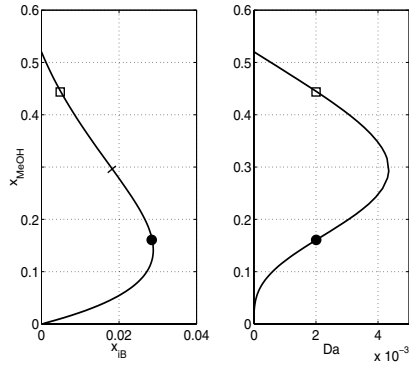
Figure 3.65: Kinetic azeotropes for low isobutene concentrations. Left: mole fraction diagram; right: x_{MeOH} depending on the Damköhler number Da. $\square$ . . . saddle, $\bullet$ . . . stable node.
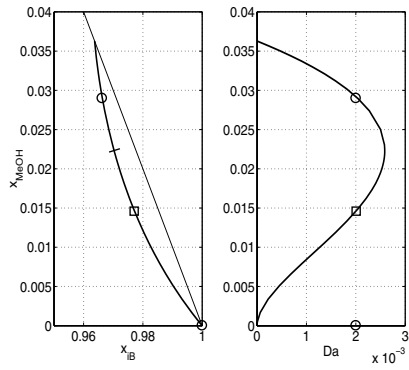

Figure 3.66: Kinetic azeotropes for high isobutene concentrations. Left: mole fraction diagram; right: x_{MeOH} depending on the Damköhler number Da. $\square$ . . . saddle, $\circ$ . . . unstable node.

For $Da > 0.00435$ the MTBE rich kinetic azeotrope disappears, too. This case is shown in Fig. 3.67 for $Da = 0.0045$. As can be seen, the distillation boundaries have disappeared and the only fixed points are pure isobutene (unstable node) and methanol (stable node).
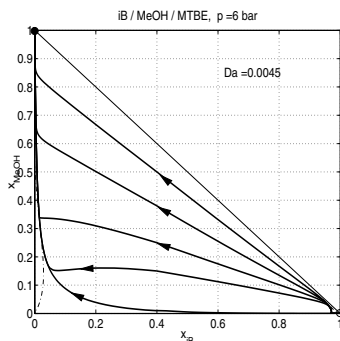

Figure 3.67: Residue curve map for the reactive system isobutene/methanol/MTBE at a pressure of 6 bar and a Damköhler number of $Da = 0.0045$.

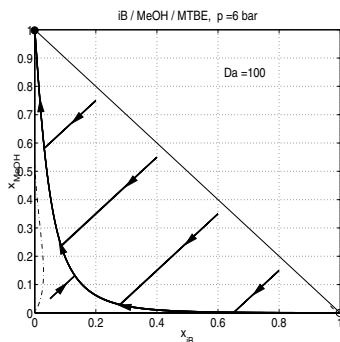Figure 3.68: Residue curve map for the reactive system isobutene/methanol/MTBE at a pressure of 6 bar near reaction equilibrium.

Increasing the Damköhler number to a very high value means that the reaction system is approaching chemical equilibrium. This situation is shown in Fig. 3.68. The fixed points are still isobutene and methanol but the trajectories directly point towards the equilibrium curve.

Conceptual design

Even though the previous trajectories are calculated for a flash cascade, they indicate the possible products and concentration profiles for a (reactive) distillation column. The design of a MTBE formation column is well known in literature. Therefore, the focus here is on the design of the MTBE decomposition column. Considering the phase portraits shown above, it is obvious that in order to obtain pure products isobutene and methanol, the reaction zone must be located in the rectifying section starting right at the top tray. It is not necessary to provide a fully catalytic column but the reaction zone must be long enough to cross the nonreactive distillation boundary. Furthermore, the amount of catalyst provided must be large enough to avoid kinetic azeotropes.
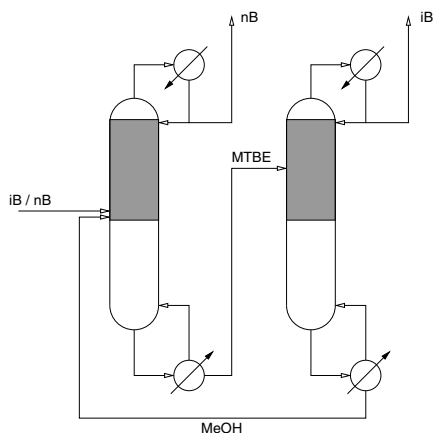

Figure 3.69: Coupled reactive distillation columns for isobutene/1-butene separation.

Fig. 3.69 shows the basic process of isobutene/1-butene separation in two coupled reactive distillation columns. The butene mixture is fed to the first RDC, denoted the *formation column* hereafter. The upper part of this column is filled with acidic ion-exchange resins as catalyst. The stripping section is nonreactive. Isobutene and methanol react to MTBE in the catalytic section as can be seen from the composition profiles in Fig. 3.70. The inert component 1-butene is withdrawn as the top product whereas MTBE is obtained in high purity in the bottom of the column. This bottom product stream is fed to the second column, the *decomposition column*. The latter is identical to the formation column with

the exception of a different feed tray position. In this column MTBE is decomposed into isobutene which is obtained as the top product and the reactive entrainer methanol. The heavy boiling methanol is withdrawn as the bottom product stream and is recycled to the formation column. For this simulation study the following data are used: butenes feed rate $F = 13.8$ mol/h, with a mole fraction of isobutene of $z_{iB} = 0.3$. The column pressures are $p = 11.14$ bar and the volume of the catalytic packing corresponds to 0.266 liters for every reactive stage.
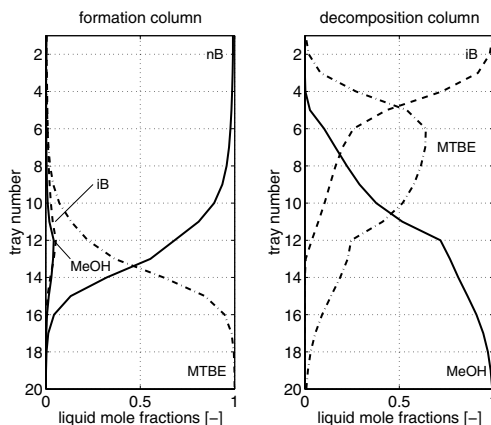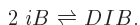

Figure 3.70: Coupled reactive distillation columns for isobutene/1-butene separation: Composition profiles (with closed methanol recycle).

If one compares the MTBE system (Figs. 3.69, 3.70) with the ideal system (Figs. 3.61, 3.62), the similarities in the formation column (MTBE and D respectively) are striking. Even though the physico-chemical properties of these systems are totally different, their input-output behavior is nearly identical. Comparing the decomposition of MTBE and D, respectively, provides interesting insights. One would expect that realizing a RDC process for a simple ideal system is much easier than for a nonideal system with azeotropes and distillation boundaries. But on the contrary, it turns out that this complex VLE behavior of the MTBE system allows to realize this coupled RDC process with only two columns. The main advantage of this system is the ability to cross the distillation boundary, enabling to obtain both products isobutene and methanol as fixed points of the column.

The process configuration and the profiles shown so far represent the ideal case where a complete conversion of the reactants to the desired products can be achieved. Unfortunately, this is only part of the truth for most real systems, as it is for the system considered here. Besides the desired etherification reaction, two important side reactions have to be taken into account. The first side reaction is the isobutene dimerization forming diisobutene (a mixture of the isomers 2,2,4-trimethyl-1-pentene and 2,2,4-trimethyl-2-pentene) [31, 68],

$$2 \ iB \rightleftharpoons DIB.$$

The second side reaction is the methanol dehydration forming dimethyl ether and water [62],

$$2 \ MeOH \rightleftharpoons DME + H_2O.$$

Taking into account these two side reactions the process is infeasible for the design and the operating conditions chosen above as can be seen in Fig. 3.71. To calculate the profiles of the formation column, the recycle from the decomposition column is opened and the methanol feed is fixed at its nominal values taken from the ideal case above.
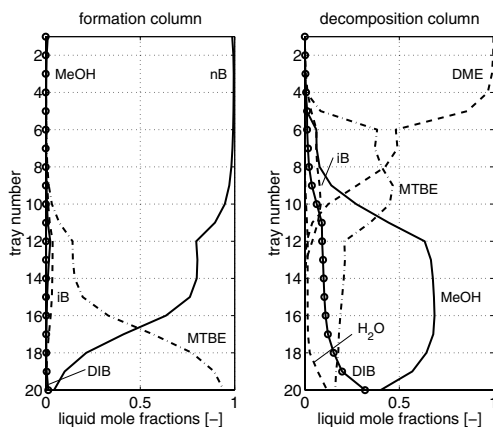

Figure 3.71: Coupled reactive distillation columns for isobutene/1-butene separation: Composition profiles for the system with side reactions (recycle opened, fixed methanol feed to the formation column).

The formation column is merely affected by the side reactions, only a small amount of di-isobutene is formed. But in the decomposition column, the isobutene from MTBE decomposition is completely converted to DIB and large amounts of dimethyl ether and water are formed. Remedies to this undesired behavior are the reduction of the column pressure and hence a column temperature reduction and a drastical reduction of the amount of catalyst in the decomposition column. With a modified design and under suitable operating conditions pure isobutene can be obtained as the top product of the decomposition column. The methanol dehydration is nearly suppresssed and a small amount of DIB is formed. As DIB is a heavy boiling component it enriches in the lower part of the decomposition column together with methanol. In order to be able to close the methanol recycle to the formation column, DIB must be removed from the system. The direct DIB/methanol separation following the decomposition column is not recommendable as these components form an azeotropic mixture. However, it is possible to close the recycle and remove the side product DIB with modest effort. In the following, two alternative process schemes are proposed.

Coupled column system – solution 1

The first feasible process configuration is shown in Fig. 3.72. The recycle stream containing both methanol and DIB is fed to the formation column. Methanol is converted to MTBE which leaves the column in the bottom product stream together with DIB. In contrast to methanol, MTBE forms a nearly ideal mixture with DIB which can be separated in a nonreactive distillation column very easily. The DIB is withdrawn in very high purity for further use whereas MTBE is fed to the decomposition column. A slight external methanol makeup stream is necessary because of the methanol losses through its dehydration.

The corresponding composition profiles for this process are shown in Fig. 3.73. As can be seen the product streams of this process consist of pure 1-butene at the top of the formation column, pure isobutene at the top of the decomposition column and high purity diisobutene at the bottom of the nonreactive separation column. Table 3.18 summarizes the operating conditions for a simulated laboratory scale column system at a constant pressure of 6 bar.
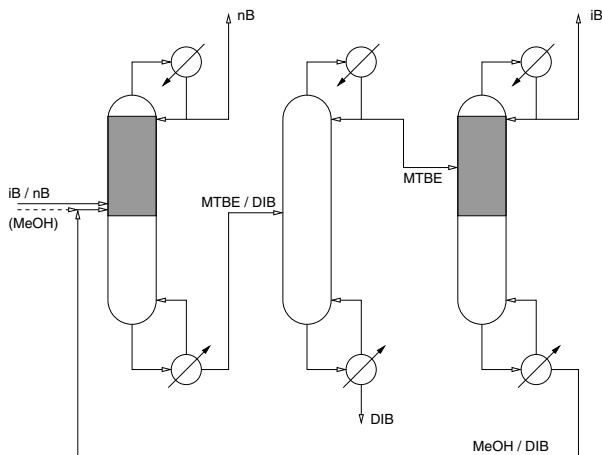
Figure 3.72: Coupled column system with removal of the side product diisobutene in a nonreactive separation column.

Feed conditions

feed	F [mol/h]	T_F [K]	
methanol (makeup)	0.05	390.8	
butenes	13.79	323.0	$z_{iB} = 0.3$

Column design and product purities

column	r	Q [W]	p [bar]	N	N_F	N_{rx}	v_{cat} [l]	component	purity
formation	5.9	371	6	30	12	2–12	0.25	1-butene	0.994
separation	2.0	67	6	30	12	—	—	diisobutene	0.999
decomposition	23.5	439	6	50	10	2–20	0.003	isobutene	0.991

Table 3.18: Operating conditions for the coupled column system with nonreactive diisobutene separation column. r... reflux ratio, Q... reboiler duty, N... number of stages, N_F... feed stage, N_{rx}... reactive section (counting from the top), v_{cat}... amount of catalyst per stage.
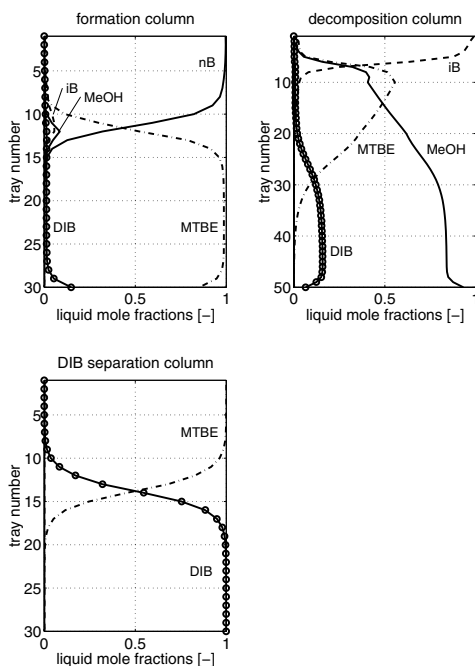
Figure 3.73: Composition profiles of the process scheme in Fig. 3.72.

Coupled column system – solution 2

The composition profiles of the formation column show that there is a region with a very high MTBE concentration in the stripping section. Exploiting this fact leads to a second solution shown in Fig. 3.74. Providing a vapor side draw pure MTBE can be withdrawn from the formation column resulting in a high purity DIB bottom product stream. Apart from the fact that MTBE is fed to the decomposition column as a vapor stream the remainder of this process configuration is identical to the previous process.

Fig. 3.75 shows the composition profiles for this configuration. Again, the three products 1-butene, isobutene and diisobutene are obtained in high to very high purity. The energy costs are comparable to those of the first solution but here only two columns are needed.
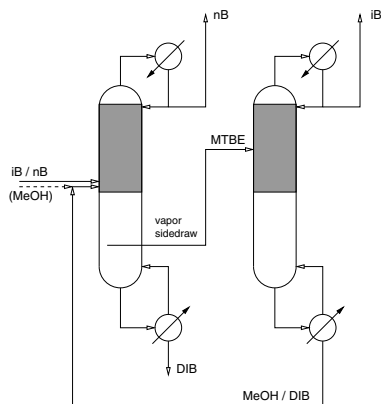
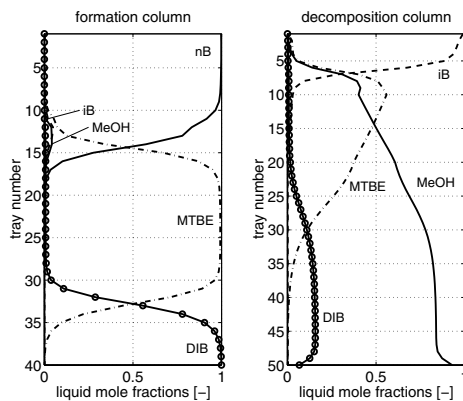Figure 3.74: Coupled column system with a MTBE vapor side draw.

Figure 3.75: Composition profiles of the process scheme in Fig. 3.74.

Approximation by an ideal system

The process simulation and optimization of the above proposed coupled column system turned out to be a very difficult task, mainly because of the size and complexity of the mathematical models. Hence, first attempts were made to develop simplified models which can be used for a preliminary design. The highly nonlinear vapor-liquid equilibrium correlations are promising candidates for model simplifications as they cause problems during the optimization calculations. In the following it is investigated how the nonideal VLE might be approximated by ideal VLE descriptions with the nonreactive ternary system isobutene/methanol/MTBE as an example. Fig. 3.63 shows the corresponding residue curve map where an ideal vapor phase and a nonideal liquid phase is assumed, resulting in the following equation

$$0 = y_i \, p - x_i \, \gamma_i \, p_{i,s}, \qquad i = 1(1)nc - 1 \tag{3.18}$$

where nc is the number of components. The saturation pressure $p_{i,s}$ is calculated with the Antoine equation

$$\log_{10}(p_{i,s}) = a_{1i} + \frac{a_{2i}}{T - a_{3i}} \tag{3.19}$$

and the liquid activity coefficients γ_i by the UNIQUAC correlation

$$\ln(\gamma_i) = \ln(\gamma_i^C) + \ln(\gamma_i^R) \tag{3.20}$$

$$\ln(\gamma_i^C) = \ln(\Psi_i/x_i) + l_i + \frac{z}{2} \, q_i \, \ln(\theta_i/\Psi_i) - (\Psi_i/x_i) \sum_{k=1}^{nc} (x_k \, l_k) \tag{3.21}$$

$$\ln(\gamma_i^R) = q_i \left(1.0 - \ln \left(\sum_{k=1}^{nc} (\theta_k \, \tau_{k,i}) \right) - \sum_{k=1}^{nc} \left(\frac{\theta_k \, \tau_{i,k}}{\sum_{m=1}^{nc} (\theta_m \, \tau_{m,k})} \right) \right) \tag{3.22}$$

where θ_i and Ψ_i depend on the composition $\mathbf{x}$, $\tau_{i,j}$ are functions of the temperature T and q_i, r_i, l_i are component-specific constants.

Following the argumentation of Vogelpohl [79], this rather complex description of the nonideal system with two azeotropes and a distillation boundary can be approximated by the much simpler description of two separate ideal systems. Assuming a constant pressure p and *constant relative volatilities* α_i, the set of equations (3.18) to (3.22) reduces to

$$y_i^* = \frac{\alpha_i \, x_i^*}{1 - \sum_{k=1}^{nc^*-1} ((\alpha_k - 1) \, x_k^*)}, \qquad i = 1(1)nc^* - 1. \tag{3.23}$$

The number of components of the ideal system nc^* is larger than the original nc as the binary azeotropes have to be defined as pseudo-components. Starting with the lowest boiling (pseudo-)component the following new components are obtained

1 . . . azeotrope isobutene/methanol
2 . . . isobutene
3 . . . azeotrope methanol/MTBE
4 . . . methanol
5 . . . MTBE

The unknown parameters α_i are fitted to the binary VLE data computed with the detailed model for a constant pressure of 6 bar. Figs. 3.76 to 3.78 show the original profiles (dashed lines) compared to the approximation with the ideal system (solid lines). The fitted values are

$$\boldsymbol{\alpha} = [\alpha_{14}, \alpha_{34}] = [35.0, 2.6]$$

for the upper distillation region (pure methanol, Fig. 3.63) and

$$\boldsymbol{\alpha} = [\alpha_{15}, \alpha_{25}, \alpha_{35}] = [8.55, 5.7, 2.85]$$

for the lower distillation region (pure MTBE, Fig. 3.63) with $\alpha_{15} = \alpha_{12} \, \alpha_{25}$.
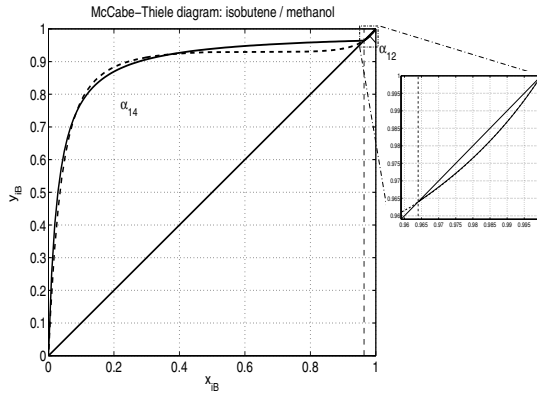

Figure 3.76: System isobutene/methanol, fitted values: $\alpha_{14} = 35.0$, $\alpha_{12} = 1.5$

Denoting the pseudo-components by the superscript "id", the transformation from pseudo-components to original components is given by

$$
\begin{aligned}
x_{iB} &= x_{iB,az12} \cdot x_1^{id} \\
x_{MTBE} &= x_{MTBE,az23} \cdot x_3^{id} \\
x_{MeOH} &= 1 - x_{iB} - x_{MTBE}
\end{aligned}
$$
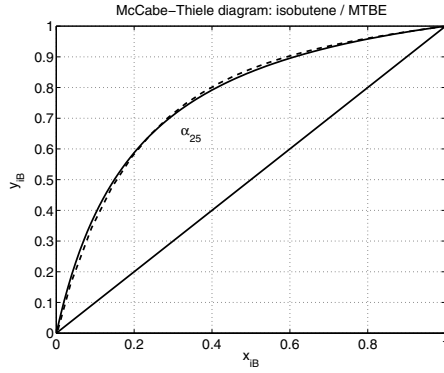
Figure 3.77: System isobutene/MTBE, fitted values: $\alpha_{25} = 5.7$
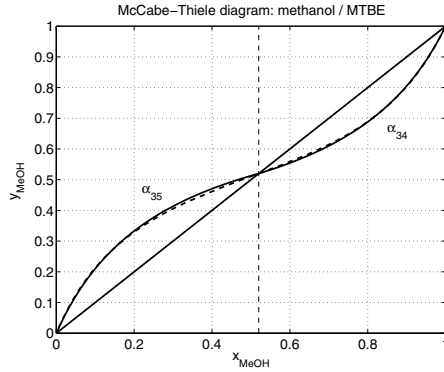
Figure 3.78: System methanol/MTBE, fitted values: $\alpha_{35} = 2.85$, $\alpha_{34} = 2.6$

for the upper distillation region and

$$
\begin{aligned}
x_{iB} &= x_{iB,az12} \cdot x_1^{id} + x_2^{id} \\
x_{MeOH} &= x_{MeOH,az12} \cdot x_1^{id} + x_{MeOH,az23} \cdot x_4^{id}
\end{aligned}
$$

for the lower distillation region. $x_{i,az12}$ are the original mole fractions of the azeotrope isobutene/methanol and $x_{i,az23}$ the corresponding values for the azeotrope methanol/MTBE.

114

Fig. 3.79 shows a comparison of residue curve maps calculated by the nonideal VLE correlation (dashed lines) with the ideal system approximation (solid lines). Even though there are quantitative differences in the trajectories, the qualitative agreement is excellent. Hence, this approach might be a valuable tool to simplify the mathematical model and ease the early process design step.

Figure 3.79: Residue curves for the ideal (solid) and the real (dashed) ternary system isobutene/methanol/MTBE.

3.3.4   Reactive Separation by Hydration

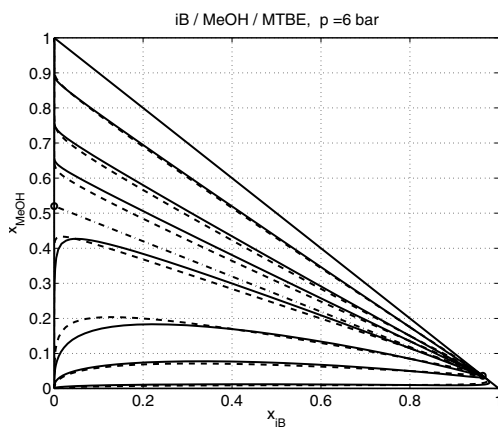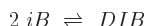The second example consideres the same separation task, the separation of isobutene and 1-butene. But in this case a different reaction scheme is applied, the hydration of isobutene to *tert*-butyl alcohol (TBA)

$$iB + H_2O \; \rightleftharpoons \; TBA.$$

This reaction system is similar to the previous case study with respect to the same side product diisobutene

$$2\,iB \; \rightleftharpoons \; DIB$$

but it widely differs in its vapor-liquid behavior as this aqueous system exhibits large miscibility gaps leading to a liquid-liquid phase split. The physico-chemical properties will be discussed in more detail below. In contrast to the previous example, in this case the TBA decomposition in a RDC is an established concept, in literature as well as in industrial practice. However, there is only little information available on a RDC process for TBA formation.

TBA formation and dehydration processes in literature

Smith [61] patented a RD process for the production of TBA. Experimental data are provided for a column operated at 11.4 bar with an isobutene/water feed ratio of roughly 1/2. The formation of some side-product diisobutene is reported. It is claimed that the catalytic section should be wetted by a patented liquid level strategy in order to assure high selectivity to TBA.

Sakuth and Peters [55] patented a RD process for TBA dehydration. They use a partial condenser to obtain a vapor product stream of high purity isobutene. Experimental data of a column operated at 2.8 bar are given. TBA is not completely converted to isobutene and water. The same process is explained in more detail in a recent paper by Tuchlenski et al. [73].

Knifton et al. [37] patented a RD process for the dehydration of TBA. They provide experimental data for different feed specifications and operating conditions. But in all cases TBA is not converted completely.

Abella et al. [2] investigated the TBA dehydration experimentally in a laboratory scale RDC. They showed that for pressures ranging from 0.7 to 1.01 bar complete conversion of TBA can be achieved. A kinetic expression from CSTR experiments is given for TBA

dehydration with water inhibition. The authors claim that one advantage of the RDC process is to overcome this product (water) limitation. The backward reaction – formation of TBA – is not taken into account.

Physico-chemical properties

Reaction kinetics and chemical equilibrium are calculated according to Velo et al. [76] for the main reaction and to Haag [31] for the side reaction. Haag considers an inhibition by methanol but in the system under consideration methanol is not present. As water and methanol adsorb similar to the catalyst considered here, the same kinetic expression is used with water replacing methanol.

$$\text{(main reaction)} \qquad r_{0,1} \;=\; k_{f,1} \,\frac{c_1\, c_2 - c_3/K_{eq,1}}{(1 + K_A\, c_3)} \qquad \text{[kmol/(eq·s)]}$$

$$\text{(side reaction)} \qquad r_{0,2} \;=\; k_{f,2} \,\frac{a_1^2}{a_1 + K_{rel}\, a_2} \qquad \text{[kmol/(eq·s)]}$$

with $k_{f,j}$, $K_{eq,1}$ and K_A dependent on the temperature T. Note that $r_{0,1}$ is formulated in concentrations c_i and $r_{0,2}$ is formulated in activities $a_i = x_i\,\gamma_i$. The component indices correspond to the following species

1 ... isobutene
2 ... water
3 ... *tert*-butanol
4 ... 1-butene
5 ... diisobutene

Tejero et al. [70] investigated the formation of byproducts during the etherification of isopropanol with isobutene. One of their observations is that TBA formation is much faster than DIB formation. The same result is obtained in numerical studies with the kinetic expressions shown above.

The system *butenes/water/TBA/DIB* is very nonideal, several binary azeoptropes and large miscibility gaps are known. As experimental data for the whole system are not available and thus complete data sets for VL(L)E correlations are lacking, the following simulations are based on the Modified UNIFAC prediction of activity coefficients. The data provided

by Gmehling et al. [30] are used. Antoine parameters are taken from the Dortmund Data Bank [18] and from Reid et al. [53] (for TBA). For two subsystems experimental LLE data are available. Fig. 3.80 shows a comparison of experimental data at different temperatures [75] with simulations based on the above mentioned assumptions for the ternary system *1-butene/water/TBA* at temperatures of 313.15 K, 373.15 K, 413.15 K and 453.15 K. It is obvious that the UNIFAC correlation is not very reliable over the whole temperature and composition range. However, if the butene concentration is rather small and the temperature, and thus pressure, is comparably high, the UNIFAC model describes the phase behavior sufficiently.
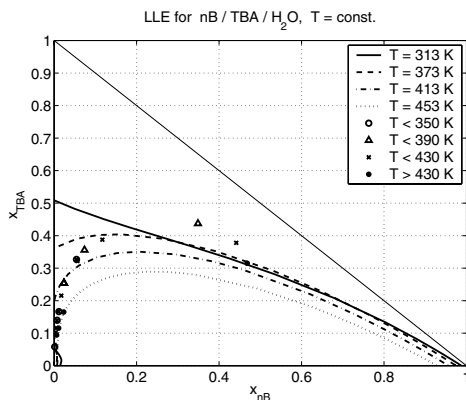
Figure 3.80: LLE of the ternary system 1-butene / H_2O / TBA at different temperatures. Simulation and experimental data.

Lee et al. [41] provide experimental LLE data for the system *water/TBA/DIB* at different constant temperatures. As can be seen in Fig. 3.81 the prediction by the model based on the UNIFAC correlation is quite good for higher DIB concentrations but it deviates from the experimental data if the DIB concentration decreases. The same behavior is observed for the remaining data sets at temperatures of 298.15 K and 318.15 K.

Column design

Taking the LLE behavior of the system into account, no phase split is expected for high temperatures, thus pressures, and very low butene concentrations. Therefore, a pressure
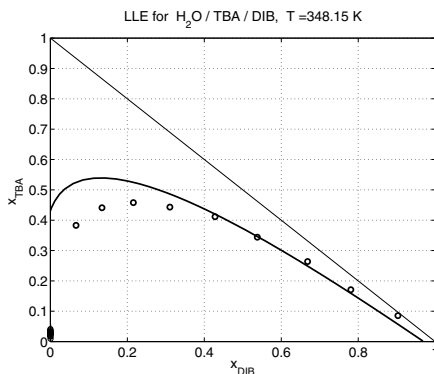
Figure 3.81: LLE of the ternary system H$_2$O / TBA / DIB at a constant temperature of 348.15 K. Simulation (—) and experimental data (o).

of 10 bar is chosen for the TBA formation column. This facilitates the contact between the main reaction partners isobutene and water. As a drawback, the byproduct diisobutene is produced in larger amounts at higher temperatures. As a consequence, this byproduct must be withdrawn from the system.

The column flowsheet is similar to that of the MTBE reactive separation system, Fig. 3.69, with the main difference that here partial condensers and decanters are used. This is due to the fact that the butenes are much more volatile than the remaining components, thus they can be separated in a partial condenser very efficiently. The remaining top product is totally condensed and split in two liquid phases, an aqueous phase and an organic phase.

Fig. 3.82 shows the configuration of this coupled process with the reaction zones inside the columns, partial condensers, decanters with different reflux strategies, partial reboilers and recycle streams. In the mathematical model no phase split is assumed inside the columns but only in the decanters. In Table 3.19 the design parameters, operating conditions and resulting product data are given. Fig. 3.83 visualizes the mole fraction profiles inside the two columns.

In a first RDC water and isobutene react to TBA which leaves the column as the bottom product together with some additional water. The product 1-butene is obtained in high purity as a vapor stream from the partial condenser. A small liquid distillate stream is withdrawn, mainly consisting of 1-butene, too.
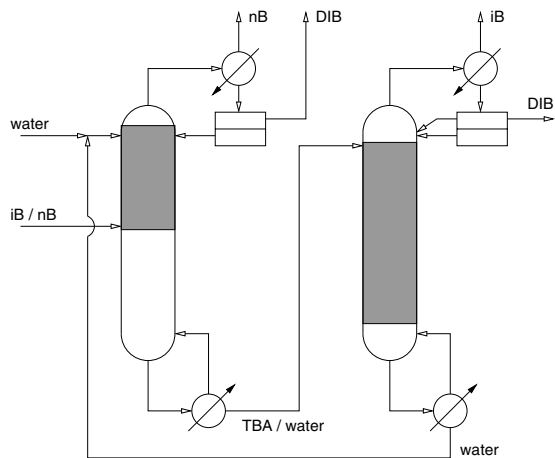
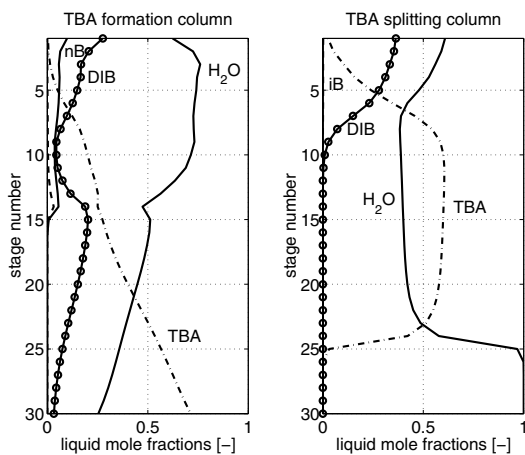Figure 3.82: Coupled column system with two partial condensers and decanters.

Figure 3.83: Composition profiles of the process scheme in Fig. 3.82.

In a second RDC, operated at 3 bar, TBA is decomposed into isobutene and water. Even though the column pressure is fairly low compared to the TBA formation column, a liquid-liquid phase split is not expected because of the in-situ removal of the highly volatile isobutene. High purity isobutene is withdrawn from the partial condenser of that column as a vapor stream. A small liquid distillate stream leaves the condenser which consists of isobutene, water, TBA and small amounts of the side product DIB.

Feed conditions

feed	F [kmol/h]	T_F [K]	
water (makeup)	0.0244	452.16	
butenes	4.1378	344.40	$z_{iB} = 0.5$

Column design

column	T_{deca}	Q [kW]	p [bar]	N	N_F	N_{rx}	v_{cat} [kg]
formation	360.0	86.3	10.0	30	2 / 14	1–14	100.0
decomposition	283.0	478.5	3.0	30	3	3–27	26.4

Product and purge flow rates of the formation column

component	V_C [kmol/h]	purity	L_{org} [kmol/h]	purity
1-butene	2.0708	0.999		
diisobutene			0.5430	0.957

Product and purge flow rates of the splitting column

component	V_C [kmol/h]	purity	L_{org} [kmol/h]	purity
isobutene	0.9358	1.000		
diisobutene			0.0455	0.971

Table 3.19: Operating conditions for the coupled column system. T_{deca}...constant decanter temperature, Q...reboiler duty, p...constant column pressure, N...number of stages, N_F...feed stages, N_{rx}...reactive section (counting from the top), v_{cat}...amount of catalyst per stage, V_C...vapor flow rate from the partial condenser, L_{org}...liquid flow rate of the organic phase from the decanter.

3.3.5 Summary

The processes proposed in these case studies combine the advantages of the reactive separation principle and the reactive distillation concept. As a first example, an ideal theoretical system is considered, demonstrating the large economical benefit of an RD realization over a conventional process configuration. The remaining two real world examples demonstrate that it is possible to reactively separate isobutene from its isomer 1-butene in two coupled reactive distillation columns. It turned out that the influence of possible side reactions has to be taken into account in order to obtain a feasible process configuration. The most important topic is the removal of heavy boiling side products in order to enable a recycle of the reactive entrainer. For this purpose, several different process configurations are proposed. In the first case study, a nonreactive separation column is provided to separate the side product. Alternatively, depending on the boiling points of the corresponding components, a vapor side draw can be used instead of the nonreactive column. In the second case study, one makes use of the liquid-liquid phase split to remove the organic side product from the aqueous phase in a decanter.

The process configurations proposed are applicable to a wide range of reactive separations, e.g. the separation of tert-olefins or cycloalkenes from their corresponding hydrocarbon mixtures:

- separation of a tert-olefin by etherification (case study 3.3.3)

$$\text{tert-olefin} + \text{alcohol} \rightleftharpoons \text{alkyl tert-alkyl ether},$$
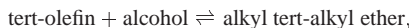
- separation of a tert-olefin by hydration (case study 3.3.4)

$$\text{tert-olefin} + \text{water} \rightleftharpoons \text{tert-alcohol},$$

- separation of a cycloalkene by esterification

$$\text{cycloalkene} + \text{carbonylic acid} \rightleftharpoons \text{carbonylic acid ester}.$$
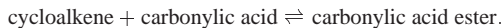
Depending on their boiling points the intermediate product or the side products are obtained at the top or the bottom of the nonreactive separation column or in the vapor side draw of the formation column, respectively. Accordingly, the liquid-liquid separation can be located at the top or the bottom of a column. In essence, economically attractive processes for the separation of closely boiling mixtures have been proposed.

Chapter 4

Conclusions

The combination of the unit operations reaction and separation in one apparatus, the reactive distillation column, shows enormous advantages for some reaction systems and is disastrous for others. The goal of this thesis is to identify criteria to decide whether reactive distillation is favorable or not for certain classes of reaction systems. First, focus is on ideal binary and ternary systems as principle mechanisms and phenomena can be examined and explained for these systems – which is not possible for real-world problems with a mess of physical properties, fittings to experimental data and so forth.

First the basics are reviewed that are necessary for a proper process design. On the one hand these are concepts like residue curve maps, reactive or kinetic azeotropes, distillation boundaries, kinetically or equilibrium controlled reactions, etc. On the other hand basic properties of mathematical modeling and optimization are briefly summarized.

The first system investigated is an ideal binary system with an isomerization reaction. Starting from the examination of basic properties like relative volatilities and reaction kinetics, different optimal processes are calculated and compared. For this simple example the transformation of principle considerations to a concrete process design is rather obvious.

The next class of examples are ideal ternary systems. Different reaction schemes are considered and it is shown how an RD process design turns from optimal to infeasible if only one physical property of the reaction system is changed. With the help of suitable mathematical modeling and MINLP optimization tools interesting inventive solutions are found for systems where reactive distillation seemed to be useless at a first glance.

The last kind of examples belong to the interesting field of reactive separation. A difficult separation task, like the separation of closely boiling mixtures, is solved by making use of the fact that one of the components to be separated reacts with a suitable reaction partner in a highly selective and reversible way. Principle properties are explained with an ideal quaternary system where the results of the previous examples can be used directly. Finally, the reactive separation scheme is investigated for the separation of the real components isobutene and 1-butene. Two different reactive entrainers are considered: The first is methanol leading to the intermediate product MTBE. In contrast to most publications on the MTBE system, the main side reactions are taken into account and it is shown that they have an essential influence on the design of this coupled process. The second reaction partner is water which leads to *tert*-butyl alcohol as the intermediate product. In this case a second liquid phase is obtained. The good news from these investigations are that the realization as a RD process saves investment costs in both cases; the bad news are that process design by rigorous mathematical modeling and optimization reaches its limits for these complex systems.

Fields of future work

The experiences with the real-world applications lead to the development of simplified models for process design purposes. First attempts were successful and should be elaborated in the future. The goal is the development of "design models" as simple as possible, as detailed as necessary. A related direction for future research is the development of models suitable for global optimization. All of the reported optimal solutions lack the confidence that there is no better solution as the available optimization algorithms are only able to determine a local optimal solution. For ideal ternary systems first attempts are promising [58].

As has been shown the optimization of the steady state design of a RD process does not guarantee that this is the best process to operate. Thus, the integration of transient behavior and process control characteristics during the design phase is a necessary extension to the proposed design procedure. One option is the formulation and solution of mixed-integer dynamic optimization problems – which is even more difficult than to solve MINLP problems. However, first approaches have been published recently [8].

Last but not least a library of reaction systems and corresponding optimal process configuration would simplify the decision which process scheme should be investigated further in the early design stage – a welcome contribution of academia to solve every-day problems in industry.

Appendix A

Model equations for a packed column

In the following, a description of the mole fractions along the height of a packed column section is derived. This leads to a mathematical model in the form of partial differential equations. For details, see Kienle [36] and references therein. The notation used in this section is summarized in the following table.

n'	holdup of the liquid phase	[kmol/m]
n''	holdup of the vapor phase	[kmol/m]
l	height of the column	[m]
z	spatial coordinate, $z \in [0, l]$	[m]
J'	liquid flow rate	[kmol/s]
J''	vapor flow rate	[kmol/s]
$r(\mathbf{x})$	reaction rate	[1/s]
$\mathbf{x}$	liquid composition	[–]
$\mathbf{y}$	vapor composition	[–]
$\mathbf{j}_a(\mathbf{x}, \mathbf{y})$	mass transfer flow rate	[kmol/m/s]
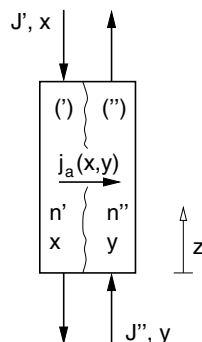
The main underlying assumptions are

- constant molar flow rates (J', J'') and holdups (n', n'')
- constant pressure over the column
- thermal equilibrium ($T' = T''$)
- no axial dispersion
- mass transfer film model with decoupled components, equimolar mass transfer and neglecting the mass transfer resistance in the liquid phase

Liquid phase

The dynamic component material balance for the liquid phase of a column section of length Δz reads

$$\frac{\partial(\Delta z\, n'\, \mathbf{x})}{\partial t} = J'\left(\mathbf{x}(z + \Delta z) - \mathbf{x}(z)\right) - \Delta z\, \mathbf{j}_a(\mathbf{x}, \mathbf{y}). \tag{A.1}$$

A Taylor series expansion for the liquid mole fractions

$$\mathbf{x}(z + \Delta z) = \mathbf{x}(z) + \frac{\partial \mathbf{x}}{\partial z}\Delta z + \dots \tag{A.2}$$

combined with Eq. (A.1) for $n' = const$ leads to

$$n'\frac{\partial \mathbf{x}}{\partial t} - J'\frac{\partial \mathbf{x}}{\partial z} = -\mathbf{j}_a(\mathbf{x}, \mathbf{y}). \tag{A.3}$$

Scaling of z, t and $\mathbf{j}_a$

$$z^* = \frac{z}{l} \qquad \rightsquigarrow \qquad \frac{1}{\partial z} = \frac{1}{l}\frac{1}{\partial z^*}$$

$$t^* = \frac{J'}{l\, n'}t \qquad \rightsquigarrow \qquad \frac{1}{\partial t} = \frac{J'}{l\, n'}\frac{1}{\partial t^*}$$

$$\mathbf{j}_a^* = \frac{l}{J'}\mathbf{j}_a$$

leads to the dimensionless form

$$\frac{\partial \mathbf{x}}{\partial t^*} - \frac{\partial \mathbf{x}}{\partial z^*} = -\mathbf{j}_a^*(\mathbf{x}, \mathbf{y}). \tag{A.4}$$

Vapor phase

Accordingly, the vapor phase component material balance for this section

$$\frac{\partial(\Delta z\, n''\, \mathbf{y})}{\partial t} = J''\left(\mathbf{y}(z) - \mathbf{y}(z + \Delta z)\right) + \Delta z\, \mathbf{j}_a(\mathbf{x}, \mathbf{y}) \tag{A.5}$$

is approximated by a Taylor series expansion of $\mathbf{y}$

$$\mathbf{y}(z + \Delta z) = \mathbf{y}(z) + \frac{\partial \mathbf{y}}{\partial z}\Delta z + \dots \tag{A.6}$$

to

$$n''\frac{\partial \mathbf{y}}{\partial t} + J''\frac{\partial \mathbf{y}}{\partial z} = \mathbf{j}_a(\mathbf{x}, \mathbf{y}) \tag{A.7}$$

with $n'' = const$. Defining the ratio of molar holdups in both phases

$$\epsilon = \frac{n''}{n'}$$

and the ratio of convective streams

$$A = \frac{J'}{J''}$$

leads to the dimensionless form

$$\epsilon \frac{\partial \mathbf{y}}{\partial t^*} + \frac{1}{A} \frac{\partial \mathbf{y}}{\partial z^*} = \mathbf{j}_a^*(\mathbf{x}, \mathbf{y}).$$

(A.8)

Mass transfer across the phase boundary
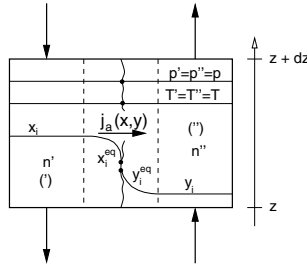
Under the assumption of equimolar mass transfer the flow rate across the phase boundary is described by

$$\mathbf{j}_a^*(\mathbf{x}, \mathbf{y}) = \frac{\mathbf{B}''}{A} \left(\mathbf{y}^{eq} - \mathbf{y} \right) = \frac{\mathbf{B}'}{A} \left(\mathbf{x} - \mathbf{x}^{eq} \right)$$

(A.9)

with dimensionless mass transfer coefficients

$$\mathbf{B}' = \frac{k'_{ik} \, a \, l}{J'}$$

and

$$\mathbf{B}'' = \frac{k''_{ik} \, a \, l}{J''}$$

and with phase equilibrium at the boundary

$$\mathbf{y}^{eq} = \mathbf{f}(\mathbf{x}^{eq}).$$

(A.10)

In general, the mass transfer coefficient matrices $\mathbf{B}'$ and $\mathbf{B}''$ are depending on the concentrations and flow rates. A simpler model can be obtained by defining mass transfer coefficients at the phase boundary

$$\mathbf{j}_a^*(\mathbf{x}, \mathbf{y}) = \frac{\mathbf{B}(\mathbf{x}, \mathbf{y})}{A}\left(\mathbf{f}(\mathbf{x}) - \mathbf{y}\right) \tag{A.11}$$

with

$$\mathbf{B}^{-1}(\mathbf{x}, \mathbf{y}) = \mathbf{B}''^{-1} + \mathbf{df_x}\mathbf{B}'^{-1}.$$

Here, $\mathbf{f}(\mathbf{x})$ is the equilibrium composition of the vapor phase and $\mathbf{df_x}$ the Jacobian matrix of the equilibrium function. If the liquid side mass transfer resistance is neglected, $\mathbf{B}$ and $\mathbf{B}''$ are identical.

Final model

Thus, the final model of a packed distillation column section results to

$$\left\{\begin{array}{rcl} \dfrac{\partial \mathbf{x}}{\partial t^*} - \dfrac{\partial \mathbf{x}}{\partial z^*} & = & -\mathbf{j}_a^*(\mathbf{x}, \mathbf{y}) \\[2mm] \epsilon\dfrac{\partial \mathbf{y}}{\partial t^*} + \dfrac{1}{A}\dfrac{\partial \mathbf{y}}{\partial z^*} & = & \mathbf{j}_a^*(\mathbf{x}, \mathbf{y}) \\[2mm] \mathbf{j}_a^*(\mathbf{x}, \mathbf{y}) & = & \dfrac{\mathbf{B}(\mathbf{x}, \mathbf{y})}{A}\left(\mathbf{f}(\mathbf{x}) - \mathbf{y}\right) \end{array}\right. \tag{A.12}$$

where $\mathbf{B}$ is a diagonal matrix according to the assumptions above.

Reactive distillation

The above developed model is valid for nonreactive systems. Assuming a single equimolar reaction in the bulk liquid phase, Eq. (A.1) is extended by a reaction term to

$$\frac{\partial(\Delta z\, n'\mathbf{x})}{\partial t} = J'\left(\mathbf{x}(z + \Delta z) - \mathbf{x}(z)\right) - \Delta z\, \mathbf{j}_a(\mathbf{x}, \mathbf{y}) + \boldsymbol{\nu}\, n'\, \Delta z\, r(\mathbf{x}) \tag{A.13}$$

Scaling of the reaction term

$$r^*(\mathbf{x}) = \frac{n'\, l}{J'}\, r(\mathbf{x})$$

leads to the final model of a packed column section for reactive distillation

$$\left\{\begin{array}{rcl} \dfrac{\partial \mathbf{x}}{\partial t^*} - \dfrac{\partial \mathbf{x}}{\partial z^*} & = & -\mathbf{j}_a^*(\mathbf{x}, \mathbf{y}) + \boldsymbol{\nu}\, r^*(\mathbf{x}) \\[2mm] \epsilon\dfrac{\partial \mathbf{y}}{\partial t^*} + \dfrac{1}{A}\dfrac{\partial \mathbf{y}}{\partial z^*} & = & \mathbf{j}_a^*(\mathbf{x}, \mathbf{y}) \\[2mm] \mathbf{j}_a^*(\mathbf{x}, \mathbf{y}) & = & \dfrac{\mathbf{B}(\mathbf{x}, \mathbf{y})}{A}\left(\mathbf{f}(\mathbf{x}) - \mathbf{y}\right) \end{array}\right. \tag{A.14}$$

Appendix B

Models for ideal ternary systems

For the design of ideal ternary systems different models are used for different purposes. In most cases, the following design procedure is applied.

- Design of the conventional process with the FUGK method.

- Optimization of different column configurations based on a steady state equilibrium stage model.

- In some cases dynamic simulations based on a dynamic equilibrium stage model.

The different models are described in the following.

B.1   FUGK shortcut method for the conventional process

The design method of Fenske-Underwood-Gilliland-Kirkbride (FUGK) for ideal multi-component distillation (e.g. [59], p. 492ff) is used for the design of the conventional process consisting of ideal reactors (CSTRs) followed by nonreactive distillation columns. Feed, distillate and bottom product specifications are given $F, \mathbf{x}_F, D, \mathbf{x}_D, B, \mathbf{x}_B$ as well as the constant relative volatility α between the key components. This method assumes an ideal split between the *light component (lk)* and the *heavy component (hk)*.

Fenske equation $\rightsquigarrow$ minimum number of theoretical stages

$$N_{min} = \log \left(\frac{x_{lk,D}}{x_{lk,B}} \frac{x_{hk,B}}{x_{hk,D}} \right) / \log(\alpha_{lk,hk})$$

Underwood equation $\rightsquigarrow$ minimum reflux ratio

$$R_{min} = \left(\frac{x_{lk,D}}{x_{lk,F}} - \alpha_{lk,hk} \frac{x_{hk,D}}{x_{hk,F}} \right) / (\alpha_{lk,hk} - 1)$$

Choose an actual value of the reflux ratio, e.g.

$$R = R_{fac} R_{min} \qquad \text{with} \qquad R_{fac} \in \{1.05 \ldots 1.5\}$$

Gilliland correlation $\rightsquigarrow$ actual number of stages

$$X = \frac{R - R_{min}}{R + 1}$$

$$Y = 1 - \exp\left(\frac{(1 + 54.4\,X)\,(X - 1)}{(11 + 117.2\,X)\,\sqrt{X}} \right)$$

$$N = \frac{N_{min} + Y}{1 - Y}$$

Kirkbride equation $\rightsquigarrow$ feed-stage location (counting from the top)

$$\frac{N_R}{N_S} = \left(\frac{B}{D} \frac{x_{hk,F}}{x_{lk,F}} \left(\frac{x_{lk,B}}{x_{hk,D}} \right)^2 \right)^{0.206}$$

$$N_F = N \frac{N_R/N_S}{1 + N_R/N_S}$$

These equations are applicable to a single distillation column. In order to obtain an overall optimal process, the Fenske, Underwood and Gilliland correlations are used together with material balances around the reactors and columns in the optimization tool GAMS. In general, the objective function to be minimized reads

$$\min\left(w_1 \sum_{k=1}^{ncol} N_k + w_2 \sum_{k=1}^{ncol} R_{fac,k} R_{min,k} D_k \right)$$

where $ncol$ is the number of columns D_k denotes the corresponding distillate flow rate. The factors w_1 and w_2 put weights on the different parts of the objective functions. In most cases, $w_2 \gg w_1$, meaning that the energy costs, represented by $R_{min,k}$, are more important than the investment costs. As the optimal solution depends on the choice of these weights anyhow, a simpler objective function can be used

$$\min\left(w_1 \sum_{k=1}^{ncol} N_{min,k} + w_2 \sum_{k=1}^{ncol} R_{fac,k} R_{min,k} D_k \right)$$

where N is replaced by N_{min}. This results in a model that is easier to solve as the strongly nonlinear expressions of the Gilliland correlation are avoided.

B.2 Equilibrium stage model

For the ideal ternary systems a simple model is developed based on the following assumptions.

- Constant liquid molar holdup on each tray, vapor holdup neglected.

- Constant molar flow rates.

- Constant pressure over the column.

- Heat effects are neglected, no energy balance.

- Saturated liquid feeds are provided.

- Ideal vapor-liquid equilibrium described by constant relative volatilities.

- Reaction in the liquid phase only.

The stages are numbered from top to bottom. In general, the total condenser represents stage 1 whereas the partial reboiler is stage N. Fig. B.1 shows one tray of a reactive distillation column with its liquid and vapor connections to the neighboring trays and a liquid feed.
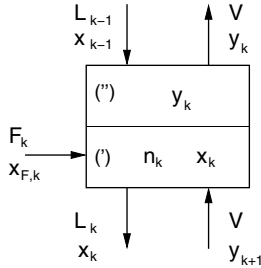

Figure B.1: Stage k of a reactive distillation column.

Component material balances $(i = 1(1)nc - 1)$

$$n_k \frac{d\,x_{i,k}}{d\,t} = F_k\,x_{i,F,k} + L_{k-1}\,x_{i,k-1} - L_k\,x_{i,k} + V\,y_{i,k+1} - V\,y_{i,k} + \sum_{j=1}^{nr} (\nu_{i,j}\,r_{0,j,k}(\mathbf{x}_k))$$

Total material balance

$$0 = F_k + L_{k-1} - L_k + \sum_{j=1}^{nr} \left(\nu_{T,j} \, r_{0,j,k}(\mathbf{x}_k) \right)$$

Ideal VLE with constant relative volatilities $(i = 1(1)nc - 1)$

$$y_{i,k} = \frac{\alpha_i \, x_{i,k}}{1 + \sum_{j=1}^{nc-1} (\alpha_j - 1) \, x_{j,k}}$$

Summation conditions

$$0 = 1 - \sum_{i=1}^{nc} x_{i,k} \qquad\qquad 0 = 1 - \sum_{i=1}^{nc} y_{i,k}$$

Extend of reaction $(j = 1(1)nr)$

$$r_{0,j,k}(\mathbf{x}_k) = m_{cat,k} \, k_{f,j} \left(\prod_{\substack{i=1 \\ \nu_{i,j}<0}}^{nc} x_{i,k}^{-\nu_{i,j}} - \frac{1}{K_{eq,j}} \prod_{\substack{l=1 \\ \nu_{l,j}>0}}^{nc} x_{l,k}^{\nu_{l,j}} \right)$$

where $m_{cat,k}$ represents the amount of catalyst on stage k and the stoichiometric coefficients are

$$\nu_{i,j} \begin{cases} < 0 & \text{for reactants} \\ > 0 & \text{for products} \\ = 0 & \text{for inerts} \end{cases}$$

The above equations are valid for the inner column stages $(k = 2(1)N - 1)$. The balance equations for the condenser $(k = 1)$ and the reboiler $(k = N)$ are slightly different as they have no top or bottom neighboring stage, respectively. In general, the feed specifications $(F_k, \mathbf{x}_{F,k})$ are assumed to be fixed and are provided as parameters or model inputs. For steady state optimization in GAMS, the left hand side of the component material balance is set to zero. In this case the model consists of a set of variables and a set of equations where the respective numbers are not required to be equal. The model equations form a *nonlinear programming (NLP)* problem which can be solved by NLP solvers like CONOPT [21] in GAMS.

To avoid a continuous feed distribution along the column height requires the introduction of binary variables $i_{F,k} \in \{0, 1\}$, leading to a more complex formulation. F_{tot} denotes the

fixed overall feed with composition $\mathbf{x}_F$ whereas F_k symbolizes the feed to every column stage. The conditions for a single feed column read

$$F_k - F_{tot}\, i_{F,k} \;\leq\; 0 \qquad\qquad k = 1(1)N$$
$$1 - \sum_{k=1}^{N} i_{F,k} \;=\; 0$$
$$F_{tot} - \sum_{k=1}^{N} F_k \;=\; 0$$

The solution of this *mixed-integer nonlinear programming (MINLP)* problem requires a different solver, e.g. DICOPT [38] in GAMS.

More complex RDC processes like the dividing wall column (Figs. 3.24, 3.33, 3.41) or the column with prefractionator (Figs. 3.25, 3.43) rely on the same model equations shown above. The only difference is that terms for liquid or vapor input or output streams have to be added to the material balances. Possibly, additional binary variables and relations have to be provided, depending on the structure to be realized.

Bibliography

[1] J. Abadie and J. Carpentier. Generalization of the Wolfe reduced gradient method to the case of nonlinear constraints. In *Optimization*, p. 37–47. Academic Press, New York, 1969.

[2] L.C. Abella, P.D. Gaspillo, H. Itoh, and S. Goto. Dehydration of tert-butyl alcohol in reactive distillation. *J. Chem. Eng. Japan*, 32(6):742–746, 1999.

[3] V.H. Agreda, L.R. Partin, and W.H. Heise. High-purity methyl acetate via reactive distillation. *Chem. Eng. Prog.*, p. 40–46, 1990.

[4] D. Barbosa and M.F. Doherty. The influence of equilibrium chemical reactions on vapour-liquid phase diagrams. *Chem. Eng. Sci.*, 43(3):529–540, 1988.

[5] D. Barbosa and M.F. Doherty. The simple distillation of homogeneous reactive mixtures. *Chem. Eng. Sci.*, 43(3):541–550, 1988.

[6] D. Barbosa and M.F. Doherty. Design and minimum-reflux calculations for single-feed multicomponent reactive distillation columns. *Chem. Eng. Sci.*, 43(7):1523–1537, 1988.

[7] D. Barbosa and M.F. Doherty. Design and minimum-reflux calculations for double-feed multicomponent reactive distillation columns. *Chem. Eng. Sci.*, 43(9):2377–2389, 1988.

[8] V. Bansal, J.D. Perkins, and E.N. Pistikopoulos. A case study in simultaneous design and control using rigorous, mixed-integer dynamic optimization models. *I&EC Res.*, 41(4):76–778, 2002.

[9] A. Brooke, D. Kendrick, and A. Meeraus, editors. *GAMS A User's Guide, Release 2.25*. The Scientific Press, San Francisco, 1992.

[10] G. Buzad and M.F. Doherty. Design of three-component kinetically controlled reactive distillation columns using fixed-point methods. *Chem. Eng. Sci.*, 49(12):1947–1963, 1994.

[11] G. Buzad and M.F. Doherty. New tools for the design of kinetically controlled reactive distillation columns for ternary mixtures. *Comp. Chem. Eng.*, 19:395–408, 1995.

[12] M.F. Cardoso, R.L. Salcedo, S. Feyo de Azevedo, and D. Barbosa. Optimization of reactive distillation processes with simulated annealing. *Chem. Eng. Sci.*, 55:5059–5078, 2000.

[13] N. Chadda, M.F. Malone, and M.F. Doherty. Effect of chemical kinetics on feasible splits for reactive distillation. *AIChE J.*, 47(3):590–601, 2001.

[14] F. Chen, R.S. Huss, M.F. Malone, and M.F. Doherty. Simulation of kinetic effects in reactive distillation. *Comp. Chem. Eng.*, 24:2457–2472, 2000.

[15] A.R. Ciric and D. Gu. Synthesis of nonequilibrium reactive distillation processes by MINLP optimization. *AIChE J.*, 40:1479–1487, 1994.

[16] CPLEX Optimization, Inc. *Using the CPLEX callable library*. NV, USA, 1989-1995.

[17] G. Damköhler. Wärmeübergangsprobleme in Chemischer Technik und Forschung. *Chemie Ingenieur Technik*, 12:469ff, 1939.

[18] DDBST. *DDB-Predict*. DDBST Software & Separation Technology GmbH, Oldenburg, 1993.

[19] M.F. Doherty and G. Buzad. Reactive distillation by design. *Chem. Eng. Res. Des.*, 70:448–458, 1992.

[20] M.F. Doherty and M.F. Malone. *Conceptual Design of Distillation Systems*. McGraw–Hill, New York, 2001.

[21] A.S. Drud. CONOPT – A large-scale GRG code. *ORSA Journal on Computing*, 6:207–216, 1994.

[22] F. Duprat, R. Gassend, and G. Gau. Reactive distillation process optimization by empirical formula construction. *Comp. Chem. Eng.*, 12(11):1141–1149, 1988.

[23] M.A. Duran and I.E. Grossmann. An outer approximation algorithm for a class of mixed-integer nonlinear programs. *Math. Prog.*, 36:307–339, 1986.

[24] T.F. Edgar, D.M. Himmelblau, and L.S. Lasdon, editors. *Optimization of Chemical Processes*. McGraw–Hill, New York, 2nd edition, 2001.

[25] B.A. Finlayson, L.T. Biegler, I.E. Grossmann, and A.W. Westerberg. Mathematics in Chemical Engineering. In *Ullmann's Encyclopedia of Industrial Chemistry, Vol. B 1*, p. 1–106 – 1–128. VCH Verlagsgesellschaft mbH, Weinheim, 1990.

[26] C.A. Floudas, editor. *Deterministic global optimization: theory, methods and applications*, volume 37 of *Nonconvex optimization and its applications*. Kluwer Academic Publishers, Dordrecht, 2000.

[27] C. Gabel, B. Schleppinghoff, H.D. Kohler, and H.V. Scheef. U.S. Patent 5,095,164, 1992.

[28] A.M. Geoffrion. Generalized Benders decomposition. *J. Optim. Theory Appl.*, 10(4):237–260, 1972.

[29] P.E. Gill, W. Murray, and M.H. Wright. *Practical Optimization*. Academic Press, London, 1981.

[30] J. Gmehling, J. Li, and M. Schiller. A modified UNIFAC model. 2. Present parameter matrix and results for different thermodynamic properties. *I&EC Res.*, 32(1):178–193, 1993.

[31] W. Haag. Oligomerization of isobutene on cation exchange resins. *Chem. Engng. Prog. Symp. Ser.*, 63:140–147, 1967.

[32] S. Hauan. *On the behaviour of reactive distillation systems*. PhD thesis, Norwegian University of Science and Technology. Trondheim, Norway, 1998.

[33] S. Hauan and K.M. Lien. A phenomena based design approach to reactive distillation. *Chem. Eng. Res. Des.*, 76:396–407, 1998.

[34] S. Hauan, A.W. Westerberg, and K.M. Lien. Phenomena-based analysis of fixed points in reactive separation systems. *Chem. Eng. Sci.*, 55:1053–1075, 2000.

[35] Ralph Joh. *Erweiterung der Anwendungsgebiete der Gruppenbeitragsmethode Modified UNIFAC (Dortmund)*. PhD thesis, Universität Oldenburg. 1998.

137

[36] A. Kienle. *Nichtlineare Wellenphänomene und Stabilität stationärer Zustände in Destillationskolonnen*. VDI Fortschritt–Berichte Nr. 3/506. VDI-Verlag, Düsseldorf, 1997.

[37] J.F. Knifton, J.R. Sanderson, and M.E. Stockton. U.S. Patent 5,811,620, 1998.

[38] G.R. Kocis and I.E. Grossmann. Computational experience with DICOPT solving MINLP problems in process systems engineering. *Comp. Chem. Eng.*, p. 307–315, 1989.

[39] A. Kröner, P. Holl, W. Marquardt, and E.D. Gilles. DIVA – An open architecture for dynamic simulation. *Comp. Chem. Eng.*, 14:1289–1295, 1990.

[40] J.W. Lee, S. Hauan, and A.W. Westerberg. Feasibility of a reactive distillation column with ternary mixtures. *I&EC Res.*, 40(12):2714–2728, 2001.

[41] Y.Y. Lee, Y.W. Lee, W.H. Hong, and H. Lee. Liquid liquid equilibria for the system water tert-butyl alcohol diisobutylene at 25, 45, and 75 degrees C. *J. Chem. Eng. Data*, 33(3):258–260, 1988.

[42] M. Mangold, A. Kienle, E.D. Gilles, and K.D. Mohl. Nonlinear computation in DIVA – methods and applications. *Chem. Eng. Sci.*, 55:441–454, 2000.

[43] K.D. Mohl. *Nichtlineare Dynamik von Reaktivdestillationsprozessen*. VDI Fortschritt–Berichte Nr. 3/747. VDI-Verlag, Düsseldorf, 2002.

[44] K.D. Mohl, A. Kienle, K. Sundmacher, and E.D. Gilles. A theoretical study of kinetic instabilities in catalytic distillation processes: Influence of transport limitations inside the catalyst. *Chem. Eng. Sci.*, 56:5239–5254, 2001.

[45] K.D. Mohl, A. Spieker, E. Stein, and E.D. Gilles. DIVA – Eine Umgebung zur Simulation, Analyse und Optimierung verfahrenstechnischer Prozesse. 1997.

[46] NAG Ltd., Oxford, England, UK. *NAG Fortran Library Routine Document*, 1993.

[47] M.J. Okasinski and M.F. Doherty. Design methods for kinetically controlled, staged reactive distillation columns. *I&EC Res.*, 37(7):2821–2834, 1998.

[48] M. Pekkanen. A local optimization method for the design of reactive distillation. *ESCAPE 5, Suppl. to Comp. Chem. Eng.*, 19:S235–S240, 1995.

[49] F.B. Petlyuk, V.M. Platonov, and D.M. Slavinskii. Thermodynamically optimal method for separating multicomponent mixtures. *Int. Chem. Eng.*, 5(3):555–561, 1965.

[50] G.G. Podrebarac, F.T.T. Ng, and G.L Rempel. More uses for catalytic distillation. *Chemtech.*, 27(5):37–45, 1997.

[51] A. Pyhälahti. Reactive Distillation in Literature. Technical report, Helsinki University of Technology, Plant Design Report Series, report no. 42, 1996.

[52] A. Rehfinger and U. Hoffmann. Kinetics of methyl tertiary butyl ether liquid phase synthesis catalyzed by ion exchange resin – I. Intrinsic rate expression in liquid phase activities. *Chem. Eng. Sci.*, 45(6):1605–1617, 1990.

[53] R.C. Reid, J.M. Prausnitz, and B.E. Polling, editors. *The Properties of Gases and Liquids*. McGraw–Hill, New York, 4. edition, 1987.

[54] E. Rév. Reactive distillation and kinetic azeotropy. *I&EC Res.*, 33(9):2174–2179, 1994.

[55] M. Sakuth and U. Peters. Offenlegungsschrift DE 195 04 555 A 1, 1996.

[56] K. Schittkowski. NLPQL: A Fortran subroutine solving constrained nonlinear programming problems. *Annals of Operations Research*, 5:485–500, 1985.

[57] E.U. Schlünder. Über den Einfluß der Stoffübertragung auf die Selektivität der thermischen Trennverfahren – dargestellt am Beispiel der Schleppmitteldestillation. *Verfahrenstechnik*, 11:682–686, 1977.

[58] A. Schöttner. Gemischt-ganzzahlige Optimierungsmodelle für das Design von Reaktivdestillationskolonnen. Master's thesis, IMO, Universität Magdeburg, 2001.

[59] J.D. Seader and E.J. Henley. *Separation process principles*. John Wiley & Sons, New York, 1998.

[60] L.A. Smith Jr. U.S. Patent 4,232,177, 1980.

[61] L.A. Smith Jr. U.S. Patent 5,221,441, 1993.

[62] W. Song, G. Venimadhavan, J.M. Manning, M.F. Malone, and M.F. Doherty. Measurement of residue curve maps and heterogeneous kinetics in methyl acetate synthesis. *I&EC Res.*, 37:1917–1928, 1998.

[63] J. Stichlmair and Th. Frey. Mixed-integer nonlinear programming optimization of reactive distillation processes. *I&EC Res.*, 40(25):5978–5982, 2001.

[64] J.G. Stichlmair and J.R. Fair. *Distillation. Principles and Practices*. Wiley-VCH, New-York, 1997.

[65] K. Sundmacher and U. Hoffmann. Development of a new catalytic distillation process for fuel ethers via a detailed nonequilibrium model. *Chem. Eng. Sci.*, 51(10):2359–2368, 1996.

[66] K. Sundmacher and A. Kienle, editors. *Reactive Distillation – Current Status and Future Trends*. Wiley-VCH, Weinheim, 2002.

[67] K. Sundmacher and Z. Qi. Conceptual design aspects of reactive distillation processes for ideal binary mixtures. *Chem. Eng. & Proc.*, 42:191–200, 2003.

[68] K. Sundmacher, G. Uhde, and U. Hoffmann. Multiple reactions in catalytic distillation processes for the production of the fuel oxygenates MTBE and TAME: Analysis by rigorous model and experimental validation. *Chem. Eng. Sci.*, 54:2839–2847, 1999.

[69] R. Taylor and R. Krishna. Modelling reactive distillation. *Chem. Eng. Sci.*, 55:5183–5229, 2000.

[70] J. Tejero, A. Calderón, F. Cunill, J.F. Izquierdo, and M. Iborra. The formation of byproducts in the reaction of synthesis of isopropyl tert-butyl ether from isopropyl alcohol and isobutene on an acidic macroporous copolymer. *React. Funct. Polym.*, 33:201–209, 1997.

[71] The MathWorks, Inc. *Using Matlab, Version 6*. Natick, MA, USA, 2000.

[72] Ch. Thiel, K. Sundmacher, and U. Hoffmann. Residue curve maps for heterogeneously catalysed reactive distillation of fuel ethers MTBE and TAME. *Chem. Eng. Sci.*, 52(6):993–1005, 1997.

[73] A. Tuchlenski, A. Beckmann, D. Reusch, R. Düssel, U. Weidlich, and R. Janowsky. Reactive distillation – Industrial applications, process design & scale-up. *Chem. Eng. Sci.*, 56:387–394, 2001.

[74] S. Ung and M.F. Doherty. Vapour-liquid phase equilibrium in systems with multiple chemical reactions. *Chem. Eng. Sci.*, 50(1):23–48, 1995.

[75] I.I. Vasileva, A.A. Naumova, A.A. Polyakov, T.N. Tyvina, V.V. Fokina, and N.G. Khrabrova. . *Zh. Prikl. Khim. (Leningrad)*, 63(6):1432–4136, 1990.

[76] E. Velo, L. Puigjaner, and F. Recasens. Inhibition by product in the liquid-phase hydration of isobutene to tert-butyl alcohol - Kinetics and equilibrium studies. *I&EC Res.*, 27(12):2224–2231, 1988.

[77] G. Venimadhavan, G. Buzad, M.F. Doherty, and M.F. Malone. Effect of kinetics on residue curve maps for reactive distillation. *AIChE J.*, 40(11):1814–1824, 1994.

[78] A. Vogelpohl. Definition von Destillationslinien bei der Trennung von Mehrstoff-gemischen. *Chemie Ingenieur Technik*, 65(5):515–522, 1993.

[79] A. Vogelpohl. On the relation between ideal and real systems in ternary distillation. *Chem. Eng. Res. Des.*, 77(A6):487–492, 1999.